

In-Plane Structural Response of Single-Storey Unreinforced Walls Constructed Using Alternative Masonry Units

by

Etobo Prince Shiso



*Thesis presented in fulfilment of the requirements for
the degree of Master of Engineering in Structural Engineering in
the Faculty of Engineering at Stellenbosch University*

The financial assistance of the National Research Foundation (NRF) towards this research is hereby acknowledged. Opinions expressed and conclusions arrived at, are those of the author and are not necessarily to be attributed to the NRF.

Supervisor:
Mrs Wibke De Villiers

April 2019

Declaration

By submitting this thesis electronically, I declare that the entirety of the work contained therein is my own, original work, that I am the sole author thereof (save to the extent explicitly otherwise stated), that reproduction and publication thereof by Stellenbosch University will not infringe any third party rights and that I have not previously in its entirety or in part submitted it for obtaining any qualification.

Etobo Prince Shiso

April 2019

Abstract

In-Plane Structural Response of Single-Storey Unreinforced Walls Constructed Using Alternative Masonry Units

E.P. Shiso

*Department of Structural Engineering,
University of Stellenbosch,
Private Bag X1, Matieland 7602, South Africa.*

Thesis: MEng (Civil)

April 2019

Studies on alternative masonry units (AMUs) at Stellenbosch University seek to reduce the environmental impact that conventional masonry units (concrete masonry units [CMUs] and fired clay) cause, by developing masonry units that are environmentally friendly, socially acceptable and structurally sound. The introduction of AMUs in the construction industry as construction components for low-income housing depends on the determination of their minimum mechanical specifications.

The three AMU types being investigated include compressed stabilized earth blocks (CSEBs), Adobe blocks, and alkali-activated concrete blocks (AACBs). Various experimental tests are being conducted in the laboratory on AMUs as well as concrete masonry blocks (CMUs), which aim to provide sufficient information on the technical performances of these masonry units.

Further, as certain areas in South Africa have been identified to be at risk of low to moderate seismic activities, the South African loading code requires that single storey masonry structures be designed for seismic actions. To use AMUs as construction components for such structures necessitates, as part of the determination of mechanical specifications, that an investigation be carried out on the seismic behaviour of a masonry structure constructed with AMUs. Such investigation is often conducted in a laboratory setting by subjecting masonry walls of pre-defined geometry and with restraint, as in a structural building system, to similar loading conditions a wall would experience during an earthquake.

In this study, in-plane shear-compression tests on large scale masonry wall, constructed with CMUs and AMUs respectively, are conducted to determine the in-plane structural response of

these walls. This was achieved by designing and constructing an appropriate test set-up capable of undertaking such tests, and by manufacturing a large quantity of masonry units.

Characterisation tests were performed on masonry units as well as wallets to determine their respective compressive strength and modulus of elasticity. Density tests were also performed on masonry units, the results of which are within the range of values provided in literature. Performed at various stages on the experimental programme and at different ages of masonry units, an increase over time in the strength and stiffness was observed in the four different masonry units. While AACBs showed a higher compressive strength than the CMUs, they had a lower modulus of elasticity. On the other hand, the Adobe blocks had the lowest compressive strength and modulus of elasticity, and exhibited little increase of these properties over time. Difficulties were encountered while performing tests on masonry wallets as adequate boundary conditions were required at the top and bottom of the specimens. However, sufficient results were obtained which were used to determine the pre-compression levels applied on top of the wall specimens.

Further, two test set-up configurations for the in-plane shear-compression tests were adopted based on the boundary conditions (BC) the wall was subjected to, i.e. fixed-free and fixed-fixed BC. The test results of AMU walls indicated that with the fixed-free BC, the specimen exhibited a rather large lateral capacity as compared to the results from a fixed-fixed BC configuration. Although difficulties were encountered while performing tests on CMU wall specimens, it was found that with few adjustments of the test set-up these tests could be performed successfully.

Forming part of the technical performances of the masonry units, the results obtained and presented in this study can further be used in forthcoming studies for validation of numerical modelling and, ultimately, the determination of minimum mechanical specifications of AMUs.

Uittreksel

In-Vlak Strukturele Gedrag van Enkelverdieping Ongewapende Mure Gebou met Alternatiewe Messelwerk Eenhede

(“In-Plane Structural Response of Single-Storey Unreinforced Walls Constructed Using Alternative Masonry Units”)

E.P. Shiso

*Departement Struktuur Ingenieurswese,
Universiteit van Stellenbosch,
Privaatsak X1, Matieland 7602, Suid Afrika.*

Tesis: MIng (Siviel)

April 2019

Studies oor alternatiewe messelwerkeenhede (AME's) by Universiteit Stellenbosch word gedoen in 'n poging om die omgewingsimpak te verminder wat deur konvensionele messelwerkeenhede (beton-messelwerkeenhede [BME's] en gebrande klei stene) veroorsaak word deur messelwerkeenhede as boukomponente te ontwikkel wat omgewingsvriendelik, sosiaal aanvaarbaar en struktureel betroubaar is. Die benutting van AME's in die boubedryf as boukomponente vir laeinkomste-behuising hang van die bepaling van hul minimum meganiese spesifikasies af.

Die drie soorte AME's wat ondersoek word, sluit in saamgeperste gestabiliseerde grondblokke (SSGB, Adobe-blokke en alkali-geaktiveerde betonblokke (AGBB's)). Verskeie eksperimentele toetse is op AME's asook BME's in die laboratorium uitgevoer met die doel om voldoende inligting oor die tegniese verrigting van hierdie messelwerkeenhede te verskaf.

Op grond van waarnemings dat sekere gebiede in Suid-Afrika 'n risiko van lae tot matige seismiese aktiwiteite loop, vereis die Suid-Afrikaanse laskode dat enkelvlak-messelwerkstrukture vir seismiese aksies ontwerp moet word. Om AME's as boukomponent vir sodanige strukture te gebruik, noodsaak, as deel van die bepaling van meganiese spesifikasies, 'n ondersoek na die seismiese gedrag van 'n messelwerkstruktuur wat met AME's gebou is. Sodanige ondersoek word dikwels in 'n laboratoriumomgewing uitgevoer deur messelwerkmure met 'n voorafbepaalde geometrie en met randvoorwaardes, soos in 'n strukturele boustelsel, aan soortgelyke lastoestande te onderwerp as wat 'n muur tydens 'n aardbewing sou ervaar.

In hierdie studie is in-vlak-skuifdruktoetse op grootskaalse messelwerkmure met onderskeidelik BME's en AME's uitgevoer om die in-vlak-strukturele reaksie van hierdie mure te bepaal. Dit is bereik deur die ontwerp en samestelling van 'n geskikte toetsopstelling en die vervaardiging van 'n groot hoeveelheid messelwerkeenhede.

Karakteriseringstoetse is op messelwerkeenhede asook klein blokmure uitgevoer om hul druksterkte en elastisiteitsmodulus te bepaal. Digtheidstoetse is ook op messelwerkeenhede uitgevoer, waarvan die resultate binne die omvang was van waardes wat in die literatuur beskikbaar is. In die toetse, wat in verskillende fases van die eksperimentele program en op verskillende ouderdomme van messelwerkeenhede uitgevoer is, is 'n toename met verloop van tyd in die sterkte en styfheid in die vier verskillende messelwerkeenhede waargeneem. Alhoewel AGBB's 'n hoër druksterkte as BME's getoon het, het dit 'n laer elastisiteitsmodulus gehad. Aan die ander kant het die Adobe-blokke die laagste druksterkte en elastisiteitsmodulus gehad, en min toename in hierdie eienskappe met verloop van tyd getoon. Probleme is ondervind met die uitvoer van toetse op klein blokmure, aangesien voldoende randvoorwaardes (RV's) aan die bo- en onderkante van die monsters nodig was. Voldoende resultate is egter verkry, wat gebruik is om die voorspanningsvlakke te bepaal wat op die bokant van die muurmonsters toegepas is.

Twee toetsopstellingskonfigurasies vir die in-vlak-skuifdruktoetse is gebruik op grond van die RV's waaraan die muur onderwerp is, naamlik vaste-vry en vaste-vaste RV's. Die toetsresultate van AME-mure het getoon dat met die vaste-vry RV, die toetsopstelling 'n redelike groot laterale kapasiteit getoon het in vergelyking met die resultate van 'n vaste-vaste RV-konfigurasie. Alhoewel probleme ervaar is toe die toetse op BME-muur toetsopstellings uitgevoer is, is gevind dat hierdie toetse met sukses uitgevoer kan word met min verstellings van die toetsopstelling.

Die resultate wat in hierdie studie verkry is en aangebied word, wat deel vorm van die tegniese evaluering van messelwerkeenhede, kan in toekomstige studies gebruik word vir data vir numeriese modellering en, uiteindelik, die bepaling van minimum meganiese spesifikasies van AME's.

Acknowledgements

I wish to offer my heartfelt gratitude to the following individuals for their outstanding contributions towards this research project:

- My supervisor, Mrs Wibke de Villiers for her encouragement, patience and guidance provided throughout this research project. I am thankful for the continued support given during my time at Stellenbosch University.
- Uncle Johan van der Merwe for his guidance and assistance during the construction of the test set-up. I thank you for the skills and knowledge you shared.
- Charlton Ramat and Lee-Roy Jones (laboratory staffs) for their incredible assistance during the experimental period spent in the laboratory.
- Dr Stephan Zeranka for his time, guidance and assistance in conducting the tests in the laboratory.
- Timothy Combrinck for his assistance in the laboratory and in performing the wall tests. Your hard work and spirit of service is greatly appreciated.
- Natalie Scheepers and Olivia van Wyk for providing great support for the administrative aspect related to my research.
- My office colleagues and friends for their encouragement and assistance as well as the wonderful moments spent together.
- My parents and family members (Nshisu's and Parsa's) for your prayers and words of encouragement. I thank you for accompanying me on this journey.
- My beautiful wife Nasim Parsa for her loving support and encouragement. Your radiant heart, kindness and patience have been a source of strength and motivation, inspiring me to give my best towards this thesis.
- My little daughter Nura Mwabile Shiso for being very patient with me in the last few weeks leading to the completion of this academic work.

Most importantly, I thank God for His protection and the strength provided to see the end of this research project.

Contents

Declaration	i
Abstract	ii
Uittreksel	iv
Acknowledgements	vi
Contents	vii
List of Figures	x
List of Tables	xiii
Nomenclature	xiv
1 Introduction	1
1.1 Thesis Statement	2
1.2 Motivation	2
1.3 Objectives and Methodology	3
1.4 Thesis Layout	3
2 Literature Review	5
2.1 Low-Income Housing (LIH) in South Africa	5
2.2 Conventional Masonry Units (CMUs)	6
2.3 Alternative Masonry Units (AMUs)	7
2.3.1 Adobe	8
2.3.2 Compressed Stabilized Earth Block (CSEB)	8
2.3.3 Alkali Activated Concrete Block (AACB)	9
2.4 Seismicity in South Africa	9
2.4.1 Design Considerations	10
2.4.2 Displacement Based Design	12
2.5 Seismic Performance of Single-storey URM Buildings	13
2.6 Experimental Studies on URM In-plane Shear Behaviour	15
2.6.1 Introduction	15
2.6.2 Failure Modes	17

2.6.3	Representation of Experimental Results	18
2.7	Various Experimental Test Set-ups	21
2.7.1	Introduction	21
2.7.2	ETH Zurich Test Set-up	22
2.7.3	EPFL Test Set-ups	23
2.7.4	Stellenbosch University Test Set-up	24
2.7.5	Other Test Set-ups	25
2.8	Concluding Summary	28
3	Materials and Block Manufacturing	29
3.1	Materials	29
3.1.1	Aggregates	29
3.1.2	Binders	31
3.1.3	Alkaline Solution	31
3.1.4	Water	31
3.2	Block Manufacturing	31
3.2.1	Concrete Masonry Units (CMUs)	33
3.2.2	Compressed Stabilized Earth Blocks (CSEBs)	36
3.2.3	Adobe	39
3.2.4	Alkali-Activated Concrete Blocks (AACBs)	40
3.3	Mortar Mix Design	43
3.4	Concluding Summary	44
4	Mechanical Properties of Masonry Structural Elements	45
4.1	Masonry Unit and Mortar	45
4.1.1	Specifications for Compressive Strength Test	48
4.1.1.1	Masonry Units	48
4.1.1.2	Mortar	49
4.1.2	Specifications for Modulus of Elasticity Test	50
4.2	Masonry Wallet	52
4.2.1	Testing Specifications	53
4.3	Density	55
4.3.1	Testing Specifications	56
4.4	Conclusion	56
5	Experimental Design	57
5.1	Compressive Strength Test	57
5.1.1	Masonry Unit Test	57
5.1.2	Mortar Test	58
5.2	Modulus of Elasticity Test	58
5.3	Tests on Masonry Wallets	61
5.4	Density test	63
5.5	In-plane Shear-Compression Test	63
5.5.1	Wall Specimens	64

5.5.2	Test Set-up and Procedure	67
5.5.3	Measurements and Data Collection	74
5.6	Conclusion	75
6	Results and Discussion	76
6.1	Masonry Unit Test Results	76
6.1.1	Compressive Strength	76
6.1.2	Modulus of Elasticity	79
6.1.3	Density	83
6.2	Masonry Wallet Test Results	84
6.3	Masonry Wall Test Results	87
6.3.1	CMU Walls	88
6.3.2	CSEB Walls	92
6.3.3	Adobe Walls	95
6.3.4	AACB Walls	98
6.3.5	Discussion on the Shear-compression Test	101
6.4	Conclusion	106
7	Conclusion	107
7.1	Block Manufacturing	108
7.2	Characterisation and In-plane Shear-compression Tests	108
7.2.1	Characterisation Tests	109
7.2.2	In-plane Shear-compression Tests	109
7.3	Observations on the Test Set-ups	110
7.4	Recommendations for Future Studies	112
	References	114
	Appendices	120
A	Masonry Unit	121
A.1	Loading Rate Summary	121
A.2	Compressive Strength Test Results	122
A.3	Modulus of Elasticity Test Results	123
B	Masonry Wallet	127
B.1	Modulus of Elasticity Test Results	127
C	Masonry Wall	128
C.1	LVDT and Applied Load Readings, & New Test Set-up	128

List of Figures

Figure 2.1	State-subsidised House Made of Fired Clay Bricks	7
Figure 2.2	South African Seismic Hazard Zones	10
Figure 2.3	Diagram Defining the Behaviour Factor (q)	11
Figure 2.4	Normalized Design Response Spectra - $S_d(T)/a_g$	12
Figure 2.5	Failure Mechanisms of a Typical Adobe Structure	14
Figure 2.6	Cracks in an Unreinforced Brick Masonry Building	14
Figure 2.7	Deformed Shape and Moment Profile of URM Wall	16
Figure 2.8	Failure Modes of Masonry Walls	17
Figure 2.9	Bilinear Envelope Idealisation of Experimental Results	19
Figure 2.10	Different Configurations for Fixed-fixed Boundary Conditions	21
Figure 2.11	ETH Zurich Test Set-up	23
Figure 2.12	EPFL Test Set-ups for Full-scale and Half-scale Walls	24
Figure 2.13	Stellenbosch University Test Set-up for Small Walls	25
Figure 2.14	Semnan University Test Set-up	26
Figure 2.15	Test Set-up with Loading Frame	26
Figure 2.16	Southeast University Test Set-up	26
Figure 2.17	Set-up used for Reinforced Concrete Block Masonry Walls	27
Figure 3.1	Grading of Materials	30
Figure 3.2	Hydraform Block Press	32
Figure 3.3	Static Compaction Process	33
Figure 3.4	Grading of CMU aggregates	33
Figure 3.5	CMU Manufacturing Process	35
Figure 3.6	Dry Density - Moisture Content Results	37
Figure 3.7	Weighed CSEB Mixtures	38
Figure 3.8	CSEB Curing in Laboratory Open Space	38
Figure 3.9	Adobe Block	40
Figure 3.10	AACB Wooden Mould	42
Figure 3.11	AACB Curing in Wooden Mould	42
Figure 3.12	Dust Layer Forming on AACBs	42
Figure 4.1	Stress-displacement Diagram of Quasi-brittle Material in Compression	46
Figure 4.2	Behaviour of Concrete under Successive Loading Cycles	47
Figure 4.3	Cycles to Determine the Stabilized Secant Modulus of Elasticity	50

Figure 4.4	Masonry Wallet, Stacked Bond Prism, and Unit-Mortar Stress State	53
Figure 4.5	Masonry Wallet Specimen	54
Figure 5.1	Test Set-up for Unit Compressive Strength	58
Figure 5.2	Modulus of Elasticity Specimens and Frames	59
Figure 5.3	Modulus of Elasticity Test Set-up for Prismatic Specimens	59
Figure 5.4	Set-up for Cylindrical Specimens	60
Figure 5.5	Wallet Specimens	61
Figure 5.6	Masonry Wallet Test Set-up	62
Figure 5.7	Masonry Bonds Adopted in Practice	64
Figure 5.8	Dimensions of Wall Specimen	65
Figure 5.9	Top and Bottom Steel Plates	66
Figure 5.10	Typical Construction of a Wall Specimen	67
Figure 5.11	Various Elements of the Test Set-up	68
Figure 5.12	Drawing of Test Set-up A	69
Figure 5.13	First Mock Wall Test	70
Figure 5.14	Components of Test Set-up B	71
Figure 5.15	Second Mock Wall Test	72
Figure 5.16	Test Set-up with Wall Specimen	72
Figure 5.17	Drawing of Test Set-up B	73
Figure 5.18	Close up View of Wall Indicating Locations of LVDTs	75
Figure 6.1	Unit Compressive Strength Results	77
Figure 6.2	Unit Modulus of Elasticity Results	79
Figure 6.3	Dry Density Results	83
Figure 6.4	Masonry Wallet Results	85
Figure 6.5	Vertical Cracks on Wallet Specimens	86
Figure 6.6	CMU-W-A: Crack Patterns	89
Figure 6.7	CMU-W-A: Test Results	90
Figure 6.8	CMU-W-B: Crack Patterns	91
Figure 6.9	CMU-W-B: Test Results	91
Figure 6.10	CSEB-W-A: Crack Patterns	93
Figure 6.11	CSEB-W-A: Test Results	93
Figure 6.12	CSEB-W-B: Crack Patterns	94
Figure 6.13	CSEB-W-B: Test Results	94
Figure 6.14	Adobe-W-A: Crack Patterns	96
Figure 6.15	Adobe-W-A: Test Results	96
Figure 6.16	Adobe-W-B: Crack Patterns	97
Figure 6.17	Adobe-W-B: Test Results	97
Figure 6.18	AACB-W-A: Crack Patterns	99
Figure 6.19	AACB-W-A: Test Results	99
Figure 6.20	AACB-W-B: Crack Patterns	100
Figure 6.21	AACB-W-B: Test Results	100

Figure 6.22	CMU-W-B: 2MN LC Force vs Vertical Displacement	102
Figure 6.23	2MN LC force vs Vertical Displacement	102
Figure 6.24	Masonry Wall Test Results	103
Figure 6.25	LVDT-6 Readings (AACB-W-A & AACB-W-B)	105
Figure A.1	CMU: Stress - Strain Responses at 28 days	123
Figure A.2	CSEB: Stress - Strain Responses at 28 days	124
Figure A.3	Adobe: Stress - Strain Responses at 28 days	125
Figure A.4	AACB: Stress - Strain Responses at 28 days	126
Figure B.1	Masonry Wallet: Stress - Strain Responses	127
Figure C.1	CMU Walls: LVDT Readings	128
Figure C.2	CSEB Walls: LVDT Readings	129
Figure C.3	Adobe Walls: LVDT Readings	130
Figure C.4	AACB Walls: LVDT Readings	131
Figure C.5	Masonry Walls: Intron MTM, 50t & 2MN LC Readings	132
Figure C.6	New Test Set-up Proposal	133

List of Tables

Table 2.1	Drift Capacity of URM Walls	17
Table 3.1	Characteristics of Aggregates	31
Table 3.2	FM values Comparison	33
Table 3.3	CMU Mix Design Quantities	34
Table 3.4	CSEB Mix Design Quantities	37
Table 3.5	Adobe Mix Design Quantities	39
Table 3.6	AACB Mix Design Quantities	41
Table 3.7	Mortar Mix Proportions	43
Table 4.1	Densities of Various Masonry Units	55
Table 6.1	Unit Compressive Strength Results with COV	78
Table 6.2	Unit Modulus of Elasticity Results with COV	80
Table 6.3	Dry Density Results with COV	84
Table 6.4	Masonry Wallet Results with COV and Mortar Characteristic	85
Table 6.5	CMU walls - Unit and Mortar Properties	89
Table 6.6	CMU walls - Results from Experimental Curves	92
Table 6.7	CSEB walls - Unit and Mortar Properties	92
Table 6.8	CSEB walls - Results from Experimental and Idealised Curves	95
Table 6.9	Adobe walls - Unit and Mortar Properties	95
Table 6.10	Adobe walls - Results from Experimental and Idealised Curves	98
Table 6.11	AACB walls - Unit and Mortar Properties	98
Table 6.12	AACB walls - Results from Experimental and Idealised Curves	101
Table 6.13	Drift Capacity Comparison	104
Table A.1	Summary of Loading Rates Used for Different Tests	121
Table A.2	Compressive Strength Test Results	122

Nomenclature

Symbols

Latin letters	Description and Units
A_i	Loaded cross-sectional area [mm ²]
d_{cr}	Displacement at crack limit [mm]
d_e	Displacement at ultimate resistance of the wall [mm]
$d_{H_{max}}$	Displacement at maximum resistance of the wall [mm]
d_u	Displacement corresponding to 20% strength degradation . . . [mm]
E_i	Modulus of elasticity of masonry specimen [GPa]
E_m	Modulus of elasticity of mortar [GPa]
E_u	Modulus of elasticity of masonry unit [GPa]
f_i	Compressive strength of masonry specimen [MPa]
f_m	Compressive strength of mortar [MPa]
f_u	Compressive strength of masonry unit [MPa]
F	Applied vertical force [kN]
$F_{i,max}$	Maximum load reached by a specimen [kN]
h	Height of the wall [mm]
h_0	Shear span [mm]
H	Applied horizontal force [kN]
H_{cr}	Resistance of the wall at crack limit [kN]
H_{max}	Maximum resistance of the wall [kN]
H_u	Ultimate resistance of the wall [kN]

NOMENCLATURE

K_e	Effective stiffness	[kN/mm]
l_w	Length of the wall	[mm]
m_{dry}	Constant mass of a specimen	[kg]
q	Behaviour factor	[–]
V_n	Volume of a specimen	[mm ³]
Greek letters Description and Units		
δ	Drift capacity	[%]
ε	Strain	[mm/mm]
ε_n	Strain normal to the applied stress	[mm/mm]
ε_p	Strain parallel to the applied stress	[mm/mm]
ν	Poisson's ratio	[–]
ρ	Dry density	[kg/mm ³]
σ	Compressive stress	[MPa]

Acronyms

Acronym	Description
AAC	Alkali-activated concrete
AACB	Alkali-activated concrete block
AMU	Alternative Masonry Unit
ASTM	American Society for Testing and Materials
BC	Boundary Condition
BNG	Breaking New Ground
CMU	Concrete Masonry Unit
COV	Coefficient of variation
CSEB	Cement stabilized earth block
DB	Displacement-based

NOMENCLATURE

dofs	degrees of freedom
EPFL	École Polytechnique Fédérale de Lausanne
FB	Force-based
FM	Fineness modulus
GGCS	Ground granulated corex slag
HCP	Hardened cement paste
LC	Load cell
LIH	Low-Income Housing
LSNC	Limit State of Near Collapse
LSSD	Limit State of Significant Damage
LVDT	Linear variable displacement transducers
MDD	Maximum dry density
MMI	Modified mercalli intensity
OMC	Optimum moisture content
RD	Relative density
SANS	South African National Standards
SH	Sodium hydroxide
SHS	Sodium hydroxide solution
SS	Sodium silicate
URM	Unreinforced masonry

Chapter 1

Introduction

Research studies on alternative masonry units (AMUs) aim at ensuring that adequate and environmentally friendly houses are provided to the low-income population in South Africa. One such research project is currently underway at Stellenbosch University and focuses on the development of AMUs to be introduced into the South African market as construction components for low-income housing (LIH) in the country.

To address the housing shortage experienced in South Africa, the government is subsidising single storey houses for the low-income population that are built with conventional masonry units such as concrete masonry units (CMUs) and fired clay bricks. The use of these units in large quantities has shown to have disadvantages, including the use of non-renewable resources in the production of fired clay bricks and the use of high temperatures and emissions of carbon dioxide in the cement production process required for cement based masonry units, all of which have negative impacts on the environment.

According to the South African Application of the National Building Regulations, LIH units can fall under Category 1 Buildings. In order to use AMUs in the construction of LIH units, technical performance requirements of AMUs need to be investigated as these are not similar to those of conventional masonry units recommended in the current South African specifications.

At Stellenbosch University, three different types of AMUs are being investigated. These include compressed stabilized earth blocks, Adobe blocks and alkali-activated concrete blocks. The technical performances of these building components are investigated through laboratory tests on masonry units and walls. The results obtained from the laboratory tests will further contribute to validating numerical models to be used in determining the minimum mechanical and environmental specifications of AMUs.

The investigation of in-plane structural response of walls constructed with AMUs is one of the mechanical performances being investigated through laboratory tests and presented in this study. This investigation contributes not only to validating the results of numerical models but also assisting further in the development of AMUs as construction components.

Certain areas in South Africa have been identified to be at risk of low to moderate seismic actions. As LIH are mainly unreinforced masonry (URM) buildings and need to be designed for seismic

actions, the tests performed in the present study will also provide an indication of the seismic behaviour of URM walls built with AMUs.

1.1 Thesis Statement

With the aim of contributing to the development of AMUs, previous research studies (e.g. [Fourie, 2017](#); [Malherbe, 2016](#)) investigated various properties of these construction components at the material level. Once introduced in the construction market, AMUs will be used to construct walls for single-storey buildings and will require to resist different forces.

In this light, the current research study is concerned with investigating and determining, at the structural level, what is the in-plane structural responses of unreinforced masonry walls constructed with AMUs, and how these compare to the walls constructed with CMUs when subjected to similar loading conditions.

1.2 Motivation

The development of AMUs as construction units for single-storey housing construction is a step forward in addressing the significant negative environmental impact that the current construction units such as concrete masonry units are causing, particularly because of the large amount of cement required for their production.

As for any construction component used for the design and erection of a structure, engineers need to ensure that structural safety is achieved by complying to the minimum design and construction requirements. The specifications for AMUs, however, are not developed as compared to the CMUs standards ([De Villiers and Boshoff, 2014](#)). Developing such standards will ensure that AMUs are also introduced and used in the construction industries, and ultimately provide a durable solution to the high demand of LIH.

Earthquakes are natural disasters which affect the integrity and safety of a given structure. Their actions on buildings can result in endangering the lives of their occupants and in other devastating consequences. A sound knowledge of the response of AMUs under seismic actions is then important for engineers and the construction industry.

Considering the complex behaviour of URM building constituents, experimental tests on these structures play an important role as they represent a basis by which numerical models of these types of structures are validated. It is hoped that the results of this research will further contribute to the efforts being made in developing AMUs as construction materials for single storey URM buildings.

Another motivation for this research comes from a desire to contribute to greater levels of social justice in society by developing materials used for masonry buildings which are affordable and can be found locally by community members. In this way, more people will benefit from the development being made.

1.3 Objectives and Methodology

In this study are presented the test results of an experimental research study on the in-plane structural response of URM walls constructed with AMUs. The following points enumerated here represent the main objectives of this research.

- i. Manufacturing blocks (CMU & AMUs).
 - Mix designs,
 - Performing characterisation tests.
- ii. Designing and constructing an experimental test set-up for in-plane shear-compression wall test.
- iii. Performing in-plane shear-compression tests on walls (1800mm × 1500mm), each constructed with CMUs and AMUs respectively.

The first objective, which follows on previous research studies under the same project, was achieved by manufacturing blocks adopting previously used mix designs (e.g. [Fourie, 2017](#)) and determining their mechanical and physical properties through experimental tests. While various experimental tests can be performed on construction materials, the tests investigated here included compressive strength and modulus of elasticity tests carried out on units and wallets, as well as material density tests. The term “wallet” is used in this study to describe a small masonry wall comprised of masonry units joint together with mortar.

A comprehensive literature review helped equip the researcher with adequate background information necessary to achieve the second objective. The design and construction of the test set-up was, however, limited by the space, resources, and material accessible in the laboratory. Effort was made nevertheless to use effectively and in the safest manner the materials and equipment available.

Using the constructed test set-up, in-plane shear-compression tests were conducted. The knowledge required in assessing the obtained results was gained through a literature review and an understanding that the obtained data will further be used in validating results from numerical models.

It should be noted that this is primarily an experimental research study seeking to perform experimental tests on manufactured solid masonry units, based on existing mix designs, and that the numerical modelling previously mentioned was not conducted. In some cases, however, the mix designs and manufacturing techniques for the units were altered mainly because of the differences in properties between the constituent materials used in this study and those used in previous ones.

1.4 Thesis Layout

The motivation of carrying out this research is to further contribute to the development of alternative masonry units at Stellenbosch University, with a focus on investigating the structural response of walls made of these units when subjected to shear-compression in-plane forces.

CHAPTER 1. INTRODUCTION

A literature review is provided in Chapter 2, where the current housing backlog in South Africa and the solution adopted involving the construction of Category 1 LIH units using conventional masonry units are discussed. Alternative masonry units, which could be adopted, are also presented. Further, as a few areas in South Africa have been identified to be at risk of seismic activities, the design and experimental test methods for masonry walls which can resist seismic loadings are discussed in this chapter.

In Chapter 3, the manufacturing process of the various masonry units is presented. This includes the mix design, the material properties and quantities for each mix, the different material used in the mixes together with the manufacturing techniques, and the curing and storage methods.

Chapter 4 provides a literature study presenting the background of the determination of mechanical and physical properties of masonry constituents. Various testing specifications and guidelines, which experimental tests are based on, are also discussed.

In Chapter 5, the experimental test set-ups used to investigate the different properties of masonry constituents are provided. The test set-ups were either adopted from previous studies or designed and constructed, the process of which is also described in detail in the chapter.

Chapter 6 provides summaries and discussions of all the test results. The behaviour of each masonry unit type as well as the difficulties encountered during the various tests are highlighted. The performance of the test set-ups and whether tests were successfully performed on masonry units is also discussed.

In Chapter 7, a conclusion of the research study is drawn, and recommendations are made based on the knowledge gained. This chapter is followed by a list of references and appendices providing additional information.

Chapter 2

Literature Review

Before presenting the research carried out in this study, this chapter will provide some background information which will include an analysis of the situation of low-income housing in South Africa; a description of the type of materials used for the construction of such houses, as well as their benefits and weaknesses; and an assessment of alternative masonry units that could be used instead. Further, the chapter will present an exploration of seismicity in South Africa and its effects on single-storey buildings; as well as a review of experimental studies carried out into the effects of seismic activity on un-reinforced masonry walls.

2.1 Low-Income Housing (LIH) in South Africa

A major challenge faced by the South African government has been to ensure that its population can have access to adequate and affordable housing, as indicated in its constitutional clause (Section 26), stating that “everyone has the right to have access to adequate housing. The government must take reasonable steps within its available resources to provide people with housing and access to land”. Since 1995, when a housing policy was put in place to eliminate the housing backlog, the government has been able to provide more than 3 million housing units to poor and low-income populations. However, based on data collected by the Department of Human Settlements in 2015, the housing backlog had only been increasing. While in 1994 it was at 1.5 million units, it had reached some 2.1 million by 2015 (Tomlinson *et al.*, 2015).

According to housing expert Mary R Tomlinson, this increase is due to a number of factors, including the formation of new families and an increase in the number of informal settlements in urban settings since 1994 (Tomlinson *et al.*, 2015). It seems there are several other factors that might have also contributed to such an increase in the backlog. For instance, Tomlinson talks about the improvement in the quality of the units constructed, which has led to an increase in cost and therefore a decrease in the number of units built per year. This has resulted in fewer units being built per annum than the government had previously planned for. The growing backlog is one among the many difficulties that the government has faced as it has attempted to implement its affordable housing policy.

In 2004, a revised housing policy called Breaking New Ground (BNG) was adopted, which aimed at providing better subsidized housing while promoting the use of alternative building

CHAPTER 2. LITERATURE REVIEW

technologies (le Roux, 2014). The BNG focuses on refining the housing environment's quality, which resulted in larger houses compared to those provided in the initial years of the housing policy (Tomlinson *et al.*, 2015). Now the government constructs 41m² low-cost single-storey housing units to address the backlog (De Villiers and Boshoff, 2014).

These housing units fall under Category 1 Buildings as introduced in the South African Application of the National Building Regulations (SANS 10400-A, 2016). These buildings have similar safety standards with other building categories. However, certain aspects, such as maintenance requirements, rain penetration, and deflection limits, may have different criteria.

Further to providing a sufficient amount of housing to its population to eliminate the housing backlog, the government is also facing various other challenges with low-income housing. These include structural issues after delivery, the provision of well-located land for residential developments, and strained housing budget provisions (Statistics South Africa, 2012).

A few studies have been undertaken to try to determine remedies to these challenges. Theart (2014) looked at the need to understand the different housing systems, which include walling systems, building materials, and housing typologies. Regarding the last one, he indicates that the location of the housing will have an impact on the design of the building. In relation to building materials, and based on Ballerino (2002) findings, Theart (2014) indicates that the choice of alternative building materials could have an impact on the construction cost of the houses and lead to other advantages. He talks particularly of two types of materials used internationally – traditional and processed – and shares the benefits and weaknesses of each.

Regarding natural materials, he mentions for instance their renewability, energy efficiency and recyclability, but also indicates that their weaknesses include their reliance on availability, their water absorption, and their resistance to natural hazards. As to processed materials, some of their benefits are that they have distinct application abilities, improved properties, and higher productivity, although they can fail to meet the realities of local conditions and have high base cost for manufacturing and transportation.

The conventional construction method mainly considered in South Africa is the massive wall system. Other walling systems include the frame and the core wall systems, which are however rarely used for low-income housing. With the massive wall system, the walls are usually built with hollow or massive bricks made of a single material which are connected together with mortar (Ballerino, 2002).

2.2 Conventional Masonry Units (CMUs)

The primary conventional masonry units adopted in South Africa for low-income housing include concrete masonry units (CMUs) and fired clay bricks. A building constructed of fired clay bricks is shown in Figure 2.1. However, the use of these materials in such large quantities has certain disadvantages, including a negative environmental impact (Reddy and Jagadish, 2003).

Fired clay bricks are made of clay and top-soils, which are both non-renewable resources. The extensive production of such bricks results in excessive extraction of such resources and contributes

CHAPTER 2. LITERATURE REVIEW

to the challenge of maintaining biodiversity. Further, high temperatures are required to produce fired clay bricks, which results in the release of greenhouse gases and an increase in waste materials in the environment (Reddy and Jagadish, 2003).

Created with cement, ‘Maxi’ blocks and hollow concrete blocks are the main concrete masonry units used in South Africa (Laing, 2011). The main negative environmental impact of the use of such units is the release of carbon dioxide (CO₂) in the production of cement, roughly 60% of CO₂ emissions come from the limestone decomposition during the clinker forming process (WBCSD, 2009). Recent studies have indicated that cement production contributes 8% of global CO₂ emissions, making it one of the largest emitters of CO₂ (Benhelal *et al.*, 2013).



Figure 2.1: State-subsidised House Made of Fired Clay Bricks (The Clay Brick Association of SA, 2018)

2.3 Alternative Masonry Units (AMUs)

With the hope of reducing the environmental impact of masonry, various studies have been undertaken to identify alternative materials which can be used in the construction industry (Benhelal *et al.*, 2013). One such research effort is also underway at Stellenbosch University. Through the different studies done at this university, an effort has been made to identify AMUs that meet various criteria, including:

- Difference in material properties between AMUs and CMUs;
- Environmental benefit;
- Cost; and
- Availability of manufacturing equipment.

Fourie (2017) gives a description of a few AMUs being discussed in the literature and presents standardized tests he performed to investigate the mechanical properties of three different types of AMUs, namely Adobe, cement stabilized earth block (CSEB), and alkali-activated concrete block (AACB), which were selected together with the benchmark CMU to be investigated at Stellenbosch University. What follows is a brief description of each of the three AMUs.

CHAPTER 2. LITERATURE REVIEW

2.3.1 Adobe

Using earth as a building material has been shown to be advantageous because of its widespread and free availability, as well as its high quality and durability in both wet and dry climates (Norton, 1986). Unfortunately, as this material is mostly used by people who cannot always afford to meet building standards, it is associated with poverty, and hence not often thought of as a quality or durable material.

Building materials made with earth are known to have moderate strength in compression and little strength in tension or bending. The compressive strength, however, can be increased by compaction and stabilization with materials such as cement or lime (Norton, 1986).

de Almeida (2012) mentions some of the characteristics of earthen materials, which include – having low cost, being locally available, and having good thermal and acoustic properties. Adobe, also known as mud brick, is among the most common building blocks manufactured using earthen material used around the world. It is generally made by compacting a mixture of earth and water in a wooden mould, then demoulding it and leaving it to dry. The compressive strength of Adobe blocks can be increased by adding straw or other types of fibres to the mix.

An Adobe unit can easily be created by anyone as long as consideration is given to the type of soil being used - its composition, plasticity, and optimum water content. The composition of a soil is characterised by the amount of clay, sand, silt, and gravel content. The soil plasticity is particularly important when considering soil stabilization (de Almeida, 2012).

2.3.2 Compressed Stabilized Earth Block (CSEB)

With the introduction of manual or mechanical pressure on blocks during production, and the addition of stabilizers to the mix design, an alternative to the Adobe block was created, called the compressed stabilized earth block (CSEB) (Pacheco-Torgal and Jalali, 2011). In addition to the many advantages of Adobe blocks, Rigassi (1985) highlights a series of other benefits to the use of the CSEBs. Among these, he mentions that the use of pressure in the production of the blocks increases the consistency of the quality of the materials and augments the compressive strength and resistance to damage and erosion from water, that the dimensions of the blocks lend themselves to great flexibility of use, and that they can be produced locally, while still meeting building standards.

While the compression is the key operation in the production of CSEBs, the quality of the produced unit depends greatly on the type of soil and all of the preliminary operations, as well as on how the blocks are treated once they are removed from the press (Rigassi, 1985).

CSEB mix generally uses three forms of stabilization processes, which are mechanical stabilization, physical stabilization, and chemical stabilization, with the most common chemical additives used being cement and lime (Rigassi, 1985).

The process of CSEB production involves a selection and processing of the soil, compaction and curing of the block. The amount of clay in the soil, the stabilizer content and the final density of the block greatly influence the characteristics of the CSEBs (Pacheco-Torgal and Jalali, 2011).

CHAPTER 2. LITERATURE REVIEW

Similar to Adobe blocks, CSEB mix requires an optimum water content. The blocks are kept humid for seven days after their production to ensure a proper hydration of cement particles (Rigassi, 1985).

2.3.3 Alkali Activated Concrete Block (AACB)

In research carried out to find concrete that can be created without cement, alkali-activated concrete (AAC) has been showing the most promising results. The initial scope of the research that led to the discovery of this alternative masonry unit was for the improvement of fire-resistant materials. Later on, it was also found that this material had other benefits, such as high strength, good durability, and low energy costs (Pacheco-Torgal *et al.*, 2014).

Alkali-activated concrete binders have been used in the previous 40 years, particularly in China and the former Soviet Union. These binders are produced through the reaction of the combination between aluminosilicates and an alkaline activator, created either at high or ambient temperatures (Garcia-Lodeiro *et al.*, 2015).

Many studies on this building component have shown that it is an eco-friendly masonry unit and more sustainable than conventional masonry. However, manufacturing AACBs is often dangerous, as they use sodium hydroxide and sodium silicate as their alkaline solution (Davidovits, 2013). As indicated by Evonik Industries (2010), pure sodium hydroxide can lead to skin injury through any amount of contact with the human body. It is important, therefore, for this risk to be considered for the labour force.

2.4 Seismicity in South Africa

There are certain areas in South Africa that have been identified as being susceptible to earthquakes of low to moderate size. These earthquakes may occur naturally or be caused by mining activities (SANS 10160-4, 2011). In the following section, the causes of earthquakes, how they are measured, and the reason why they are a concern for engineers are discussed.

To understand how natural earthquakes occur, Tarbuck and Lutgens (2011) explain that the outer solid layer of the earth, called Lithosphere, is comprised of several plates that can move on the softer layer below it, called the Asthenosphere. The plates move along the fault lines, which are made of rocks. These movement take place over the years causing an accumulation of strain energy as the solid rocks resist deformations (Bhattacharya *et al.*, 2014). Once the rocks can no longer resist the movement and break apart, the strain energy is suddenly released causing the movement of the plates and the propagation of shock waves. This causes the movement of the ground known as an earthquake.

In the process of mining activity, on the other hand, the removal of large volumes of rock can cause extreme pressure on other surrounding rock, leading to tremors at the surface of the earth (Van Der Kolf, 2014). Regardless of the cause, the consequences of earthquakes can be devastating, resulting in human deaths and destruction of infrastructures.

CHAPTER 2. LITERATURE REVIEW

The severity of an earthquake can be indicated by its magnitude or its intensity. The magnitude quantifies the energy discharged during an earthquake, represented by the Richter scale. The intensity, measured using the Modified Mercalli Intensity (MMI) scale, indicates the effect of the earthquake on the location where it takes place based on observations of the behaviour, and the structural damaged caused. Earthquakes with a magnitude of 4.5 or less on the Richter scale are considered minor quakes. Those with an intensity above 5 can lead to structural damage. In certain parts of South Africa, natural earthquakes of magnitudes between 6 and 7 on the Richter scale have been recorded (Kijko *et al.*, 2002).

2.4.1 Design Considerations

Loss of human life resulting from earthquake activities is not directly caused by ground motions; casualties are due to collapsing structures. These observations have resulted in a significant amount of research being carried out to understand the behaviour of structures during earthquake activities, leading to the writing of new building codes and guidelines (Bhattacharya *et al.*, 2014).

The South African structural loading code, namely SANS 10160-1 (2011), consists of eight parts. SANS 10160-4 (2011) is the part that addresses “*seismic actions and general requirements for buildings*”. This code regulates the design of buildings by providing rules, limitations and strategies for the construction of adequate structures capable of avoiding catastrophic structural failures and loss of life. However, the function of a structure may not be maintained, nor significant damage prevented, even if the design of the building adheres to the code.

The code also maps out, as shown in Figure 2.2, the zones in the country prone to seismic activities, and for which structures are to be designed accordingly. Zone I represents areas of natural seismicity and Zone II, areas of natural and mining-induced seismicity. These zones indicate regions with a peak ground acceleration- a_g that has a 10% probability of being exceeded in a 50-year period. Measured at the surface of the earth during an earthquake event, the peak ground acceleration is often used for seismic design.

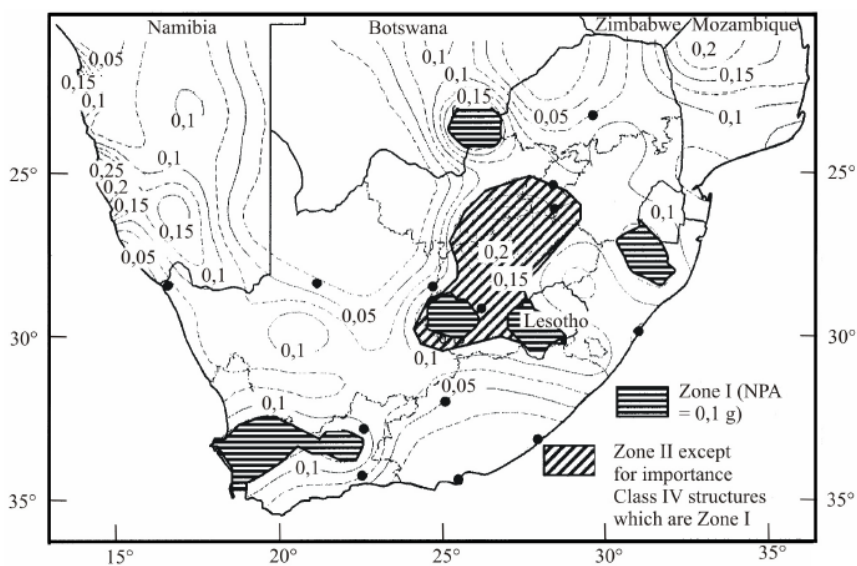


Figure 2.2: South African Seismic Hazard Zones (SANS 10160-4, 2011)

CHAPTER 2. LITERATURE REVIEW

SANS 10160-4 (2011) requires that a single-storey building be designed with plan layout which provides adequate lateral stability, i.e. a simple box plan. The area of openings in a given wall should not be greater than a third of the total wall area. Proper ties and anchorages need to be provided to ensure that loads are adequately transferred between horizontal and vertical structural elements.

An important step in the design process presented in the code is the investigation of the ground conditions on which a structure is to be erected. The ground is then categorized according to the four specific ground types identified in the code. This is done due to the fact that layers of different soil types have the capacity to amplify or damp seismic waves before they attain the surface of the earth (Tomažević, 1999).

Seismic action at a given point can be represented in different forms. These include ground acceleration, power spectrum, and response spectrum (Tomažević, 1999). In SANS 10160-4 (2011), the “*elastic response spectrum*” is used to represent the seismic action.

Due to the non-linear material stress strain characteristics of masonry structures, the behaviour of such structures during seismic actions can only be accurately predicted by performing direct non-linear dynamic analysis (Tomažević, 1999). However, design codes such as SANS 10160-4 (2011) provide simple linear elastic analysis methods in which the elastic response spectrum is reduced by a behaviour factor, q . This factor also considers the capacity to dissipate energy and the non-linear behaviour of structures (Tomažević, 1999).

In a simplified way, Tomažević (1999) explains the behaviour factor to be the ratio between the elastic seismic load H_e and the ultimate design load H_{du} ($q = H_e/H_{du}$). These two loads are obtained from a comparison between two envelope curves idealising the seismic response of a structure – a perfectly elastic envelope and a linear elastic perfectly plastic envelope, with similar initial stiffnesses, as shown in Figure 2.3. Due to some ductile behaviour observed in masonry structures, they can displace more than predicted if they behaved according to the idealized linear elastic envelope – displacement at the seismic load H_e . The ultimate design load H_{du} corresponds then to the load that will occur at maximum displacement.

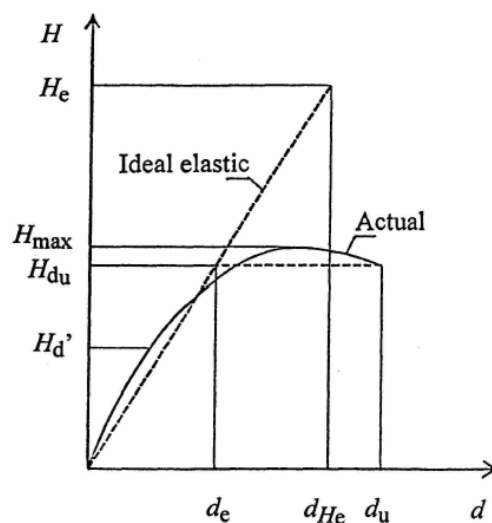


Figure 2.3: Diagram Defining the Behaviour Factor (q) (Tomažević, 1999)

CHAPTER 2. LITERATURE REVIEW

From experiments the values of the behaviour factor for unreinforced masonry (URM) have been proven to be $q = 1.5$ (Tomažević, 1999). This value is also proposed in SANS 10160-4 (2011). With a set of equations provided in the code, four different response spectra can be produced for the respective ground type. The response spectra are normalised in relation to the peak ground acceleration, a_g , to produce the normalized design response spectra $S_d(T)/a_g$. Figure 2.4 shows, for a behaviour factor $q = 1.0$ and 5% damping, the normalised design response spectra as presented in SANS 10160-4 (2011) for the four ground types,.

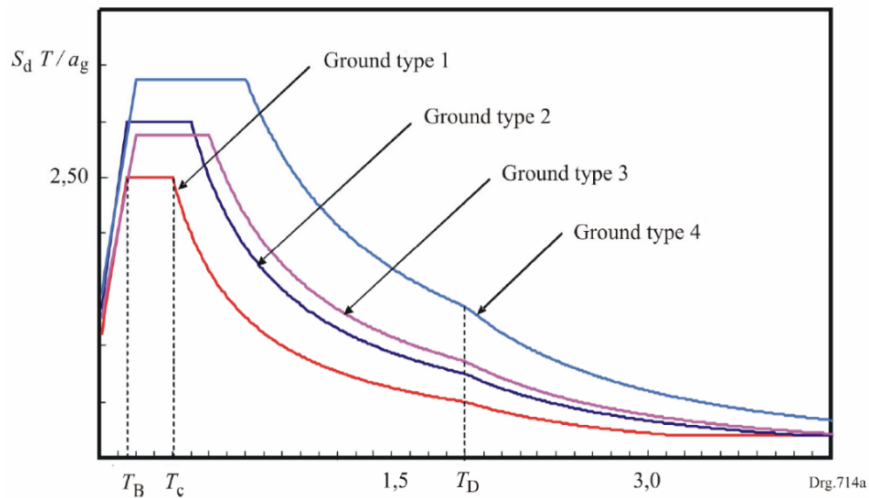


Figure 2.4: Normalized Design Response Spectra - $S_d(T)/a_g$ (SANS 10160-4, 2011)

The design base shear is determined on the basis of the normalized design response spectra corresponding to the fundamental period of vibration (T) of the structure in the direction being analysed, and the nominal vertical load applied on the structure. The principles for the distribution of the design base shear along the height of a structure are provided in the code. These should be considered and used to design for internal forces acting on individual structural elements.

Together with the recommendations provided in SANS 10160-4 (2011), the designer should also consider the recommendations and requirements provided in SANS 10164-1 (1989) when designing structural URM elements. The design of URM structural elements according to SANS 10160-4 (2011) as well as SANS 10164-1 (1989) are not discussed in detail here as this is beyond the scope of the current section.

2.4.2 Displacement Based Design

Design codes such as SANS 10160-4 (2011) provide seismic design guidelines that use a force-based (FB) approach, which express seismic loads as forces and use linear elastic analysis methods together with the behaviour factor q (Petry, 2015). A FB approach does not fully represent the non-linear characteristic of structures such as masonry and it is considered to be conservative (Petry, 2015).

The development of the displacement-based (DB) approach has been undertaken as an alternative to the FB approach. A number of researchers have proposed various DB design methods which

considers the non-linear behaviour of structures and which have been shown to be suited to the assessment of existing masonry structures (Petry, 2015). Although proper design guidelines have not been fully applied yet, seismic designs based on DB design approach have resulted in more reliable and cost effective designs (Salmanpour, 2017).

2.5 Seismic Performance of Single-storey URM Buildings

Historically, masonry buildings have performed poorly during seismic activities. Structural damage and collapse during earthquakes have been observed for a significant number of masonry buildings. This is a major reason why these buildings are considered inadequate for earthquake prone regions (Tomažević, 1999).

Observations on single-storey masonry buildings indicate two types of structural behaviour of the walls, depending on the direction of the seismic motion. Out-of-plane bending deformation occurs to walls perpendicular to the seismic motion, while walls parallel to the motion are subjected to in-plane bending and shear causing horizontal and diagonal cracks in the wall (Tomažević, 1999).

The three main types of masonry structures include reinforced, confined, and URM structures. Of these, the URM is the type of structure considered in this study. Some of its advantages are that it is low in cost, it has adequate thermal insulation, and, due to its satisfactory compression capacity, it can be used to carry vertical loads (Tomažević, 1999). However, URM is structurally a non-ductile material and can only withstand small lateral loads and displacements, while earthquakes induce large lateral loads and displacements (Tomažević, 1999).

Although URM buildings are low in cost and can be constructed easily, they are susceptible to damage from earthquake activities. These buildings can generally be divided in three categories: Adobe, brick and stone masonry (Bhattacharya *et al.*, 2014).

Due to the advantages of Adobe structures, as outlined in Section 2.3.1 of the current chapter, they have been popular around the world over the years. A typical single-storey Adobe house is constructed using sun-dried blocks joined with mud mortar and built on foundations made of medium to large-grade rocks. Depending on the region, the roof would consist of timber joists or bamboo, covered by either clay tiles, corrugated metal sheets, or thatch (Bhattacharya *et al.*, 2014).

Brick masonry houses are also widely constructed around the world. They are made of fired brick units bonded together with mortar. Adhesion between mortar and bricks significantly influences the ability of the wall to resist the shear stresses induced during an earthquake. The strengths of both mortar and the brick are largely influenced by the quality and quantity of their constituent materials (Bhattacharya *et al.*, 2014).

Stone masonry buildings include rural houses – which are mainly small single-storey dwellings containing small openings for doors and windows that are built as separate buildings for a single family – and urban housing – which are homes built in urban communities with buildings sharing common walls. These types of masonry buildings are found in North Africa, the Mediterranean Europe, the Middle East, and other parts of Asia (Bhattacharya *et al.*, 2014).

CHAPTER 2. LITERATURE REVIEW

[Bhattacharya et al. \(2014\)](#) reported that these types of URM buildings have demonstrated similar failure mechanisms from earthquake activities. The common type of failure in the three URM building categories involves junction failure with out-of-plane collapse of walls.

Catastrophic failures occur in Adobe structures due to their low ductility, which makes them very brittle structures. As shown in Figure 2.5, their failure mechanisms include the separation of walls at corners (i) or roofing (iii), diagonal (ii) and vertical (iv) cracking in the wall, and out-of-plane failure (v).

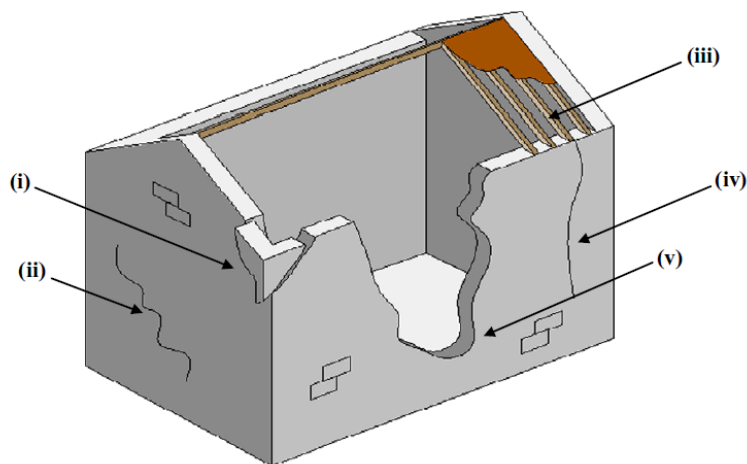


Figure 2.5: Failure Mechanisms of a Typical Adobe Structure ([Bhattacharya et al., 2014](#))

The failure mechanisms observed in brick masonry structures include shear cracks in walls and junction failure of the corner resulting in out-of-plane collapse, which in turn leads to the disintegration of floors and roofing and, ultimately, the collapse of the whole building. Figure 2.6 shows various cracks in a brick masonry building after an earthquake event.



Figure 2.6: Cracks in an Unreinforced Brick Masonry Building([Bhattacharya et al., 2014](#))

Common failures observed in stone masonry buildings include out-of-plane overturning of long-span walls, in-plane shear cracks, junction failure which leads to out-of-plane collapse and de-lamination, and which occurs when two external walls disintegrate due to lateral motion if they are not sufficiently attached together ([Bhattacharya et al., 2014](#)).

2.6 Experimental Studies on URM In-plane Shear Behaviour

2.6.1 Introduction

Studies on the seismic behaviour of URM walls include experimental tests, conducted in laboratories, which aim at simulating the observed failure mechanism of masonry walls after earthquakes. This is usually done by subjecting masonry walls of similar geometry and restraint as in a structural building system to the same load conditions as they are subjected to in a building during an earthquake. The shear behaviour of URM is then determined by conducting different tests such as diagonal compression tests and simple monotonic or cyclic tests. Studies have shown that these tests provide similar values of tensile strength (Tomažević, 2000).

The seismic resistance capacity of masonry structures is influenced by various factors including strength and stiffness degradation, energy absorption capacity, and ductility. However, most of these factors can only be determined by conducting cyclic loading tests similar to what the masonry structure would be subjected to during a seismic event. To this end, different research laboratories have developed various testing devices which apply lateral and vertical loading patterns in various ways (Tomažević, 2000).

In the laboratory, however, it is difficult to represent the conditions of a masonry wall as they would be in a real building. In order to minimize uncertainties and to ensure that the measured parameters recorded in the laboratory can be accurately evaluated, testing set-ups that provide simplified and controlled boundary conditions are designed with various mechanical systems. The applied vertical load is usually kept constant throughout the test. The displacement and rotation of the wall, as well as the supporting system, are measured throughout the test (Tomažević, 2000).

During tests conducted in the laboratory to simulate seismic actions on masonry structures where local failure modes, such as out-of-plane failure, are prevented, it has been observed that the global behaviour of these structures is particularly governed by the in-plane response of shear-dominated failure mechanisms as these indicate a lower displacement capacity compared to other failure modes (Salmanpour *et al.*, 2012).

When trying to understand the seismic response of a structure, attention is given to understanding and determining its deformation capacity. For URM, the deformation capacity is expressed in terms of drift capacity, δ , which represent the ratio of the horizontal displacement at the top of the wall (u_{hor}) and the wall height (h) as denoted in Equation (2.1). Furthermore, the ultimate drift capacity is the point at which the lateral strength drops by 20% of the maximum strength (Beyer and Petry, 2015).

$$\delta = \frac{u_{hor}}{h} \quad (2.1)$$

Many experimental tests are carried out on wall specimens having a height smaller than the wall height in an actual building. A few reasons for testing smaller walls include the size of the test stand, which might not be able to accommodate full-scale specimens; decreasing the complexity of the test setup; and the specimen representing only a small section of the wall, such as spandrels (Beyer and Petry, 2015).

CHAPTER 2. LITERATURE REVIEW

Furthermore, investigations into the deformation capacity of URM have considered walls in multi-storey buildings where these walls are connected by vertical and horizontal structural elements such as columns and slabs. These elements determine the wall's boundary conditions and act as coupling elements between walls when in-plane loading is applied to the wall. Three coupling levels are distinguished based on the stiffness and strength of the coupling elements: (i) weak coupling is considered when the horizontal elements of each storey only induce equal displacement on the walls with negligible transfer of shear forces or bending moments, (ii) intermediate coupling implies that there is a limited transfer of bending moment that is not negligible, (iii) strong coupling refers to the development of a framing action by the vertical and horizontal structural elements which remains elastic when horizontal loading is applied (Petry and Beyer, 2014).

A typical URM wall can be represented by a deformed shape with moment profile as illustrated in Figure 2.7, where h is the wall height, h_0 is the shear span, M_{top} and M_{bot} are moments at the top and bottom of the wall, V and H are the vertical and horizontal forces, u_{hor} is horizontal displacement at the wall top, and δ is drift capacity. Note that some of the symbols in Figure 2.7 have been changed to harmonize with the ones used in this study.

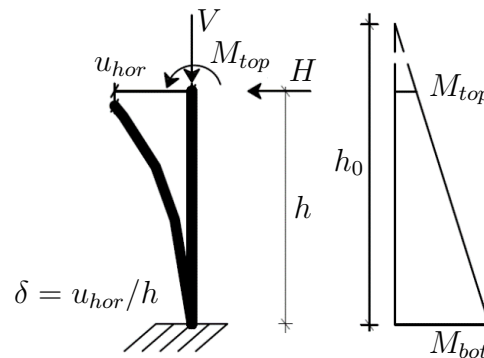


Figure 2.7: Deformed Shape and Moment Profile of URM Wall (Beyer and Petry, 2015)

Laboratory experimental setups aim at replicating the boundary conditions of a wall when lateral in-plane loading are applied. Petry and Beyer (2014) conducted quasi-static cyclic tests on six identical URM walls. The aim of the tests was to investigate the effects of different boundary conditions in relation to the shear span, the applied ratio and the restraint of the moment at the top of the wall. Their findings, which were based on their own experimental studies as well as a review of previous experimental data, indicate the following;

- Increasing the applied axial load ratios results in a decrease of the drift capacity of the wall. Strength degradation is achieved faster because the shear cracks tend to pass through the bricks and not through the joints. The axial load ratio is defined as the ratio of the applied stress on the wall and the compressive strength of masonry wallets.
- Increasing the shear span results in an increase of the deformation capacity.
- The dataset indicated that an increase in the test unit size resulted in a decrease of the deformation (drift) capacity of the wall.

CHAPTER 2. LITERATURE REVIEW

The fixed-end boundary condition is usually simulated by either the static approach, where the shear span, h_0 , is kept at $0.5h$, or the kinematic approach, where only translation movements with no rotations are allowed on the loading beam (Salmanpour and Mojsilović, 2015). These two approaches have been implemented in various experimental set-ups by using either mechanical devices or two vertical actuators, which can either be force controlled independently (static approach) or couple mixed force-displacement controlled (kinematic approach). Experimental observations have proven that due to the non-linear behaviour of masonry and their heterogeneity, the static approach, although easier to implement than the kinematic approach, can result in unrealistic boundary conditions (Salmanpour and Mojsilović, 2015).

BS EN 1998-3 (2005) provides values for the drift capacity of URM walls built with conventional masonry units for flexural and shear failure modes. The values, summarized in Table 2.1, correspond to the drift capacity at the Limit State of Significant Damage (LSSD) as well as the ultimate drift capacity at the Limit State of Near Collapse (LSNC). In the LSSD, although the URM wall is damaged, it still has some residual lateral capacity (strength and stiffness) and is able to sustain vertical loads. In the LSNC, however, the wall is severely damaged with little lateral capacity and it has exploited its full displacement capacity. For the flexural failure mode, BS EN 1998-3 (2005) takes into account the boundary conditions in terms of the shear span h_0 . In Table 2.1, l_w represents the length of the wall.

Table 2.1: Drift Capacity of URM Walls (BS EN 1998-3, 2005)

Failure Mode	Drift Capacity [%]	
	LSSD	LSNC
Flexural	$0.8 \cdot (h_0/l_w)$	$(4/3) \cdot 0.8 \cdot (h_0/l_w)$
Shear	0.4	$(4/3) \cdot 0.4$

2.6.2 Failure Modes

Various characteristics – such as the geometry, the quality of materials, the load application and boundary conditions – influence the type of failure mode of masonry walls under in-plane seismic loads. From analysis of earthquake damages as well as experimental results, three types of failure modes have been identified, namely sliding shear, diagonal shear, and flexural failure (Tomažević, 1999). These failure modes are illustrated in Figure 2.8.

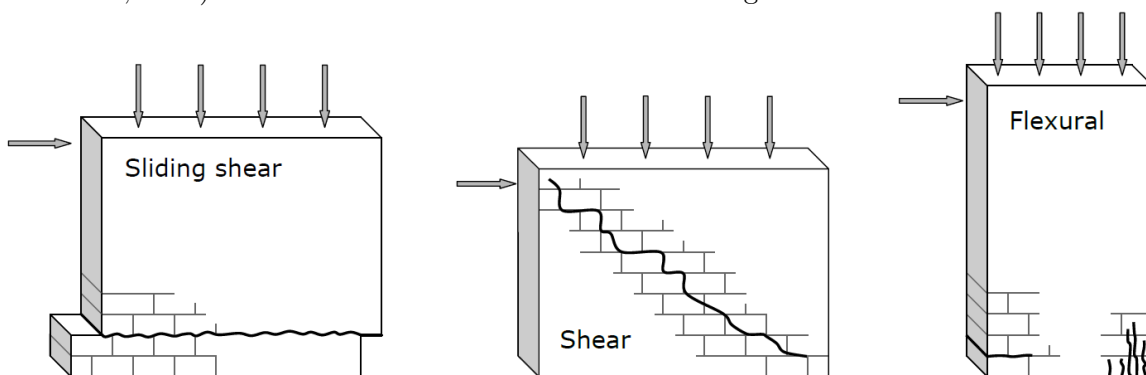


Figure 2.8: Failure Modes of Masonry Walls (Tomažević, 1999)

CHAPTER 2. LITERATURE REVIEW

Sliding shear failure occurs mainly due to use of poor-quality mortar and low vertical load acting on the wall. Loads induced by seismic actions shear the wall in two parts along one of the horizontal mortar joints. The upper part normally slides in relation to the bottom part through the horizontal joint (Tomažević, 1999). From experiments, the response of the wall with this type of failure mode is very stable and is characterised by a high energy dissipation, an elastic perfectly plastic behaviour with large displacement capacity ((Salmanpour *et al.*, 2013).

Diagonal shear failure, often referred to as shear failure and considered as the typical failure mode for masonry walls subjected to in-plane seismic actions, occurs due to an increase of the principal tensile stresses within the wall that supersede the in-plane tensile capacity of masonry materials. The principal tensile stresses are developed by simultaneous application of vertical and horizontal loads which cause diagonal cracks within the wall. The cracks will follow the mortar joints in a stair-case shape, or go through the masonry units (Tomažević, 1999). Masonry walls resulting in this type of failure mechanism have shown moderate energy dissipation, a rapid decrease in strength and stiffness, and low displacement capacity (Salmanpour *et al.*, 2013). In the case of squat walls built with poor-quality mortar, diagonal cracks may form along the mortar joints causing a sliding movement of one part of the wall in relation to the other. This type of failure is described by Salmanpour (2017) as sliding shear failure with similar wall response as previously mentioned.

Flexural failure occurs due to an increase in shear capacity and a high moment/shear ratio in the wall. An increase in the horizontal load induces tension cracks in the bed joints resulting in crushing of masonry units in the compressed zones (Tomažević, 1999). Walls with flexural failure have a nonlinear elastic response characterised by moderate energy dissipation and low strength degradation. Further, when the applied vertical load is lower than the compressive strength of masonry, substantial displacement may occur (Salmanpour *et al.*, 2013).

The mortar joints have a major influence on the masonry response when loaded in different conditions. Depending on the quality of mortar, shear failure can occur along the mortar joint as previously mentioned. Another failure can occur on the unit-mortar interface due to an increase in the tensile stresses acting normal to the joints, this may ultimately lead to the separation of the interface (Parisi and Augenti, 2012).

With regards to shear tests, another characteristic of the masonry joints, which has been demonstrated to significantly contribute to the shear resistance of masonry (van Zijl, 2004), is the dilatant behaviour. Dilatancy in masonry is characterised by a volume increase of the mortar joint due to shearing deformation (van Zijl, 2004). If confining boundary conditions resist this volume increase, a pressure build-up will occur, resulting in a shear strength increase of the unit-mortar interface with the normal compressive force applied (Parisi and Augenti, 2012).

2.6.3 Representation of Experimental Results

Experimental tests on masonry walls and buildings are necessary to simulate and understand the effects of seismic actions. The results of such tests are used to further develop computational models to predict the behaviour of structural masonry under seismic loads (Tomažević, 1999).

CHAPTER 2. LITERATURE REVIEW

Once obtained, the experimental results are represented by a hysteresis envelope, which is then simplified and idealised with a bi- or trilinear envelope as suggested by Tomažević (1999). In the case of an idealised bilinear envelope, as shown in Figure 2.9, three limit states are considered:

- **Crack limit:** Corresponding to the displacement d_{cr} and resistance of the wall H_{cr} . This limit state is characterised by the development of the first significant cracks and the change in the slope of the hysteresis envelope.
- **Maximum resistance:** Corresponding to the displacement $d_{H_{max}}$, attained at the maximum resistance H_{max} of the wall.
- **Ultimate resistance:** Corresponding to the maximum displacement d_{max} , attained during the test with a resistance $H_{d_{max}}$.

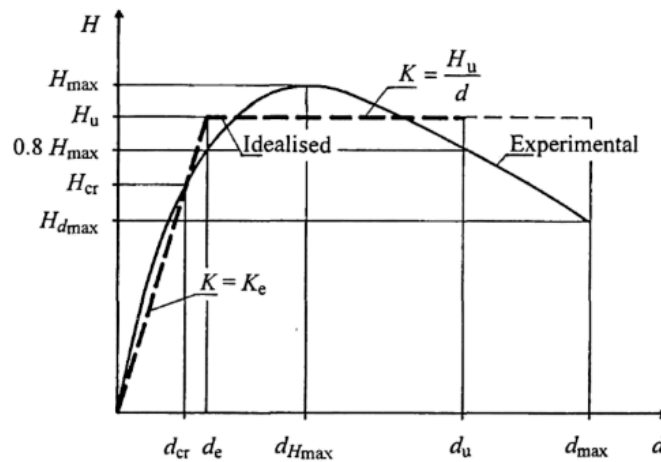


Figure 2.9: Bilinear Envelope Idealisation of Experimental Results (Tomažević, 1999)

From the idealised envelope thus represented, a few parameters can be determined based on practical equations which have been developed from a series of experimental tests on masonry walls subjected to seismic loads. These experiments were conducted by Tomažević (1999) and the equations presented by this author have also been used by other researchers.

The effective stiffness K_e corresponds to the first slope of the idealised envelope and represents the secant stiffness of the experimental envelope at the crack limit. It is represented in Equation (2.2).

$$K_e = \frac{H_{cr}}{d_{cr}} \quad (2.2)$$

Where:

K_e	Effective stiffness
H_{cr}	Resistance at crack limit
d_{cr}	Displacement at crack limit

As suggested by Tomažević (1999), the resistance at crack limit is calculated by multiplying the maximum attained resistance of the wall H_{max} by a reduction factor C_{cr} obtained from experimental data. The value of the reduction factor has been determined to be $C_{cr} = 0.7$.

CHAPTER 2. LITERATURE REVIEW

Equation (2.3) is then used to calculate H_{cr} .

$$H_{cr} = 0.7 \times H_{max} \quad (2.3)$$

When idealising experimental results, the energy dissipation capacity of the wall is considered by ensuring that both areas under the idealised and experimental curves are equal. This allows for the evaluation of the ultimate resistance H_u of the idealised envelope. Once the effective stiffness K_e has been calculated for Equation (2.2), Equation (2.4) can be used to calculate the ultimate resistance H_u , in which A_{env} represents the area below the experimental envelope.

$$H_u = K_e \left(d_{max} - \sqrt{d_{max}^2 - \frac{2 \times A_{env}}{K_e}} \right) \quad (2.4)$$

The ultimate resistance H_u is primarily a characteristic of the idealised envelope. In the case of the idealised bilinear envelope shown in Figure 2.9, H_u represents the maximum idealised capacity of a wall (Tomažević, 1999). From an evaluation of test results from more than 60 walls, Tomažević (1999) has suggested an expression (Equation (2.5)) of the ultimate resistance H_u in terms of the maximum experimental resistance of a wall H_{max} .

$$H_u = 0.9 \times H_{max} \quad (2.5)$$

The idealised elastic limit can be represented as the limit at which the ultimate resistance, H_u , is reached, which occurs at displacement d_e . The displacement, d_e , can be calculated using Equation (2.6).

$$d_e = \frac{H_u}{K_e} \quad (2.6)$$

Another property of masonry that can be calculated from the idealised envelop is the ultimate ductility factor μ_u . The expression shown in Equation (2.7) defines the ultimate ductility factor as a ratio between the ultimate idealised displacement d_u and the idealised elastic limit d_e . The ultimate idealised displacement, also known as the ultimate displacement capacity, is commonly defined, and accepted by many researchers, to be the displacement corresponding to 20% strength degradation (Salmanpour *et al.*, 2012). However, Tomažević (1999) pointed out that this value is arbitrarily taken as such.

$$\mu_u = \frac{d_u}{d_e} \quad (2.7)$$

The value of the ultimate ductility factor μ_u for URM, has been limited to values between 2.0 - 3.0. Used for the seismic resistance verification, these limits account for excessive damage of the structural URM wall (Tomažević, 1999).

2.7 Various Experimental Test Set-ups

2.7.1 Introduction

The shear force and displacement (drift) capacities of an URM wall are typically determined by conducting shear-compression tests. Characterized by two forces being applied vertically as well as horizontally in the plane of the wall, two major decisions need to be taken with regard to the three in-plane degrees of freedom (dofs) at the top of the wall. The first is in relation to the way the horizontal force or displacement needs to be applied, which can either be increased monotonically or be through cyclic displacements; the latter being a common method presented in various literature. The second and third dofs are in relation to how the axial force or displacement as well as the in-plane moment or rotation are controlled (Wilding *et al.*, 2018).

In a typical shear-compression test set-up of URM walls, the base of the specimen is always founded on a stiff foundation, inducing a fixed boundary condition. A stiff loading beam is often attached to the top of the specimen, which reduces to three the in-plane dofs (Wilding *et al.*, 2018).

The control of the top dof determines the boundary conditions for the test set-up. Either fixed-fixed or cantilever boundary conditions have been used for different tests with the fixed-fixed boundary condition being the most common, and which is achieved with various configurations implemented at the top of the wall (Wilding *et al.*, 2018).

While performing a cyclic test, the top horizontal displacement is controlled by a predetermined cyclic loading protocol. The control of the vertical movement can either be achieved through a static, controlled axial force and top moment, or through a kinematic, controlled axial displacement and top rotation (Wilding *et al.*, 2018). As shown in Figure 2.10, Wilding *et al.* (2018) distinguish four different ways in which doubly-fixed boundary conditions can be implemented in the in-plane shear-compression tests of URM. These include force, mixed and displacement control of vertical actuators, as well as a cantilever of half the wall height.

In Figure 2.10, the control of the vertical movement is represented by the symbol N which can either be in terms of the vertical force V , or vertical displacement w . The top rotation of the loading beam is represented by θ_{Top} . The subscripts 1 and 2 are used to differentiate between the two apparatus controlling the vertical movement of the loading beam.

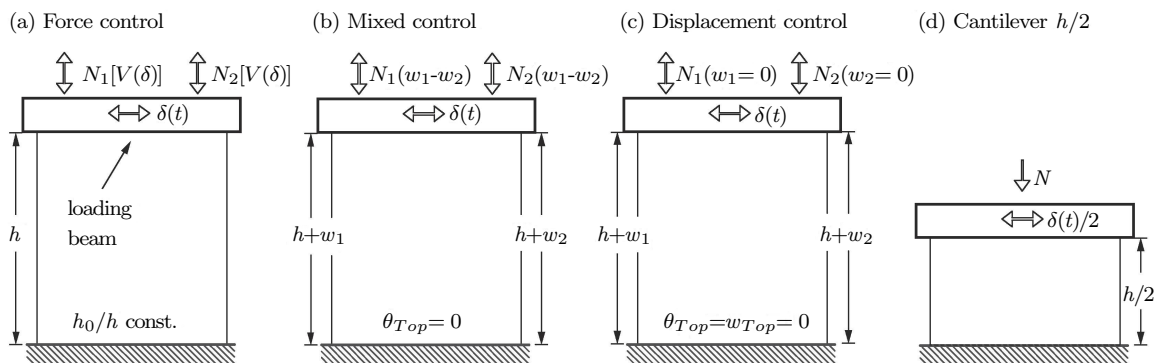


Figure 2.10: Different Configurations for Fixed-fixed Boundary Conditions (Wilding *et al.*, 2018)

CHAPTER 2. LITERATURE REVIEW

With the force control approach, the horizontality of the loading beam is achieved by altering the moment at the top of the wall in such a way that the top and bottom moments are equal, and the total normal force induced by the two actuators is kept constant. This approach is frequently used to maintain the shear span (h_0) at half the wall height, but it can also be used to simulate any other shear span (Wilding *et al.*, 2018).

The main characteristic of the mixed control approach is that an equal vertical displacement at the two wall ends can be achieved while maintaining a constant normal force. This configuration result in zero rotation induced at the top of the wall. The mixed control approach is suggested to provide more realistic boundary conditions and can be implemented by using either two servo-hydraulic actuators or one hydraulic actuator with other devices to maintain the zero rotation (Wilding *et al.*, 2018).

The displacement control is achieved by restraining the change in the height of the wall as well as the top rotation. This is done by using two servo-hydraulic actuators or by means of rollers placed between the loading beam and the upper support. However, with this configuration, as soon as the wall cracks, the normal force applied to the top of the wall changes (Wilding *et al.*, 2018).

Another way of simulating fixed-fixed boundary conditions on a wall specimen is by testing half of the wall as a cantilever. The test of the half-wall is conducted by following the other test control modes and applying a constant axial load. Using this approach, the half-wall is confined resulting in a suppression of diagonal crossing shear cracks that would normally result in a failure mode from a cyclic test with fixed-fixed boundary conditions (Wilding *et al.*, 2018).

The choice between the different test configurations mainly depends on the test set-up. Depending on the capacity of a laboratory and the testing equipment available, simple or sophisticated testing procedures can be performed to simulate seismic loads. For most simple tests, monotonic lateral displacements are statically applied, whereas with a sophisticated set-up, real seismic actions can be simulated with displacements applied dynamically (Tomažević, 1999).

The sections that follow present a few examples of experimental test setups which have been built and used in various laboratory to perform in-plane shear-compression tests on masonry walls.

2.7.2 ETH Zurich Test Set-up

The test set-up shown in Figure 2.11, presented by Salmanpour (2017), was used to perform in-plane shear tests on URM walls at the structural engineering laboratory of ETH Zurich. In this set-up three servo-hydraulic actuators, one horizontal and two vertical, were used to apply the horizontal and vertical forces. The two vertical actuators were connected to a steel reaction frame, whereas the horizontal actuator was attached to a reaction wall.

Constructed on a 350mm thick reinforced concrete foundation, the wall specimen was first constructed in the laboratory open area before being carefully moved and placed in the test set-up. Using post-tensioned steel bars, the concrete foundation was tensioned to the strong floor. Connected to the top of the wall, a steel loading beam with a depth of 450mm was used to

CHAPTER 2. LITERATURE REVIEW

apply the vertical loads from the three servo-hydraulic actuators. A sliding system prevented any out-of-plane movement of the loading beam.

With this set-up, two different boundary conditions, i.e. cantilever and fixed-end, could be simulated. The full pre-compression force was applied by the two vertical actuators before applying the horizontal static-cyclic load in a displacement-controlled manner.

The results of the tests performed suggest that changing the boundary conditions from fixed-ends to cantilever, on two identical wall specimens, will result in the failure modes changing from shear to flexural failure. Similarly, increasing the pre-compression level resulted in a change from flexural and sliding failure modes to shear failure mode, and contributed to an increase of the compressive and shear stiffness of the masonry specimen.

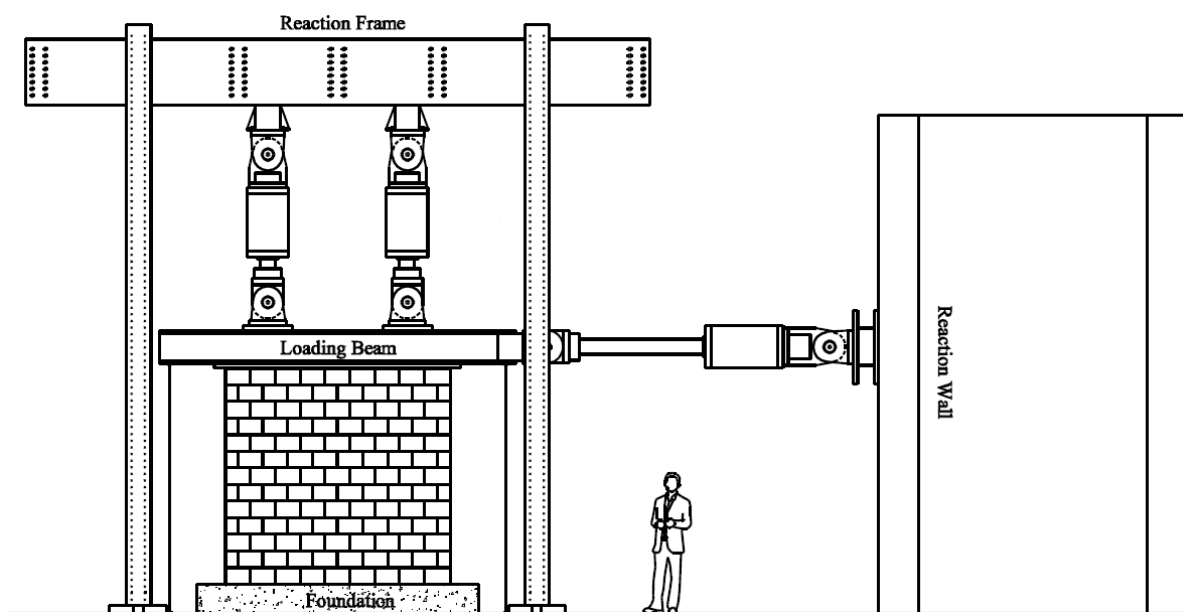


Figure 2.11: ETH Zurich Test Set-up (Salmanpour, 2017)

2.7.3 EPFL Test Set-ups

The test set-ups shown in Figure 2.12 were used in the structural laboratory of École Polytechnique Fédérale de Lausanne (EPFL) (Petry, 2015) to test wall specimens representing the first-floor wall of a four-story building. The wall specimens used in both test set-ups were built on steel plates that had a layer of quartz sand glued onto them. After each wall was built, and before the beginning of the test, another steel plate, with a similar layer of quartz sand, was mortared at the wall top after which the loading beam was placed on the specimen.

Using a crane, the wall specimen was then transported to the test set-up where the bottom steel plate was bolted to the concrete foundation, which was attached to the strong floor of the laboratory.

In Figure 2.12, the set-up on the left was used to perform full-scale masonry wall tests. Three actuators with similar force and displacement capacities were used to apply the moment as well

CHAPTER 2. LITERATURE REVIEW

as the axial and shear forces on the wall. With this configuration, different boundary conditions were applied on the wall. The two vertical actuators were coupled with the horizontal actuator allowing for a control of the shear span. The set-up on the right of Figure 2.12 was used to test half-scale masonry walls. Three actuators (two vertical and one horizontal) were used and controlled in a similar manner as those used for full-scale tests. In this configuration two beams bolted together were used as one deep loading beam.

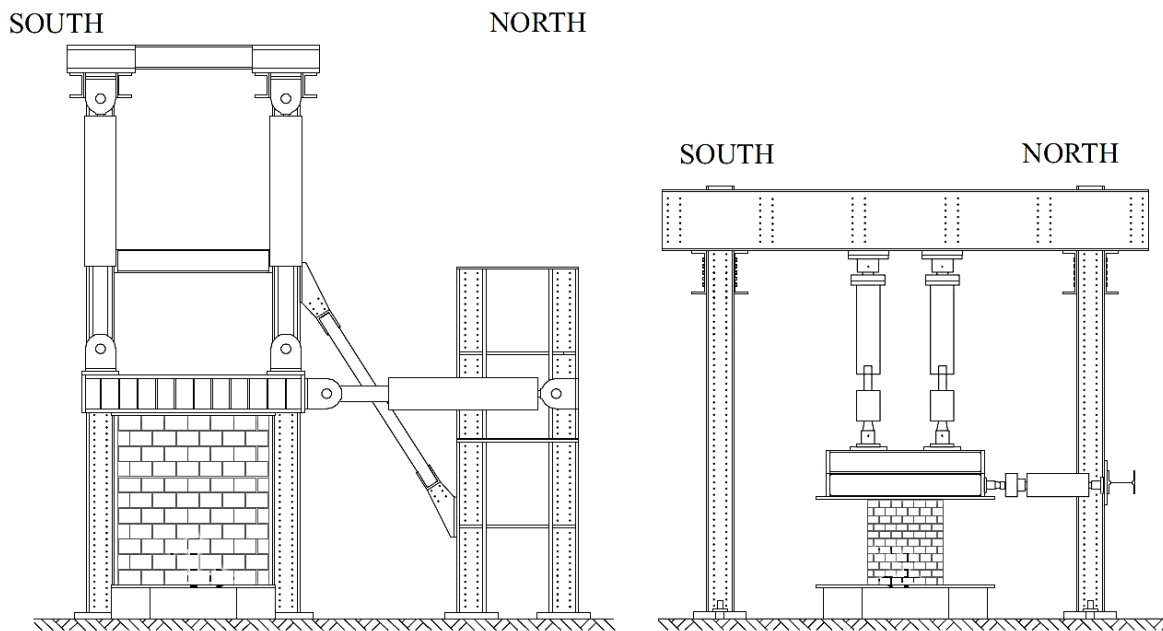


Figure 2.12: EPFL Test Set-ups for Full-scale and Half-scale Walls (Petry, 2015)

2.7.4 Stellenbosch University Test Set-up

De Beer (2016) designed and built the test set-up shown in Figure 2.13 to test unreinforced masonry shear wall specimens in the structural laboratory at Stellenbosch University. The specimens were small walls with dimensions 1150 x 935 mm and were built between two reinforced concrete beams. Each specimen was then placed in the testing set-up by means of an overhead crane and both concrete beams were attached at the bottom to a steel beam, which was connected to the strong floor of the laboratory and, at the top, to a steel load spreader beam (De Beer, 2016).

A 500 kN Instron testing machine was utilized for the application of the horizontal force on the spreader beam in a pulling action. Gravity load applied on the specimen was achieved by means of post-tensioning rods together with coil springs to reduce an increase in the forces generated in the rods due to opening cracks and the dilatancy behaviour of masonry. Two additional sets of vertical rods were used at one end of the beam, reducing the uplift of the wall specimen and the rotation of the loading beam due to the applied shear force, and ensuring that the specimen failed with a diagonal shear crack (De Beer, 2016).

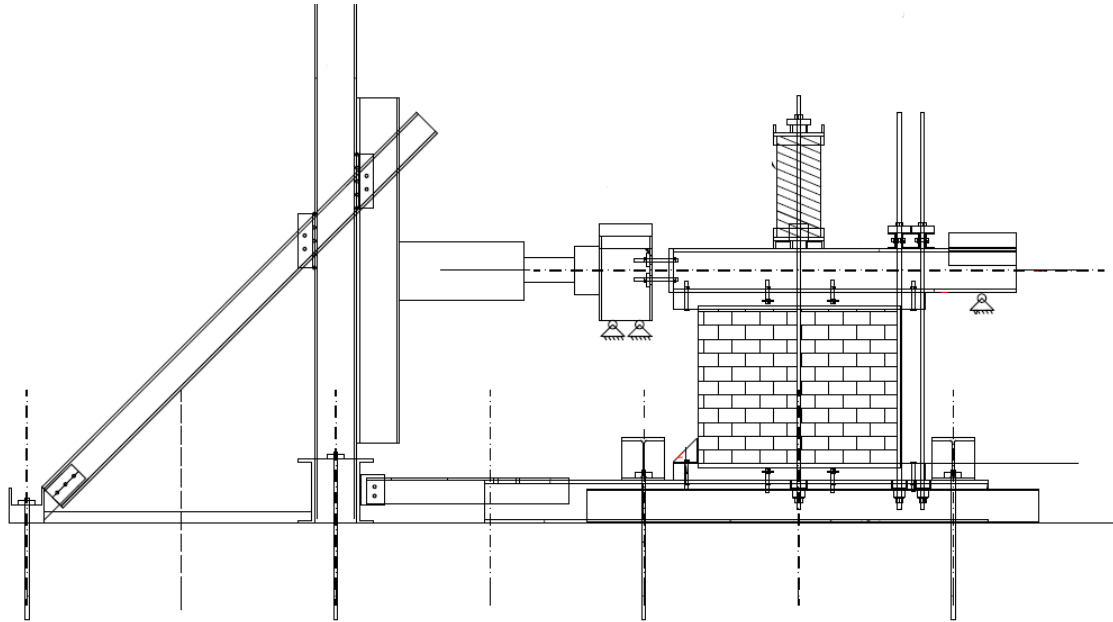


Figure 2.13: Stellenbosch University Test Set-up for Small Walls (De Beer, 2016)

2.7.5 Other Test Set-ups

In the laboratory of Semnan University, Iran, the test set-up shown in Figure 2.14 was used to determine the effect of openings in masonry walls when subjected to in-plane shear loads. Built in a rigid steel frame, the wall specimen was subjected to lateral cyclic loading which was applied by means of two hydraulic jacks located on top and on the two sides of the specimen in a displacement controlled manner. A third hydraulic jack, positioned at the top of the specimen, applied a static axial load. All the loads were applied through a rigid steel beam placed on top of the wall (Karimi *et al.*, 2016).

The displacements induced by the two horizontal hydraulic jacks were monitored through two linear variable displacement transducers (LVDTs), one placed by each horizontal hydraulic jack. The loads were measured by means of load cells which were placed between the specimen and the loading frame. The frame was securely attached to the laboratory floor and lateral bracings were utilized to prevent any out-of-plane movements of the specimens (Karimi *et al.*, 2016).

To assess the behaviour and the shear strength of ancient Italian brick masonry, the set-up shown in Figure 2.15 was used to perform experimental tests on wall specimens made with the above-mentioned brick masonry. The walls were constructed and tested in a special loading frame fitted with three independent hydraulic jacks, two of which were used to apply the vertical loads, and the third, the monotonic horizontal load. Three load-cells were used to monitor the loads applied by the three jacks (Capozucca and Sinha, 2004).

Each wall specimen was built with a flange on one side of the wall (T-shaped wall) and a steel plate glued with epoxy resin which was used as a slab at the top of the wall. The flange was made with mortar due to the scarcity of ancient bricks. Once the full pre-compression load was applied to the flange and the top of the wall, the shear force was then applied in stages until failure of the specimen (Capozucca and Sinha, 2004).

CHAPTER 2. LITERATURE REVIEW



Figure 2.14: Semnan University Test Set-up (Karimi *et al.*, 2016)

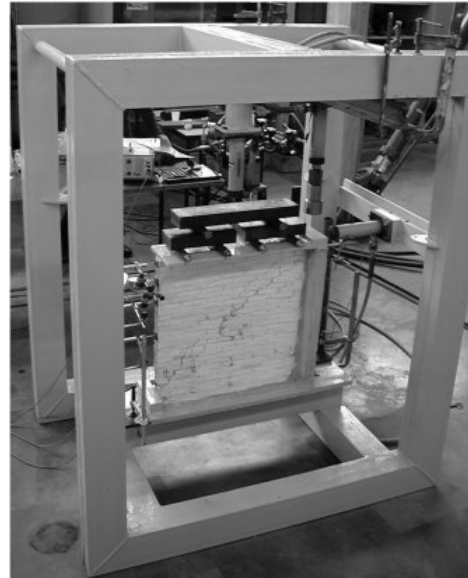


Figure 2.15: Test Set-up with Loading Frame (Capozucca and Sinha, 2004)

The test set-up from Key Laboratory of RC&PC Structures of the Ministry of Education – Southeast University – China, shown in Figure 2.16, was used to test self-insulating concrete masonry shear walls under in-plane cyclic loading. Each wall specimen was reinforced with steel bars and built on a foundation beam anchored to the laboratory floor. The axial load was applied by the vertical jack, connected to the crossbeam of a steel frame, and kept constant throughout the test. The horizontal cyclic loads were applied by the horizontal hydraulic actuator which was mounted to a reaction wall (Mohamad and Chen, 2017).

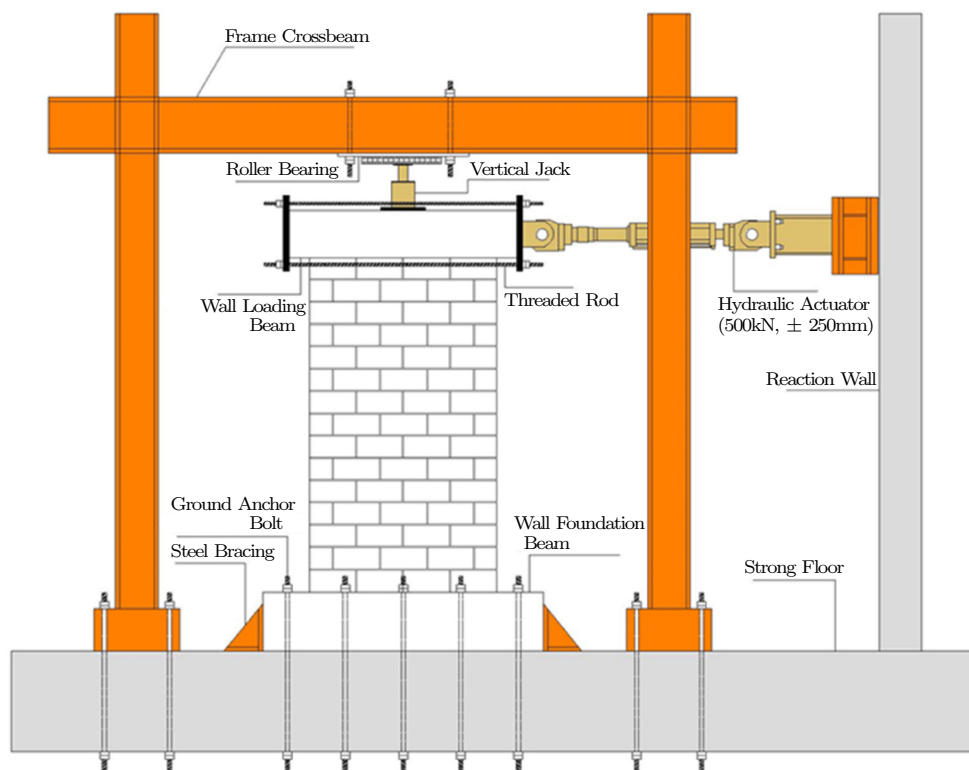


Figure 2.16: Southeast University Test Set-up (Mohamad and Chen, 2017)

CHAPTER 2. LITERATURE REVIEW

With the vertical reinforcement of the wall anchored in both the foundation and loading beams, each wall was designed to have reinforcements that ensured that the nominal shear strength of the wall was greater than the nominal flexural strength. The failure mode sought here was flexural failure as opposed to shear failure (Mohamad and Chen, 2017). In the case of reinforced masonry shear walls, researchers (e.g. Mohamad and Chen, 2017; Voon and Ingham, 2006) have stated that flexural failure is the preferred failure mode as it is characterised by a ductile behaviour of the wall specimen and an effective energy dissipation through reinforcement yielding.

Once the vertical load was fully applied and maintained constant, the horizontal cyclic load was then applied in two steps; first in a force controlled manner until the yielding of flexural reinforcement, and then in a displacement control until failure of the specimen. The loads were applied through a loading beam whose lateral stability was achieved by means of transverse rollers (Mohamad and Chen, 2017).

The test set-up shown in Figure 2.17 was used by Haach *et al.* (2009) to perform in-plane static cyclic tests on reinforced concrete block masonry walls. These tests aimed at contributing further to the knowledge gained on the performance of reinforced masonry walls and the influence of the added horizontal and vertical reinforcement when the walls are subjected to seismic actions. Each masonry wall specimen was built with horizontal and vertical reinforcement as well as reinforced concrete beams placed at the top and bottom of the wall. The vertical reinforcement were anchored in the concrete beams to ensure uniform distribution of the applied loads.

To avoid uplift of the wall base, the bottom concrete beam was fixed to steel beams through steel bolts. Two adjustable clamping angles were used on each side of the concrete beam to prevent slippage of the specimen. The steel beams were connected to the strong floor through steel rods. The vertical load was applied by means of an actuator with vertical steel cables anchored at the strong floor. The load was then distributed at the wall top through a stiff steel beam and a set of steel rollers allowing displacement of the wall with respect to the vertical actuator. The horizontal load was applied with another actuator and transmitted to the wall by means of two steel plates attached to the top concrete beam.

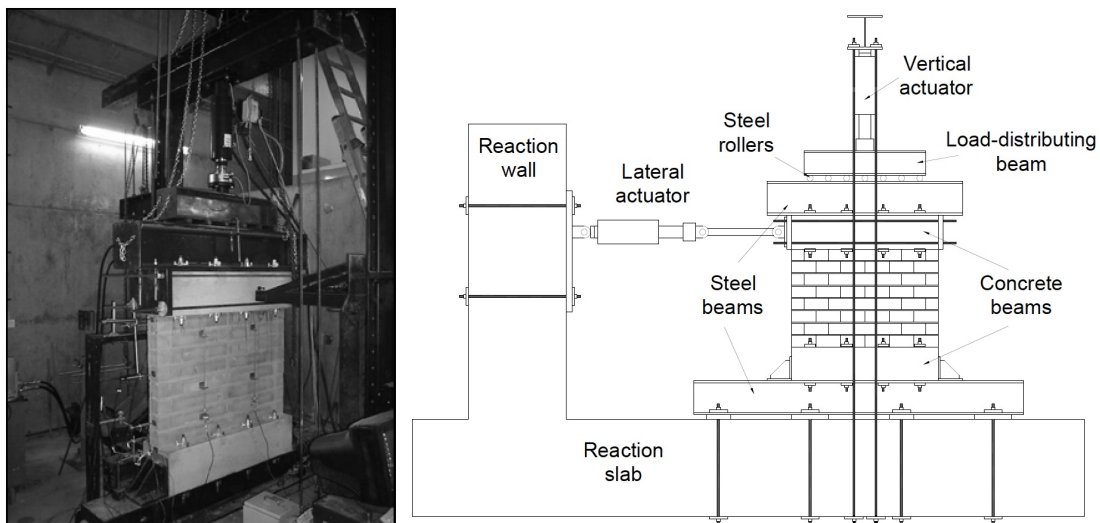


Figure 2.17: Set-up used for Reinforced Concrete Block Masonry Walls (Haach *et al.*, 2009)

2.8 Concluding Summary

This literature review presented a few topics regarding South African housing. It looked at the challenge faced by the South African government of ensuring that its population has access to adequate and affordable housing. While it has been able to provide more than 3 million housing units to poor and low-income populations, due to various reasons, the housing backlog has only been increasing. Several studies have indicated that alternative building materials could reduce the construction cost of houses and lead to other advantages.

The main conventional masonry units used in South Africa for low-income housing include CMUs and fired clay bricks. When used in large quantities, both of these materials present certain disadvantages, including having a negative environmental impact. Various studies have been undertaken to identify alternative materials that can be used in the construction industry without these consequences. For instance, at Stellenbosch University, alternative masonry units have been identified as a feasible option based on the difference in material properties, the cost and environmental benefit of the units, and the availability of manufacturing equipment. Three of these alternatives are Adobe, cement stabilized earth block, and alkali-activated concrete block.

In considering what materials to use for the construction of low-income housing, it is also important to be aware of seismicity in South Africa. The country has areas identified to be at risk of low to moderate size earthquakes, which occur due to both natural causes and mining activities. In either case, their consequences can be devastating and can result in loss of human life, mostly because of falling structures.

Masonry buildings have performed poorly during seismic activities, making them inadequate for earthquake prone regions. Of the three main types of masonry structures, un-reinforced masonry (URM) is the type considered in this study. While it has multiple advantages, it can only withstand small lateral loads and little displacement. Studies have shown that the three types of URM buildings (i.e. Adobe, brick, and stone) have demonstrated similar failure mechanisms from earthquake activities. To assist with the construction of these structures, the recommendations and requirements provided in [SANS 10160-4 \(2011\)](#) as well as [SANS 10164-1 \(1989\)](#) should be considered in the design process.

To study the seismic behaviour of URM walls various tests are conducted in laboratories, each using different testing devices, in an attempt of replicating the observed behaviour of masonry walls after earthquakes. In this way, a range of test configurations and load applications can be considered. From the tests conducted, three distinct failure modes have been identified – sliding shear, diagonal shear, and flexural failure. The results obtained by the experimental tests can be used to further develop computational models that can predict the behaviour of structural masonry which are under seismic loads.

As it is difficult to represent the real conditions of a masonry wall in the laboratory, testing set-ups are designed with various mechanical systems that provide simplified and controlled boundary conditions. The shear force and the displacement capacities of URM walls are typically determined by conducting shear-compression tests. Several experimental test set-ups have been presented, which are considered in the design of the test set-up used in this study.

Chapter 3

Materials and Block Manufacturing

The walls and wallets built for the investigation presented in this study were constructed with blocks that were manufactured by the author. The block manufacturing process, being an important aspect of the project, needed to be set up in such a way that the blocks would be created with high quality control in order to ensure similar mechanical properties of each individual block type. This chapter will provide information on the masonry units as well as the mortar used to build the wallets and walls. The themes that will be discussed include the materials used for the fabrication of the different masonry units; the mix designs and the manufacturing process for each type of masonry unit; and the mortar design used to construct the different walls.

3.1 Materials

The materials used to manufacture the different masonry units include fine and coarse aggregates, binders, an alkaline solution, and water. The total amount of material needed for the block manufacturing process was determined based on the total amount of blocks required for the unit, wallet and wall tests, and according to the CMU and AMU mix proportions proposed by [Fourie \(2017\)](#).

The properties of some of these materials had to be determined according to the relevant South African National Standard (SANS) requirements, which provided a sound starting point for determining the proportions needed of the materials to be used in the various mixes and ensured that the masonry units being manufactured had similar properties to the units produced by [Fourie \(2017\)](#). Further descriptions of the materials used in this study are provided in this section.

3.1.1 Aggregates

The aggregates used in the mix designs for the CMUs and AMUs included two types of fine sand known as Philippi and Malmesbury, a coarser sand known as Crusher dust, 13-mm Greywacke stone, and clay soil. The aggregates that were not available in the laboratory, in particular the sands, were obtained from a local materials supplier. Before being used, they were dried in the laboratory open area and stored in the laboratory silos. Grading of the sands was conducted by performing a sieve analysis according to [SANS 201 \(2008\)](#) after which the fineness modulus

CHAPTER 3. MATERIALS AND BLOCK MANUFACTURING

(FM) was determined. The relative density (RD) of the aggregates was determined following the guidelines set in [SANS 5844 \(2014\)](#).

Different batches of Malmesbury and Philippi sands were available to be used in the different unit mixtures. For the purpose of this study, the four different sands were respectively identified as Malmesbury sand #1, Malmesbury sand #2, Philippi sand #1 and Philippi sand #2.

Malmesbury sand #1 was used in the CMU and Adobe mixtures, and Malmesbury sand #2 was used in the AACB mixture. Philippi sand #1 was used in the CSEB and Adobe mixtures whereas Philippi sand #2 was used for the different mixes of mortar.

In addition to the use of fine sands in different mixtures as described above, the crusher dust was used in the CMU mix, the 13-mm stones in the AACB mix, and a yellow clay soil sourced locally from a brick manufacturer was a constituent material for the Adobe and CSEB mixtures.

The gradings of the different materials, shown in [Figure 3.1](#), indicate that both Philippi sands are very fine, with Philippi sand #2 being slightly finer. Malmesbury sand #2 is slightly coarser and shows a much better grading than the other three finer sands. As the mix proportions for the different units used in this study were adopted from the mix designs proposed by [Fourie \(2017\)](#), his suggestion of blending the sand for appropriate grading was also adopted.

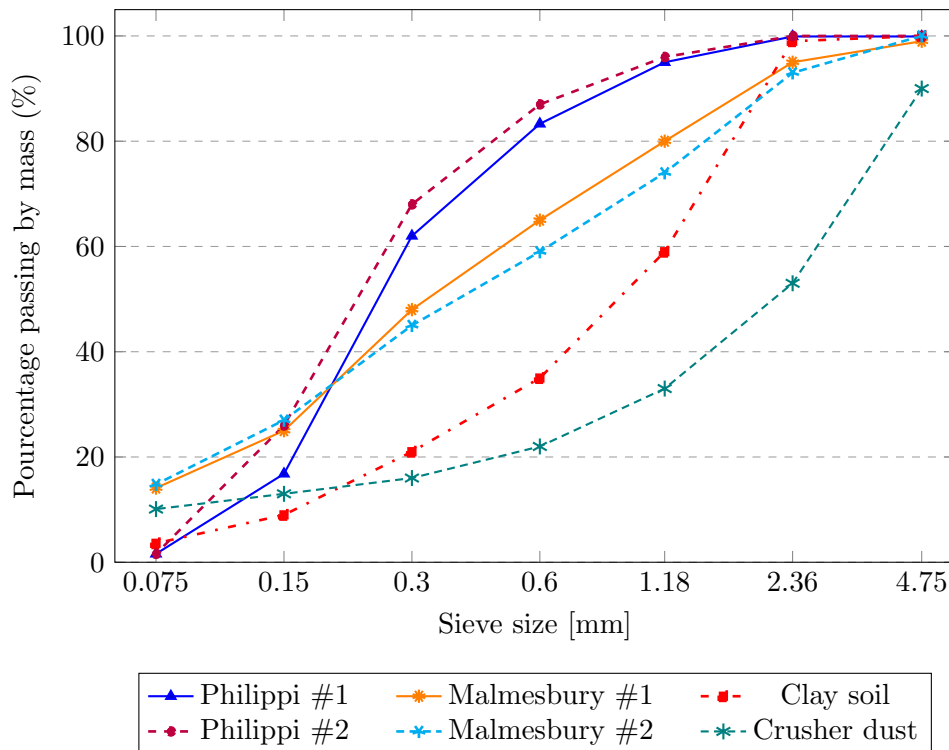


Figure 3.1: Grading of Materials

The fineness modulus (FM), the relative density (RD), as well as the particle shapes of the aggregates used in manufacturing the bricks are given in [Table 3.1](#).

Table 3.1: Characteristics of Aggregates

Material	FM	RD	Particle Shape
Malmesbury sand #1	1.87	2.56	Round
Malmesbury sand #2	2.03	2.55	Round
Philippi sand #1	1.43	2.61	Round
Philippi sand #2	1.23	2.63	Round
Crusher dust	3.72	2.69	Angular
13 mm Greywacke stone	-	2.74	Angular

3.1.2 Binders

The binders comprised of CEM II 42.5 N and CEM II 52.5 N Portland cement, ground granulated corex slag (GGCS), and fly ash. These materials were constituents of the different mix designs and influenced the strength of the respective units being manufactured. The author ensured that each of these materials was acquired from the same supplier and that, once the block manufacturing process had started, the required materials were sourced from the same batch.

3.1.3 Alkaline Solution

An alkaline solution of sodium silicate and sodium hydroxide was used in manufacturing the AACBs. Obtained in pellet form, the sodium hydroxide needed to be dissolved in potable tap water and left to cool down for about two hours as the solution produces heat.

The mass per litre of solution of sodium hydroxide pellets is determined by the concentration required in the solution. It was essential to take necessary precautions while working with the chemicals, such as avoiding any skin contact.

3.1.4 Water

Water is an important constituent of concrete mixes as it is needed for workability and enables the hydration process. The total amount of water in a mix is often determined by the properties desired in the final mix and its constituents. As it is also required in the manufacturing of the blocks presented here, ordinary municipal tap water, classified as potable water, was used in the different mixes.

3.2 Block Manufacturing

Fourie (2017) presents an extended study on the mix designs and the manufacturing process for each type of masonry unit. The processes outlined in his notes, which include the mix design, mixing procedure and curing, were followed for the manufacturing of blocks in this study.

The four different types of masonry blocks presented in this experimental study include concrete masonry unit (CMU) and three alternative masonry units (AMUs), namely compressed stabilised earth blocks (CSEBs), Adobe blocks, and alkali-activated concrete blocks (AACB). These blocks were used to construct the CMU and the three different types of AMU walls and masonry wallets. CMUs are frequently used in the construction of low-income housing throughout South Africa

CHAPTER 3. MATERIALS AND BLOCK MANUFACTURING

and, for the tests performed in this study, CMU specimens were used as a benchmark for the test results obtained from the AMU specimens.

The methods used in the block manufacturing process varied according to the differences in the mix proportions of each block type, as well as the characteristics of the materials used. The blocks were manufactured in the materials laboratory at Stellenbosch University. A 50-litre pan mixer was used to mix the different materials for each mixture. Once the mixture was ready, the block was created either by compaction in a manual earth block press (CMU, CSEB and Adobe) or by casting it in wooden moulds (AACB).

The dimensions of each block were determined based on the manual earth block press available in the laboratory. Manufactured by *Hydraform*, this block press, shown in Figure 3.2 can produce a masonry unit, which is 290mm long, 140mm wide and 116mm high.

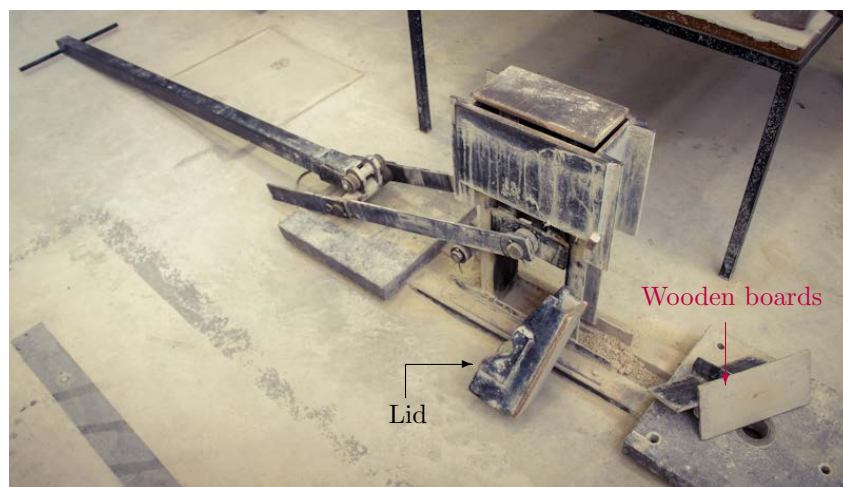


Figure 3.2: Hydraform Block Press

Compaction techniques as described by Venkatarama Reddy (2012) are of two types, “static and dynamic compaction”. These techniques are used, through the application of compaction energy, to convert loose materials into a dense and stable unit. The process of compacting materials by using the manual earth block press can be described as a static compaction technique whereby the materials placed in the block press chamber are compacted by using a piston. The compaction energy required to make the block will vary according to the characteristics of the material mixture placed in the press chamber (Venkatarama Reddy, 2012). Figure 3.3 illustrates the different steps necessary in the static compaction process for a given soil mixture.

The following sections present the manufacturing processes of each of the masonry unit types investigated in this study. It should be noted that the purpose of this study was not to produce new mix designs of the different units manufactured. While existing mix designs were adopted, as new materials were used which had different properties from the materials on which the mix designs were based, trial mixes were made to assess the quality of the mixes. Where the trial mixes confirmed to be adequate, the existing mix design was kept unchanged, otherwise, any required adjustments to a given mix design were made accordingly.

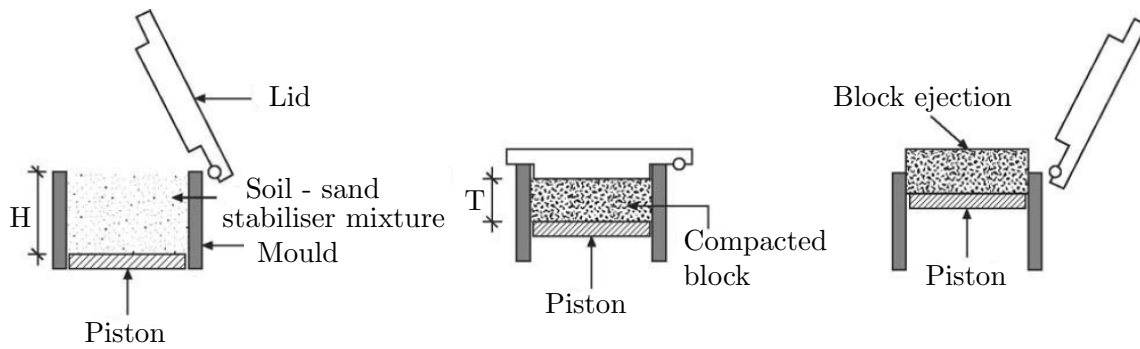


Figure 3.3: Static Compaction Process (Venkatarama Reddy, 2012)

3.2.1 Concrete Masonry Units (CMUs)

The first set of blocks created for this experimental study were CMUs. The mix design for these blocks was the one presented by Fourie (2017), who tried to design a mix that would resemble as closely as possible that used in practice while following the CMU mix design steps and manufacturing procedures provided by Jablonski (1996), who used the fineness modulus (FM) to decide on the proportions for the mix.

The CMU mix design proposed by Fourie (2017) had a high content of crusher dust in an attempt of raising the FM value for blended aggregates to the recommended FM values. For both the Malmesbury sand #1 and Crusher dust available in the laboratory, it was noted, as shown in Table 3.2, that these aggregates were respectively finer and coarser than the Malmesbury sand and Crusher dust used by Fourie.

Based on the aggregate proportions in the CMU mix design proposed by Fourie (2017), the FM of the blended aggregates was found to be 3.14, calculated according to the aggregate proportioning procedure proposed by Jablonski (1996). A similar FM value for the blended aggregates was found with the aggregates used in the current study, according to their respective gradings. It was therefore decided that the same aggregate proportions would be used in this study. The gradings of the two sands used in the CMU mix together with the blended sand are shown in Figure 3.4.

Table 3.2: FM values Comparison

CMU Aggregates	FM	
	Fourie	Shiso
Malmesbury sand	1.87	2.33
Crusher dust	3.72	3.52

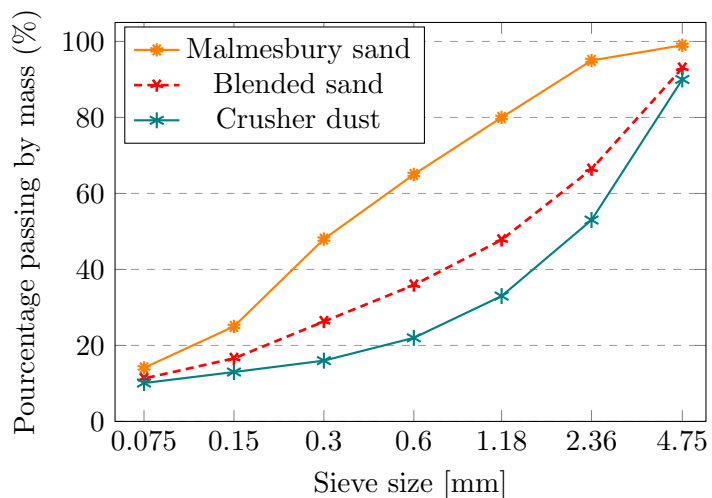


Figure 3.4: Grading of CMU aggregates

CHAPTER 3. MATERIALS AND BLOCK MANUFACTURING

For the blended aggregates, the proposed mix design includes water and two types of binders, cement and fly ash. A 1:10 ratio of binder to aggregate was chosen, which is in the range of the cement to aggregate ratio recommended by Jablonski (1996). Of the amount of binder required, 75% was cement. The fly ash, representing 25% of the total required binder, was added to increase the cohesiveness of the mix, due mainly to the manufacturing method.

Fourie (2017) determined the water content by eye inspections and trial mixes. The optimum water content suggested for the CMU mix was 9.1% of the total mixture. Using the same water content and mix proportions of dry materials, a trial mix was performed in a small quantity in order to assess the quality of the mixture and the unit produced. By inspecting the unit produced, which resembled the unit produced by Fourie, it was decided to adopt, for this experimental study, the same mix design quantities shown in Table 3.3.

Table 3.3: CMU Mix Design Quantities

Constituents	kg/m ³
Malmesbury Sand	607
Crusher dust	1316
CEM II 42.5 N	144
Fly Ash	48
Water	212
TOTAL	2328

A 50 l (liter) pan mixer was used to mix all of the constituents of the CMU mix. Each unit was created by compacting 10.5kg of the wet mixture. This mass, which was suggested by Fourie (2017), was found through trial and error to be the optimal mass for compaction of a CMU. It required less compaction effort while achieving sufficient cohesion for the unit to be removed from the block press and placed on the table used mainly to dry the unit for 24 hours.

The total volume of mixture in the 50 l pan was determined in such a way as to produce eight units per mix. The required mass of each constituent was thus determined accordingly and in such a way to minimize wasted materials. Once the different constituents of the mix had been weighed, the dry materials (binders and aggregates) were first placed in the pan mixer before adding water. To achieve a homogenous mix, first the dry materials were mixed for a duration of about two minutes, then, while the mixing continued, water was added. The materials were then mixed for another three to four minutes.

Using small containers available in the laboratory, 10.5kg of the final wet mixture was subsequently weighed from the 50 l pan and placed in the small containers. As shown in Figure 3.5, a total of eight small containers, each filled with wet mixture, were prepared and moved to the area where the block press was located.

For the unit creation, the block press chamber was carefully, and in consecutive layers, filled with the wet mixture, and roughly levelling each layer with a small masonry trowel. Once all the mixture was in the press chamber, the lid positioned on the top of the chamber, the unit was

CHAPTER 3. MATERIALS AND BLOCK MANUFACTURING

compressed by operating the lever arm, which prevents the lid from moving from the top and controls the movement of the piston within the chamber.

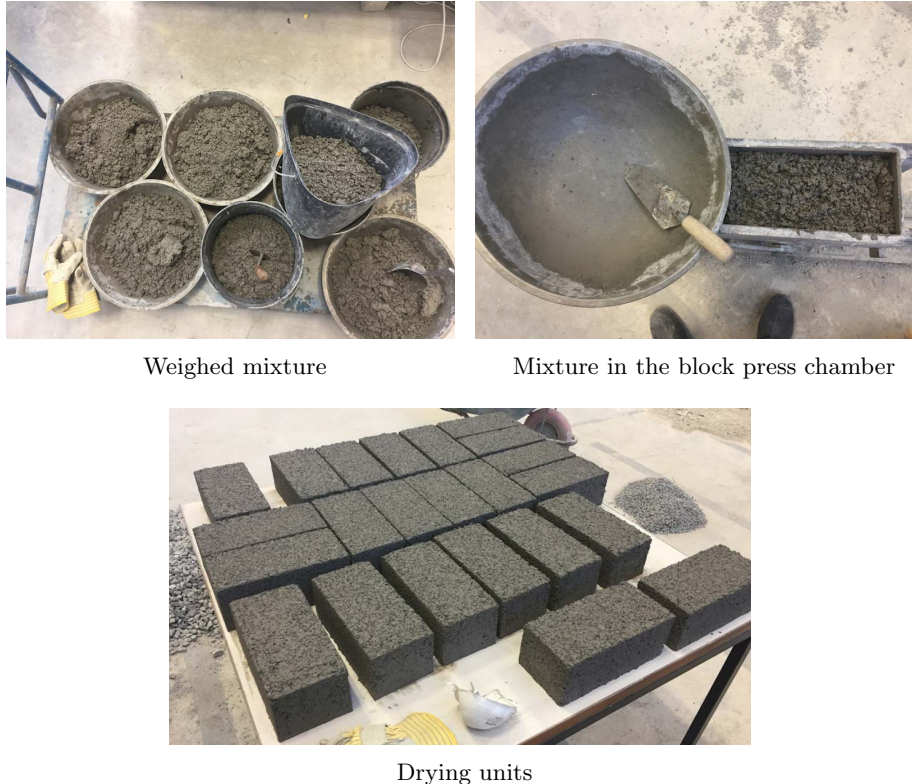


Figure 3.5: CMU Manufacturing Process

Because of the nature of the CMU mixture, care needed to be taken when removing the unit from the press and placing it on the table. As shown in Figure 3.2, two wooden boards cut to match the side dimensions of the unit (290mm × 160mm) were used to move each unit. Once the unit was compacted and lifted out of the chamber, the wooden boards were placed on each side of the unit. Just enough pressure was put on the board to be able to grip the unit and then the unit was carefully turned on its side, either right or left, while making sure that the block was resting on the side and that there was no pressure put on it by holding it.

Placing the unit on its side and resting it on the wooden board while holding it ensured that no deformation of the unit was induced by the pressure required to hold. Such deformation can occur if a unit is removed directly from the block press in its original position.

With the unit resting on the board, it was carried to the table where, once again, it was turned back to its original position and slowly placed on the table. As illustrated in Figure 3.5, the process just mentioned was followed for the remaining wet mixture. After each batch of units was made from a given mix, the block press chamber was cleaned and prepared for the next batch. This was then repeated for all of the subsequent mixes.

The units thus made were left to dry for 24 hours before being placed in the curing tanks, which were filled with water. The units remained in the curing tanks until they were tested or used to construct wallets and walls. Approximately 235 units were required for all of the tests performed

in this study. As only one unit could be produced with the block press at a time, an average of 16 units were produced each day and the total amount of units was produced after a period of three weeks.

3.2.2 Compressed Stabilized Earth Blocks (CSEBs)

The first type of AMUs manufactured were the compressed stabilized earth blocks (CSEBs). Similar to CMUs, the CSEB mix design used for this study was based on the mix design proposed by [Fourie \(2017\)](#), with the decision of adopting his mix design based on the trial mix with the materials available in the laboratory. The same manufacturing process for CMUs illustrated in Section 3.2.1, using the manual block press (see Figure 3.2), was followed.

[Fourie \(2017\)](#) used an adaptation of a CSEB mix design developed in a previous study at the Stellenbosch University by [Malherbe \(2016\)](#). He presented a mix design that contains a fine sand known as Philippi, CEM II 52.5 N as the only binder, and the clay soil, with 10% moisture content determined with the modified Proctor test.

The clay soil, which was obtained from a local brick manufacturer, contained large clay clumps, requiring for it to be mechanically crushed in the open space of the laboratory and then sieved through a sieve with a 2.36mm aperture. [Fourie \(2017\)](#) found that during the mixing process, clumps would form in the pan mixer because to the high clay and low water content in the mix. These clumps had to be broken by hand before placing the mixture in the block press chamber.

For this experimental study, a trial mix was first carried out with the mix design proposed by [Fourie \(2017\)](#). Once all the materials were put together, it was found that the mixture was too dry and, once compressed, it did not hold its shape as it was extracted from the block press.

Due to the difference in material properties, an optimum moisture content (OMC) for the blended dry materials, henceforth referred to as dry mixture, had to be determined based on the modified Proctor test. The guidelines provided in [SANS 3001-GR30 \(2015\)](#) were followed to perform the above mentioned test. It should be noted that the same mix proportions for the dry materials of the CSEB design mix proposed by [Fourie \(2017\)](#) were used.

Four dry mixture samples, each weighing 7kg, were prepared for the test. Each sample was tested one after the other with a determined moisture content added to each. The moisture content of the first sample was estimated based on an expected moisture content. Water was added to the dry mixture and was thoroughly mixed in to achieve a homogeneous mix. The sample was then laid in five layers in a cylindrical mould with a known mass and volume and compacted using an electric compacting machine.

Five cycles of 11 evenly distributed blows were applied by the compacting machine with a tamper in order to compact the sample. Once all five layers were compacted, the cylindrical mould was removed from the testing machine and cleaned of any excess materials after which the mass of the mould with the compacted material was determined. The material was then removed from the mould before testing the next sample.

CHAPTER 3. MATERIALS AND BLOCK MANUFACTURING

The moisture content of the subsequent samples was adjusted as specified in the code and compacted with the machine in the same manner as for the first sample. Using the determined mass of each sample, the dry densities were determined and plotted on the graph shown in Figure 3.6 with their corresponding moisture contents. With the parabolic curve fitted to the data, the OMC was determined at the maximum dry density (MDD) obtained for the specified compaction effort.

From the obtained results, the optimum moisture content of the mix was found to be 11.3%. The compaction effort from the compacting machine can be characterized as dynamic compaction. In contrast, as previously described, the compaction effort exerted with the manual block press was static. It was decided that the OMC would be increased to 12% in order to ensure that the resulting mixture will be suitable to be used in the block press and would hold its shape once compacted.

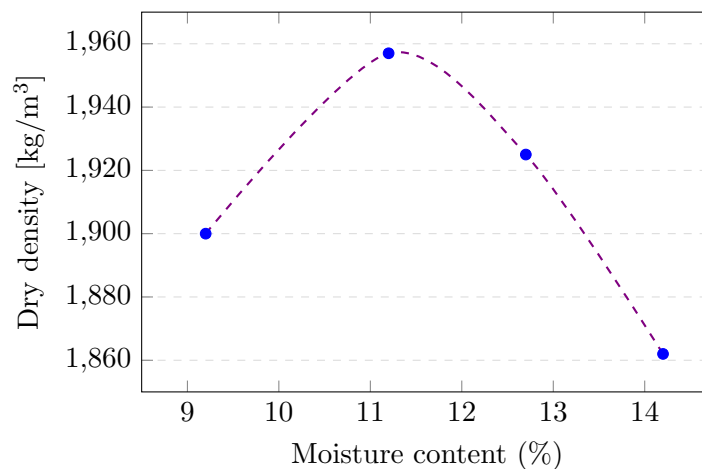


Figure 3.6: Dry Density - Moisture Content Results

CEM II 52.5 N cement, Philippi sand #1, and a clay soil sieved through a sieve with a 2.36mm aperture were used together with water for the CSEB mix. The final mix design quantities are presented in the Table 3.4.

Table 3.4: CSEB Mix Design Quantities

Constituents	kg/m ³
Philippi Sand	1198
Clay Soil	798
CEM II 52.5 N	200
Water	264
TOTAL	2460

The CSEB manufacturing procedure was similar to the procedure outlined in Section 3.2.1 for the production of CMUs. A 50 l pan mixer was used to combine the materials such that eight blocks were created from one mix. The total mass of the mixture in each of the small containers that was prepared for a block was 9.4kg, similar to that used by Fourie (2017). The dry materials

CHAPTER 3. MATERIALS AND BLOCK MANUFACTURING

were mixed together before adding water. The clumps that were formed during the mixing process, mainly due to the clay soil and low water content, were broken up by hand before the wet mixture was weighed.

As the compaction process of each unit took some time, the mixture in the small containers was covered with a polythene sheet to prevent the mixture from drying out through evaporation, as shown in Figure 3.7. The mixture was then placed in layers in the chamber of the block press. Each layer was slightly compacted and levelled with a masonry trowel to ensure all the material fit in the chamber.

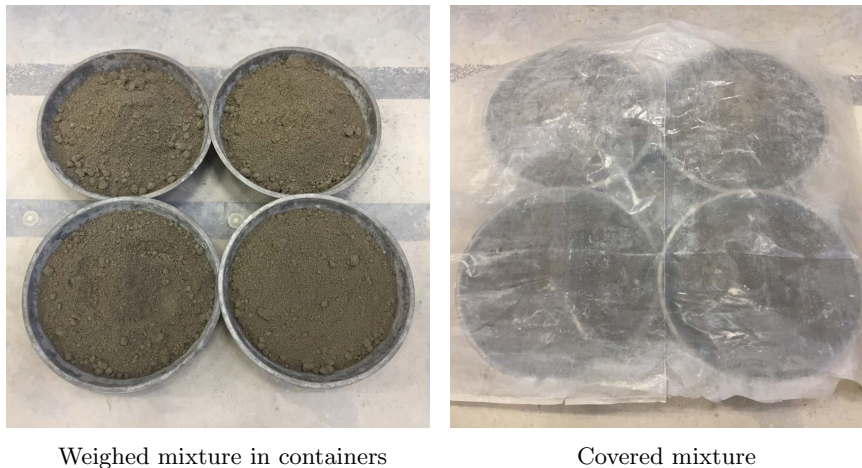


Figure 3.7: Weighed CSEB Mixtures

Once compressed, the two wooden boards were again used to move the block to the curing area. The block held its shape well after compaction, which made it easy to move and lift from the press without needing to turn it on its side as had been done for the CMUs.

The CSEB were then cured. The blocks were first placed on polythene sheets in an allocated area of the laboratory open space and covered with other polythene sheets to reduce evaporation (see Figure 3.8). For seven days, the units were sprayed every 24 hours with a mist of water after which they were moved to a climate-controlled room which was kept at a temperature of 25°C and 65% relative humidity.



Figure 3.8: CSEB Curing in Laboratory Open Space

CHAPTER 3. MATERIALS AND BLOCK MANUFACTURING

Similar to the CMUs, the total number of CSE blocks required for this study was approximately 235 blocks. These were produced over a period of three weeks, with an average of 16 blocks manufactured per day. Once cured, the blocks were stored in the climate-controlled room until they were used for tests or for building wall and wallet specimens.

3.2.3 Adobe

Adobe blocks were the second type of AMUs and third unit type created after CSEBs. These units were created by mixing soil and water. In practice, the soil used for Adobe mix, is often comprised of a certain percentage of clay, silt, sand, and gravel blended together. These constituents are often located near the manufacturing site. Other materials may be added to improve the properties and qualities of the blocks.

[Fourie \(2017\)](#) proposed a soil mixture, for Adobe blocks, composed of two types of fine sands and clay soil. Philippi sand #1 and Malmesbury sand #1 were the fine sands used to manufacture Adobe blocks during this experimental study. As these blocks rely on the clay for their strength, once crushed the clay soil was sieved through a sieve with 1.18mm aperture. [Fourie](#) found, through trial and error, that the optimum water content for the mix was approximately 13% of the soil mixture.

A common method of creating Adobe blocks involves using wooden moulds with no base. The mixture is placed in the mould and tamped down by hand. With this method however, the exact amount of mixture placed in the mould is not known, and it is often necessary to line the interior of the mould with a polythene sheet in order to reduce friction and deformation of the block once extracted. For these reasons and in order to produce blocks with as much consistency as possible, it was decided that the Adobe blocks would be manufactured in the same manner as the CMUs and CSEBs, using the manual block press.

Trial mixes were performed based on the mix design proposed by [Fourie \(2017\)](#) in order to assess the workability of the mix and to determine the amount of material required for a unit that can be compacted and extracted with ease from the block press, that will retain its shape once out of the press chamber, and that will have similar density to the units produced by [Fourie](#). Based on the trial mixes prepared in this way, the mix design proposed by [Fourie](#), shown in Table 3.5, was adopted and it was found that a suitable unit could be created by compacting 9.3kg of the mixture.

Table 3.5: Adobe Mix Design Quantities

Constituents	kg/m ³
Philippi Sand	809
Malmesbury Sand	809
Clay Soil	534
Water	275
TOTAL	2428

CHAPTER 3. MATERIALS AND BLOCK MANUFACTURING

Similar to the process of manufacturing CMUs and CSEBs, the 50 l pan mixer was used to produce Adobe blocks. With each mix, enough material was weighed to produce 8 blocks. Clumps would form during the mixing process, which needed to be broken down by hand before the units were compacted. Figure 3.9 shows a typical Adobe block after compaction as well as the handling process using wooden boards.

Due to the nature of the Adobe mixture, it was necessary to regularly clean the block press chamber for ease of extraction, particularly the bottom plate of the chamber. As with CMUs, the Adobe block needed to be handled gently and the same technique that had been employed for CMUs was adopted whereby two wooden planks were used to remove the units from the block press. Once formed, the units were left to dry in the open area of the laboratory in a space prepared for this purpose. An average of 16 units were produced per day and the total amount of units required for this study was prepared within a period of three weeks.



Figure 3.9: Adobe Block

3.2.4 Alkali-Activated Concrete Blocks (AACBs)

The Alkali-Activated Concrete Blocks were the third AMU type and last set of blocks manufactured. The constituents of these blocks include the aggregates, binders, and an alkaline solution. The mix design of AACBs differ from conventional concrete mixes as it is not based on the water binder ratio.

The AAC mix designs have been reported to be complex in nature and not straightforward [Fourie \(2017\)](#). No significant amount of time was dedicated to designing an AACB mix for this study. However, a few studies have been undertaken at Stellenbosch University such as the one carried out by [Barnard \(2014\)](#), who used mixes provided in literature to design a mix for an AAC that can be cured at room temperatures.

The mix design proposed by [Fourie \(2017\)](#) did not show any workability from the trial mixes performed and based on materials constituents available in the laboratory. However, another mix design was provided by [Schmidt \(n.d.\)](#), and was used for the purpose of this study. The mix design shown in Table 3.6 produced AAC mix which was much more workable allowing the

CHAPTER 3. MATERIALS AND BLOCK MANUFACTURING

blocks to be cast easily. The constituents include 13mm Greywacke stone, Malmesbury sand #2, two types of binders (i.e. fly ash and slag), and the alkaline solution.

Table 3.6: AACB Mix Design Quantities

Constituents	kg/m ³
13 mm Greywacke Stone	1000
Malmesbury Sand	700
Fly Ash	350
Slag	100
Sodium Silicate (SS)	70
Sodium Hydroxide Solution (SHS)	90
Water	120
TOTAL	2428

The stone and sand were already available in the laboratory. It was found that the age of binders played an important role in the workability and setting time of the mix. The binders stored for a long time (more than a year) resulted in a mix that set rapidly and required more water to be added. However, the mix obtained with newer batches of fly ash and slag was workable and provided enough time for casting the blocks.

The alkaline solution consisted of a mix of sodium silicate and sodium hydroxide. These two constituents were weighed and added separately into the AAC mix. Sodium silicate (SS) came in a liquid state while sodium hydroxide (SH) came in pellets and needed to be dissolved in water (W) in order to make the sodium hydroxide solution (SHS). The concentration of sodium hydroxide in the SHS was based on a SH:W ratio of 0.4. Once made, the SHS produced heat and needed to cool down for about two hours before being used in the mixing process. Due to the corrosive nature of SH (Evonik Industries, 2010), these products were handled with great care using gloves, masks, and glasses as it was essential to avoid all sort of skin contact with the mixture.

A 50 l pan mixer was used to produce the AAC mixtures. As a first step, the dry materials were placed in the pan and mixed for approximately two minutes. The SHS was then added followed by the SS and water and the mixing continued for another two minutes. Once all of the materials were thoroughly mixed, forming a homogeneous mixture, blocks were immediately cast by placing the mixture into wooden moulds (see Figure 3.10) created for this purpose. The inner dimensions of each mould were 290mm long, 140mm high and the width of 116mm, thus producing blocks with the same dimensions as the blocks manufactured with the manual block press. However, the bedface of the block was at a right angle to the casting direction.

The moulds were vibrated to remove the air from the mixture. Although an important step in the AAC block manufacturing, the vibrating time should be kept to a minimum as it was found that the stones in the mixture would segregate if the mixture in the mould is vibrated for too long. With each mix, six blocks were cast along with one cylinder specimen, which was prepared for the modulus of elasticity test (see Figure 3.11). The blocks created were then left to cure for 24 hours, after which they were demoulded and stored in the climate-controlled room as was the

CHAPTER 3. MATERIALS AND BLOCK MANUFACTURING

case for CSEBs. The temperature in the room was maintained at 25°C and the relative humidity at 65%.

With six blocks produced from each mix, it was possible to manufacture 18 blocks in a day, with the SHS prepared two hours before mixing. Once the blocks were demoulded, the moulds needed to be cleaned and prepared for the next set of blocks. This process was time consuming and, as a result, the total amount of AAC blocks required for the experiment was reached within a period of four weeks.



Figure 3.10: AACB Wooden Mould



Figure 3.11: AACB Curing in Wooden Mould

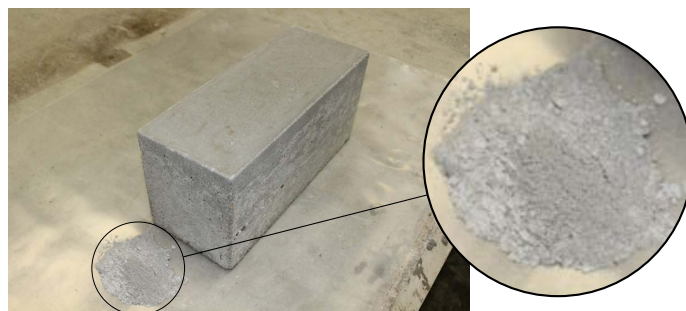
While the AACBs were left to cure in the climate-controlled room, it was realized that a powdery substance with crystal-like shapes would form on the surface of the units as shown in Figure 3.12. The exact cause of this behaviour was not known to the author as this was not investigated in the study presented here.



Blocks in curing room



Before cleaning the block



After cleaning the block

Figure 3.12: Dust Layer Forming on AACBs

The blocks were, however, thoroughly cleaned with a brush before they were used for the various tests as well as in the construction of wallets and walls. It is suggested that further investigation into this matter be carried out in future studies.

3.3 Mortar Mix Design

The main functions of mortar are highlighted in [SANS 10164-1 \(1989\)](#), which include providing an even bed for equal distribution of applied loads over the structural unit area, bonding the structural units together and contributing to resisting lateral forces, and to provide sealed joints to prevent penetration of rain.

Based on the characteristics of the masonry units and the type of loadbearing walls being considered, three different classes of mortar are provided in [SANS 10164-1 \(1989\)](#) together with their limiting proportions for the mixes. The mortar mixture is often comprised of cement and/or lime, aggregates, and water; additives may also be added to improve the properties of mortar, such as workability ([Tomažević, 1999](#)).

As the four unit types investigated in this study had different properties, such as their compressive strength, an attempt was made to design four different mortar mixes with compressive strengths similar to the respective masonry units. Due to the large variability in the compressive strengths of the units and the limited time available to perform trial mixes, it was decided that only one type of sand - Philippi sand #2 - and the CEM II 42.5 N cement would be used for all four mortar designs.

The initial step was to perform small trial mixes using the appropriate cement to sand ratio by mass to provide a linear estimate of the change in strength. The water content was estimated by eye. The mortar mixes were cast in 100mm × 100mm cubes which were tested for compressive strength after seven days (Testing age of wall and wallets specimens). After the linear estimate of the mortar strengths was plotted, the cement to sand (c:s) ratio by mass, for each of the four mortar mixes, was determined using the plotted graph and based on a mortar compressive strength, that would correspond to the compressive strength of each of the four masonry units, respectively.

However, the final water content of each mix was determined by a professional bricklayer based on the quality of each masonry unit and the workability of the mix. The final mortar mixes are shown in [Table 3.7](#). For the construction of the wall specimens a stronger mortar was used for the bottom and top mortar joints (see “All Units” in [Table 3.7](#)).

Table 3.7: Mortar Mix Proportions

Constituents (kg)	CMU	CSEB	Adobe	AACB	All Units
CEM 52.5 N					1
CEM 42.5 N	1	1	1	1	
Philippi Sand	2.5	4	6.5	2.5	1
Water	0.725	1.2	2	0.725	0.4

3.4 Concluding Summary

This Chapter looked at various features of the masonry units manufacturing process and the mortar that was required for testing to be carried out on units, wallets, and walls in this study. Efforts were made to manufacture blocks with a high degree of quality control in order to ensure that each of the blocks of a particular block type had similar mechanical properties. The materials used for manufacturing the CMUs and AMUs, and the reasons for the selection of these materials were described.

The blocks were primarily manufactured using two methods - compaction in a manual earth block press and casting in wooden moulds - according to the differences in the mix proportions of each block type and the characteristics of the materials used. While existing mix designs were adopted, trial mixes were performed to assess the quality of different mixes. While efforts were made to follow the mix designs proposed by [Fourie \(2017\)](#), changes had to be made in the case of the CSEB mix design and, in the case of AACBs another mix design was used for the purpose of this study as the one presented by [Fourie](#) did not show any workability from the trial mixes performed, and based on the material available in the laboratory. All together, a total number of 940 masonry units were manufactured.

With regard to the mortar, an attempt was made to design four different mixes, using one type of sand and cement. Each mix was designed in such a way as to have a compressive strength similar to of the respective masonry units. While small trial mixes were used to provide a linear estimate of the change in strength, the final water content of each mix was determined by a professional bricklayer according to the quality of each masonry unit and the workability of the mortar mix.

Chapter 4

Mechanical Properties of Masonry Structural Elements

The use of numerical methods and programs allows for the performance of structural analysis with a high degree of accuracy. However, the characteristics and properties of the element under consideration are essential for the validation of numerical methods. In the case of a masonry structural element such as a wall, mechanical properties of its constituents, i.e. masonry units, mortar and masonry assemblage, need to be determined.

The mechanical properties of a wall element are dependent on the intrinsic mechanical properties of masonry and units, and include compressive strength, shear strength, modulus of elasticity, Poisson's ratio, shear modulus, and fracture energy, to name a few. This study focused on an investigation, through experimental tests, of some of the above mentioned mechanical properties which are presented in this chapter. These include compressive strength and modulus of elasticity tests performed on units, masonry wallets and mortar, as well as unit density tests.

4.1 Masonry Unit and Mortar

Quasi-brittle materials - for instance, bricks, mortar, ceramic, rock and concrete - have been known to have, in different phases, material defects, such as voids and flaws, resulting from the heterogeneity of the mixture of constituents (Lourenço, 1998). This aspect is very determinant in the way these materials behave when subjected to a given stress or deformation. One of the mechanical behaviours of such materials, defined by Lourenço as softening, is characterised by a gradual reduction of mechanical resistance of a material specimen or structure subjected to a continuously increasing deformation.

These materials contain inclusions and micro cracks which are initially stable. When a deformation is progressively subjected to them, because of the change of internal stiffness and strength it causes, a growth of the micro cracks then occurs (Lourenço, 1998). Once the peak load is reached, the growth of micro cracks accelerates resulting in larger cracks, known as macro cracks, which are unstable. During both a deformation controlled and energy-based test, the growth of macro cracks causes the softening of the material, requiring a reduction of the applied load to avoid an uncontrolled crack growth (Lourenço, 1998).

CHAPTER 4. MECHANICAL PROPERTIES OF MASONRY STRUCTURAL ELEMENTS

When a compressive test is conducted on a brittle or quasi-brittle material, the softening behaviour is based on the boundary conditions and the size of the specimen tested during the experiment. With the result thus obtained, Lourenço (1998) defines a material property, known as compressive fracture energy G_c , as the integral of the stress (σ)-displacement (δ) diagram describing the inelastic behaviour of such material. The σ - δ diagram shown in Figure 4.1 describes the characteristic of quasi-brittle materials when subjected to a compressive stress. In the diagram, f_c represents the compressive strength of the material. Micro and macro cracks are also represented on the diagram.

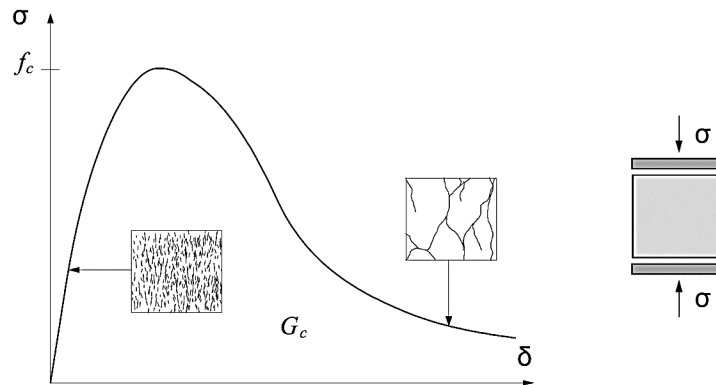


Figure 4.1: Stress-displacement Diagram of Quasi-brittle Material in Compression (Lourenço, 1998)

The compressive strength of masonry units has been accepted by many researchers as a way through which the quality of the unit is assessed (Morel *et al.*, 2007). When compressive strength tests are conducted experimentally, the specimen is often subjected to an axial load uniformly exerted through two stiff and flat steel plates. The test specimen tends to expand laterally due to the applied load. However, at the contact with the test specimen, the steel plates induce frictional resistance which prevents any lateral movement along the interface and confines the specimen. This restraint thus created results in an increase of the apparent strength of the specimen. If the distance between the steel plates, determined by the size of the specimen, increases, the restraint decreases (Morel *et al.*, 2007).

While conducting compressive strength tests on materials that can be cast (e.g. concrete and mortar), standard specimen size and shape, i.e. cube and cylinder, which are used to accommodate the change in compressive strength due to confinement, are specified. Although the test results are not representative of the true strength of the material, a geometric comparison between test samples yield to outcomes which can be utilized with the specified design requirements. However, masonry units are preformed specimens of varying dimensions. As the specified standard specimen size may not be applicable for these materials, the compressive strength test results are normalized by shape factors prescribed in international standards, which aim at removing the restraint effect (Morel *et al.*, 2007).

The modulus of elasticity is a mechanical property of material which provides an indication of the stiffness of a material. The commonly measured value of the modulus of elasticity is known as Young's modulus (E). This value, together with the Poisson's ratio (ν), are necessary for theoretical design calculations and numerical modelling techniques (Domone and Illston, 2010).

CHAPTER 4. MECHANICAL PROPERTIES OF MASONRY STRUCTURAL ELEMENTS

Once known, the modulus of elasticity value can be used to calculate the stresses resulting from strains induced on the material. The strains are often caused by applied loads, temperature changes, and constrained movements.

The modulus of elasticity is normally determined during a compression test by measuring, while the test is underway, the arising strain (ε_p) parallel to the applied compressive stress (σ). The modulus of elasticity value is then calculated using Equation (4.1) (Domone and Illston, 2010).

$$E = \sigma / \varepsilon_p \quad (4.1)$$

While performing the compression test, if the strain (ε_n) perpendicular to the compressive stress (σ) is also measured, Poisson's ratio (ν) can be determined using Equation (4.2) (Domone and Illston, 2010).

$$\nu = -\varepsilon_p / \varepsilon_n \quad (4.2)$$

Because of the minor imperfections and micro cracks present in masonry units and bond layers, as well as the difference in stiffness between units and mortar, masonry exhibits non-linear behaviour resulting in a parabolic stress-strain curve with an early elastic region. Similarly to concrete, the presence of micro cracks in the transition zone between the aggregate and the hardened cement paste (HCP) creates a relatively weak region which ultimately influences the overall concrete strain. Although initially stable, the length, number and width of these cracks in a specimen will progressively increase with a rise in the stress level resulting in non-linear stress-strain behaviour (Domone and Illston, 2010).

Subjecting the specimen to stress levels below the ultimate capacity in successive loading and unloading cycles, has shown, at zero load, significant diminishing hysteresis loops and residual strains. If the stress levels in a given cycle do not exceed the stress level of the first or previous cycles, the subsequent loading cycles will not propagate as many cracks as the first loading, resulting in smaller hysteresis loops as shown in Figure 4.2.

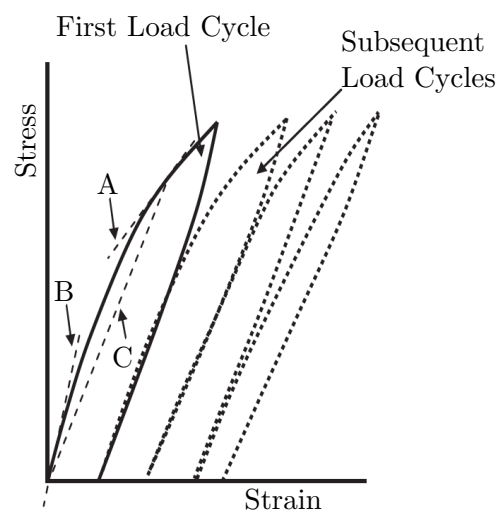


Figure 4.2: Behaviour of Concrete under Successive Loading Cycles (Domone and Illston, 2010)

CHAPTER 4. MECHANICAL PROPERTIES OF MASONRY STRUCTURAL ELEMENTS

Due to the non-linear stress-strain curve of concrete, the modulus of elasticity value can either be denoted in terms of the slope of the tangent to the curve at any given point (line A or B in Figure 4.2) or the slope of the line between the origin and a pre-determined point on the curve (line C in Figure 4.2). The latter is known as the secant modulus and the former, the tangent modulus (Domone and Illston, 2010).

A typical test is performed on cylindrical or prismatic specimen, which has a length at least twice its lateral dimension, loaded longitudinally to a given stress while measuring the arising strain. Usually, the specimen is subjected to a few loading/unloading cycles to minimize the hysteresis effects (Domone and Illston, 2010).

4.1.1 Specifications for Compressive Strength Test

4.1.1.1 Masonry Units

Generally, masonry unit specimens are tested in the bedface orientation, the same orientation they are used for masonry construction, and in the similar manner cast concrete and mortar are tested, that is using a testing device that can apply a stress through either a force or displacement control manner.

In this study, the compressive strength test was conducted following the guidelines presented in the European standard BS EN 772-1 (2011): *Determination of compression strength*. The standard specifies that the minimum number of specimens to be tested is six. A testing machine with a capacity to crush all specimens at an appropriate loading rate is required.

The specimen should be prepared by ensuring that the faces through which the loads will be applied are plane within the provided tolerances; this can be done either by capping or grinding the faces. Various conditioning regimes are specified in the standard. Based on the nature of masonry units being investigated in this study, the adopted conditioning methods are conditioning to the air dry condition and conditioning by immersion.

As per the standard, specimens conditioned to the air dry condition should be stored for at least 14 days in the laboratory space where free air circulation is achieved, and a temperature higher than 15°C with a relative humidity less or equal to 65%. Specimens conditioned by immersion should be immersed in water at a temperature of 20°C ± 5°C for a minimum period of 15h after which they are allowed to drain for 15 to 20 minutes before they are tested.

Once the loading face has been prepared as specified, the necessary dimensions (length and width) should be measured and used to determine, in square millimetres, the gross area of the specimen. The testing machine should also be wiped clean and prepared for the test. A pre-determined loading rate based on the rates specified in the standard is used for the loading application.

The maximum compressive strength (f_u) of the specimen is calculated through the division of the maximum load achieved by the loaded area as shown in Equation (4.3). For a given unit type sample, the compressive strength of the sample is then calculated as the average strength value of the individual specimens. The coefficient of variation (COV) of the sample is also calculated.

$$f_u = \frac{F}{A} \quad (4.3)$$

Where:

f_u	Compressive strength of the unit specimen, [MPa]
F	Maximum load reached, [N]
A	Loaded cross-sectional area, [mm ²]

In order to use the experimental test results for design application, the compressive strength of masonry units should be converted to the normalised compressive strength. This conversion takes into consideration the confinement of the specimen resulting from the use of steel plates during the test. An informative annex provided in [BS EN 772-1 \(2011\)](#) allows for the conversion, which is based on the converted air-dry compressive strength of the unit and the appropriate shape factor provided in the annex.

4.1.1.2 Mortar

The compressive strength of mortar is determined in the same manner as concrete, by casting cubes of 100mm side dimension in lubricated moulds. This dimension is recommended for concrete of maximum aggregate sizes of 20mm or less. The moulds are accurately created in such a way that opposite faces are smooth and parallel ([Domone and Illston, 2010](#)).

It has been observed that the cracking patterns resulting from the compressive strength test on cubes have a double pyramid shape after failure, indicating that the stresses within the cube are not uniaxial but the concrete specimen is rather in a triaxial stress state due to the boundary conditions. In the cube-testing machine, the specimen is placed in between two stiff steel platens with similar dimensions as the specimen loading face. Owing to the Poisson effect, the applied compression force induces tensile strain in steel plate as well as the specimen. The difference in stiffness between steel and concrete, and the friction at the steel plate-concrete interface restrain the concrete against outward expansion leading to the triaxial stress state ([Domone and Illston, 2010](#)).

Although the restraint in the cube test may result in failure at a higher stress as opposed to the true unrestrained strength, the test is used for its simplicity and enables comparison between different concretes. To overcome the restraint effect in the cube test, various guidelines around the world recommend a cylindrical test, as the restraints around the middle section of the cylinder specimen are reduced, because of the length of the cylinder, resulting in near uniaxial failure. The strength from the cylindrical test is often assumed to be about 20% lower than the cube strength ([Domone and Illston, 2010](#)).

The compressive strength test of mortar was performed according to the specifications provided in the South African Standards, [SANS 5863 \(2006\)](#): *Concrete tests - Compressive strength of hardened concrete*. At the time of testing, the specimens were taken from the curing tank. The dimensions of the loading face were recorded, and the specimen was tested immediately while still saturated as prescribed in the code. Once the test is completed, the compressive

CHAPTER 4. MECHANICAL PROPERTIES OF MASONRY STRUCTURAL ELEMENTS

strength (f_m) of the mortar specimen is calculated, similarly to the unit compressive strength, using Equation (4.3). The mortar compressive strength is determined by taking the average compressive strength of all the specimens.

4.1.2 Specifications for Modulus of Elasticity Test

The modulus of elasticity of masonry units as well as mortar were determined following the guidelines and recommendations given in the European standard [BS EN 12390-13 \(2013\)](#): *Determination of the secant modulus of elasticity in compression*. The American standard [ASTM C469/C469M-14 \(2014\)](#): *Static modulus of elasticity and Poisson's ratio of concrete in compression*, was also consulted to ascertain the modulus of elasticity of cylinder specimens.

[BS EN 12390-13 \(2013\)](#) standard provides guidelines to determine the secant modulus of elasticity, following two methods, on cylinder or prismatic specimens either cast or taken from an existing structure. As per the standard, a testing machine is required to perform the test, which should be able to execute programmable loading cycles, apply the loads at a constant loading rate within the specified tolerances, and maintain a constant load at selected values with less variation. Strain measuring instruments are also required to track and record the strain or length changes at a gauge length between two-thirds of the section width or diameter of the specimen and half of the specimen length.

The standard provides guidelines to determine the dimensions of the test specimen. The diameter or width, expressed as dimension d , should be at least 3.5 larger than the maximum aggregate size, and the L/d ratio of the length to the diameter or width should be limited to $2 \leq L/d \leq 4$. A companion specimen with the same dimensions and created in the same manner as the test specimen is required to determine the compressive strength in order to define the stress levels to be used during the elastic modulus cyclic test.

Two methods are provided in the standard to determine either the initial and stabilized secant modulus of elasticity (Method A) or just the stabilized secant modulus of elasticity (Method B). The later is used in the present experimental study. The test is carried out by applying three loading cycles on the specimen, as illustrated in Figure 4.3. To minimise the hysteresis effects, the stabilized secant modulus of elasticity is determined on the third cycle.

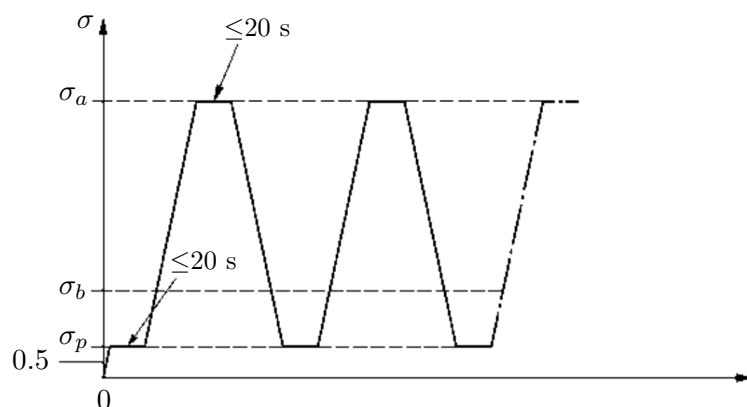


Figure 4.3: Cycles to Determine the Stabilized Secant Modulus of Elasticity ([BS EN 12390-13, 2013](#))

CHAPTER 4. MECHANICAL PROPERTIES OF MASONRY STRUCTURAL ELEMENTS

Once the strain (or length change) measuring instruments are attached, the specimen is centrally positioned in the testing apparatus. The preload stress- σ_p is applied and maintained for a period less than 20 s, then a gradual stress increase to the upper stress- σ_a occurs at a constant rate of 0.6 ± 0.2 MPa/s. Once reached, the upper stress is held for a duration not exceeding 20 seconds before reducing the stress, at the same loading rate, to the preload stress, where it is also held for a period less than 20 s. The loading and unloading processes for the second and third cycles are repeated in the same manner.

At the end of each cycle, the average strain is determined along each measuring line. Based on the change in length measured, the strain is calculated using Equation (4.4).

$$\varepsilon = \frac{\Delta L}{L} \quad (4.4)$$

Where:

ε	Strain due to applied stress, [mm/mm]
ΔL	Change in length corresponding to the vertical deflection , [mm]
L	Gauge length, [mm]

Once the test is completed and the data recorded, the stabilized secant modulus of elasticity of a given material is determined from the loading cycles results using Equation (4.5).

$$E_c = \frac{\sigma_a^m - \sigma_p^m}{\varepsilon_{a,3} - \varepsilon_{p,2}} \quad (4.5)$$

Where:

E_c	Modulus of elasticity of specimen, [GPa]
σ_p^m	Measured value of preload stress, [MPa]
σ_a^m	Measured value of upper load stress, [MPa]
$\varepsilon_{p,2}$	Average strain resulting from $\sigma_{p,2}$ (Second loading cycle)
$\varepsilon_{a,3}$	Average strain resulting from $\sigma_{a,3}$ (Third loading cycle)

[ASTM C469/C469M-14 \(2014\)](#) standard provides a similar method to [BS EN 12390-13 \(2013\)](#) for the determination of the modulus of elasticity. However, provisions for determining the chord modulus of elasticity within the stress range of 0 to 40% ultimate compressive strength are given in [ASTM C469/C469M-14 \(2014\)](#). A testing machine capable of imposing a load at a rate of 241 ± 34 kPa/s is required.

The main readings required for the calculations are the applied stress and longitudinal strain at;

- (1) The point when the longitudinal strain is 50 millionth, and
- (2) The point when the applied load is 40% of the ultimate load, determined from the companion specimen.

CHAPTER 4. MECHANICAL PROPERTIES OF MASONRY STRUCTURAL ELEMENTS

However, when intermediate readings are recorded, the stress-strain results' graph can be plotted. As the applied forces are known and the loading area can be determined, the stress is calculated by dividing the applied forces by the loading area, and the strain, as per Equation (4.4). The chord modulus of elasticity is then calculated using Equation (4.6).

$$E_c = \frac{\sigma_2 - \sigma_1}{\varepsilon_2 - 0.000050} \quad (4.6)$$

Where:

E_c	Modulus of elasticity of specimen, [GPa]
σ_2	Stress corresponding to 40% of ultimate load, [MPa]
σ_1	Stress corresponding to longitudinal strain of 50 millionths, [MPa]
$\varepsilon_{p,2}$	Longitudinal strain produced by σ_2

4.2 Masonry Wallet

A masonry wallet is comprised of masonry units joint together with mortar in a given pattern. The load bearing capacity of a wall structure subjected to vertical and lateral loads is often determine by testing masonry wallets (Tomažević, 1999).

A significant feature of URM elements is that they are known to have a very low tensile strength. This property has been a determinant reason for loading masonry structures only in compression unless they are reinforced or prestressed (Zucchini and Lourenço, 2007). The compressive strength of masonry wallet is thus considered as a very important structural property.

The mechanical properties of a structural masonry wall are dependent of the intrinsic mechanical properties of masonry as well as the interaction between the constituents of the masonry (Tomažević, 1999). Masonry units and mortar, the main constituents of masonry, are generally known to have different mechanical properties, i.e. compressive strength and stiffness. As a result, the strength and stiffness of masonry is believed to generally be between that of the two constituents (Kaushik *et al.*, 2007).

Uniaxial compressive strength of masonry is obtained by conducting tests on standard specimens according to a set of guidelines. Masonry wallets are typical specimens recommended in the standards, however due to the size and cost related to testing these specimens, the stacked bond prisms can also be used. However, the test results obtained from the stacked bond prisms are slightly different from the masonry wallet test results, with the later giving a good indication of the uniaxial compressive strength and considered as the standard test (Zucchini and Lourenço, 2007).

The difference in strength and stiffness between the masonry unit and mortar result in different internal stress states in these materials when the masonry is subjected to a uniaxial compressive force. It has been observed that, when the masonry unit is stronger and stiffer than the mortar, the bonds and shear stress at the unit-mortar interface confine laterally the mortar, resulting in internal stress states of triaxial compression in mortar and bilateral tension combined with axial

CHAPTER 4. MECHANICAL PROPERTIES OF MASONRY STRUCTURAL ELEMENTS

compression in the masonry unit (Kaushik *et al.*, 2007). However, it has also been reported that the opposite stress states, i.e. triaxial compression in masonry unit and lateral tension with axial compression in mortar joints, would develop in a masonry specimen constructed with soft units and stiff mortar. Furthermore, tests conducted on prism specimens constructed with soft bricks and a combination of different mortar grades have shown an increase of the masonry compressive strength due to an increase in the mortar strength which increased the bond strength (Kaushik *et al.*, 2007).

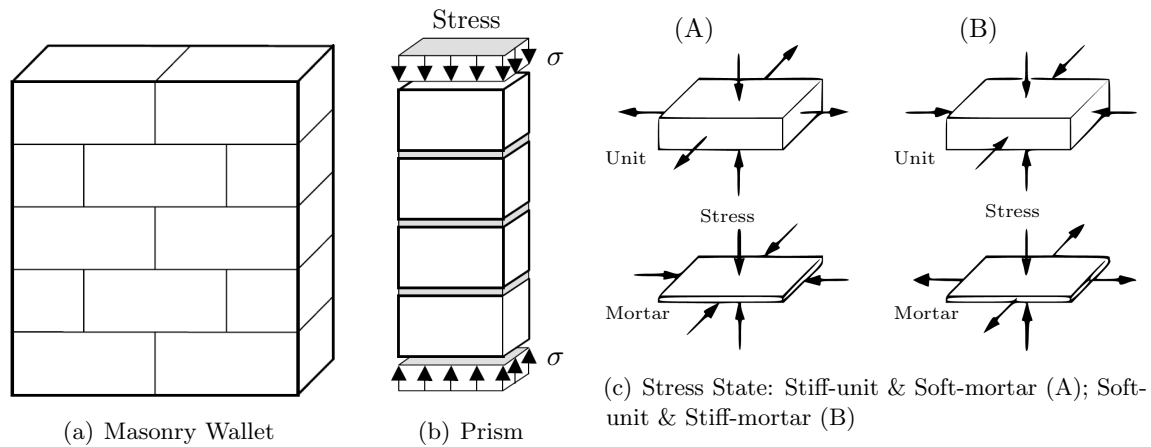


Figure 4.4: (a) Masonry Wallet, (b) Stacked Bond Prism, and (c) Unit-Mortar Stress State (Zucchini and Lourenço, 2007; Wu *et al.*, 2013)

Figure 4.4 shows a graphical representation of a masonry wallet, a typical stacked bond prism under uniaxial compressive stress and the resulting internal stress states of unit and mortar which are dependent on their respective stiffnesses. Failure in masonry is generally correlated to the difference in elastic properties of its constituents (Zucchini and Lourenço, 2007), with the stress states initiating vertical cracks in the units (Wu *et al.*, 2013).

4.2.1 Testing Specifications

The uniaxial compressive strength of masonry is required in order to perform the in-plane shear test on masonry walls, as the pre-compression levels are determined from the compressive strength. As mentioned earlier, masonry wallets provide a better indication of the masonry uniaxial compressive strength, therefore these are used in this study.

Guidelines provided in BS EN 1052-1 (1999): *Methods of test for masonry - Part 1: Determination of compressive strength*, are followed to perform the uniaxial compressive strength and the modulus of elasticity tests on masonry wallets subjected to a load applied at right angle to their bed joints. The South African standards SANS 10164-1 (1989) provides practical guidelines for the design of loadbearing URM walls, constructed in areas other than earthquake prone areas.

The testing machine required should be able to apply an evenly distributed compressive load onto the specimen such that uniform displacements are induced across the loaded area. The standard specifies that at least three masonry specimens should be tested, the sizes of which are dependent on the unit sizes, as shown in Figure 4.5.

CHAPTER 4. MECHANICAL PROPERTIES OF MASONRY STRUCTURAL ELEMENTS

Each specimen is built on a flat horizontal surface, in such a way that the top and bottom load distribution faces are flat and parallel to each other. During the construction of the specimens, samples of the mortar used should cast in cubes and tested for compressive strength at the age at which wallet specimens are tested. For the first three days after they are built, the specimens should receive appropriate curing to prevent drying.

At the time of test, the specimen is placed centrally and in full contact with the testing apparatus. The applied load is gradually increased such that failure of the specimen occurs after 15 to 30 minutes from the commencement of loading. To determine the modulus of elasticity, displacement measuring devices are fitted onto the specimens to measure the change in height.

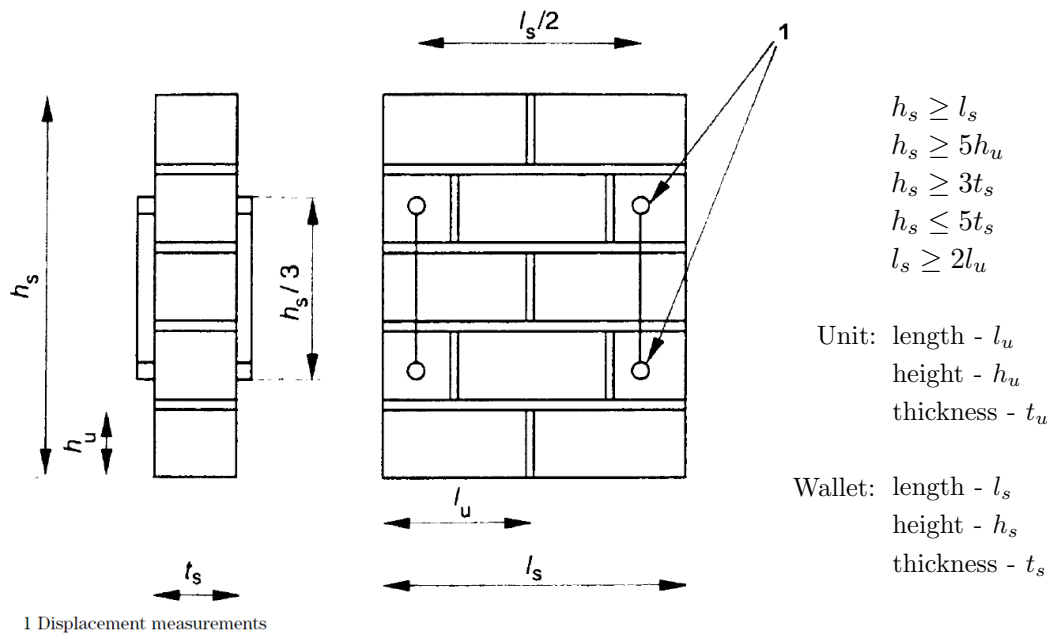


Figure 4.5: Masonry Wallet Specimen

The required measurements to be recorded include: the loaded cross-section dimensions, the maximum load attained, the load when cracks appeared, the time elapsed between the commencement of loading until the maximum load, and the displacement at the four points shown in Figure 4.5. Once the test is completed, the compressive strength of each masonry specimen is calculated using Equation (4.7).

$$f_i = \frac{F_{i,max}}{A_i} \quad (4.7)$$

Where:

- f_i Compressive strength of the masonry specimen, [N/mm²]
- $F_{i,max}$ Maximum load reached by each specimen, [N]
- A_i Loaded cross-sectional area of the specimen, [mm²]

CHAPTER 4. MECHANICAL PROPERTIES OF MASONRY STRUCTURAL ELEMENTS

The modulus of elasticity is then calculated, using Equation (4.8), as a secant modulus from the mean of the strains at the four measuring positions and obtained at a stress equal to a third of the maximum stress achieved.

$$E_i = \frac{F_{i,max}}{3 \times \varepsilon_i \times A_i} \quad (4.8)$$

Where:

E_i	Modulus of elasticity, [N/mm ²]
ε_i	Calculated mean strain

The mean compressive strength (f) and the modulus of elasticity (E) of the wallet specimens tested are calculated thereafter to the nearest 0,1 N/mm².

4.3 Density

Also investigated in this study is the density of a masonry unit, a physical property used in numerical modelling. For the unit manufacturing process as well as mechanical property tests, the density can be related to packing of materials and is used as quality control.

The purity of materials and the unit manufacturing process influence the density. In structural masonry, and in the design of loadbearing walls, the density is an important characteristic of masonry unit as it influences the weight of the wall, as well as the compressive strength and thermal properties of the unit (Fourie, 2017). It is generally recognized that the denser the unit, the higher its compressive strength. However, higher unit density may result in an increase of the units cost if they are not produced near the construction site, and a decrease in the thermal resistance (Deboucha and Hashim, 2011).

Based on the properties of the constituent material, the density of masonry units varies from one unit type to another. It is often used to classify the various types of concrete masonry blocks (i.e. dense, lightweight, aerated). The density of concrete block as well as AACB increases with age, the former due to the geopolymerisation reaction and the latter due to the hydration process of concrete. Table 4.1 shows the range of densities of various masonry units.

Table 4.1: Densities of Various Masonry Units

Masonry	Density, [kg/m ³]	Source
Dense concrete blocks	1700 - 2200	(Deboucha and Hashim, 2011)
Lightweight concrete blocks	600 - 1600	
Aerated concrete blocks	400 - 950	
Fired clay bricks	1400 - 2400	
Calcium silicate bricks	1600 - 2100	
CSEBs	1700 - 2200	
AACBs	1800 - 2300	(Abdullah <i>et al.</i> , 2015)
Adobes	1570 - 2000	(Brown and Clifton, 1978)

CHAPTER 4. MECHANICAL PROPERTIES OF MASONRY STRUCTURAL ELEMENTS

4.3.1 Testing Specifications

Guidelines provided in the European standard [BS EN 772-13 \(2000\)](#): *Methods of test for masonry - Part 13: Determination of net and gross dry density of masonry units*, are followed for the density tests performed on the manufactured masonry units.

Placed in a well ventilated oven, which can maintain a temperature of $70 \pm 5^\circ\text{C}$, the specimen units are dried to a constant mass (m_{dry}) which is achieved when the mass loss observed after two subsequent unit weighing within a 24 hours interval, is not more than 0.2% of the total mass.

Once the constant mass is reached, the volume (V_n) of the specimen is determined based on the unit dimensions (length \times width \times height) and subtracting any indentations. The dry density (ρ) is calculated using Equation (4.9).

$$\rho = \frac{m_{dry}}{V_n} \quad (4.9)$$

4.4 Conclusion

In this chapter, a description was given of the mechanical properties of masonry structural elements which are investigated in this study through the following tests: compressive strength and modulus of elasticity tests of units, masonry wallets and mortar; and unit density tests. These tests were performed using different testing standards and procedures due to the lack of prescribed South African standards. However, where possible, the guidelines provided by the South African standards were followed. In the next chapter, there will be a discussion on the experimental test set-ups used to performed these tests during this study.

Chapter 5

Experimental Design

This chapter presents the various test set-ups that were used to perform the experimental tests outlined in this study. These tests include the compressive strength and the modulus of elasticity tests performed on units, on masonry wallets as well as on mortar; and the density test and the in-plane shear-compression test conducted on masonry walls. While some of the test set-ups were adopted from previous studies, the set-up for the shear-compression wall test was designed and constructed by the researcher of this study.

5.1 Compressive Strength Test

5.1.1 Masonry Unit Test

For each type of masonry unit, compressive strength tests were conducted at 28 days and at the time of the in-plane shear wall tests. The units selected for the test were randomly picked to ensure that the compressive strength test results give a good representation of the strength of units manufactured on different days. In the case of the tests performed at 28 days of age, eight specimens were selected from eight different manufacturing days.

The compressive strength test was performed using a 2MN Instron Materials Testing Machine and the testing procedures outlined in [BS EN 772-1 \(2011\)](#) were followed. This test had previously been conducted at Stellenbosch University with a loading rate chosen to be 0.75 mm/min. While the rate used for this study was selected in accordance to the guideline, due to the large difference in compressive strength between units, the units with higher strength took longer to reach failure.

Before starting the test, each specimen needed to be grinded to ensure that the top loading face was flat, horizontal and parallel to the bottom face. The specimen was then weighed for quality control, and the dimensions of the loading face measured. The specimen was then placed in the testing machine and in the bedface orientation between two 20mm steel plates through which the load was applied as shown in [Figure 5.1](#). After the peak load was attained, the load application continued until a 50% load reduction of the peak load was reached.

Once the test was completed, the peak load from the Instron Testing Machine was recorded, while the steel plates were cleaned and prepared for the next test. The compressive strength (f_u) of each masonry unit was then determined using [Equation \(4.3\)](#).

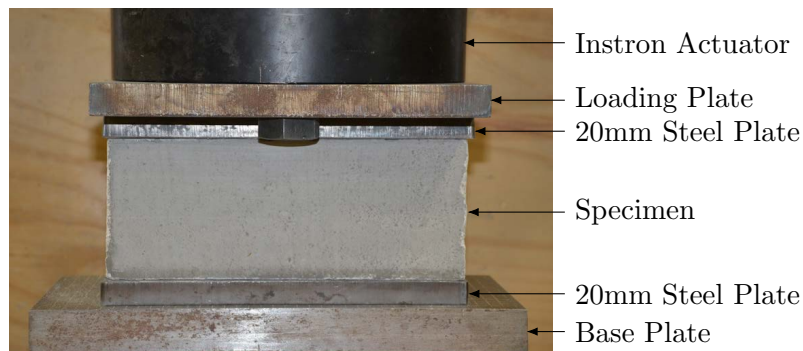


Figure 5.1: Test Set-up for Unit Compressive Strength

5.1.2 Mortar Test

Four different mortar types, used in the construction of masonry wallets and walls, were designed to have approximately similar compressive strength as the masonry unit type. Three cube specimens of 100mm side dimension were cast for each mortar type. The cubes were left to dry in the moulds for 24 hours after which they were removed and placed in the curing tank until tested at 7 days of age (age at which wall specimens were tested).

The test was performed immediately after removing the specimens from the curing tank. Using a Contest Grade A compression testing machine which is operated at a loading rate of 180 kN/min, the load was applied on the plane faces that were in direct contact with the surface of the mould, until failure. The peak load at failure was recorded and the compressive strength (f_m) was determined as described in Section 4.1.1.2.

5.2 Modulus of Elasticity Test

When conducting modulus of elasticity tests, the guidelines provided in [BS EN 12390-13 \(2013\)](#) were followed for the secant modulus of elasticity, and [ASTM C469/C469M-14 \(2014\)](#) for the chord modulus of elasticity. The two standards were adopted mainly because of the use of various testing machines and the difference in shape of the test specimens.

The CMU, CSEB and Adobe specimens were prismatic specimens cut from the masonry units respectively. The dimensions of these specimens were determined according to [BS EN 12390-13 \(2013\)](#) such that the length to width ratio L/d fell in the range $2 \leq L/d \leq 4$. As the unit is used in the masonry in the bedface orientation, the height of the unit (116mm) was therefore the length of the specimen. Based on the range of L/d ratio recommended in the standard, the maximum value of d was calculated to be 58mm which was adopted as the width of the prismatic specimen.

The three above-mentioned specimens were cut using the laboratory electric table saw cutting machine and were tested using a 2MN Instron Materials Testing Machine. Each specimen had a height of 116mm with squared-shaped top and bottom faces of 58mm side dimension (see Figure 5.2(a)). The top loading face of the CMU and CSEB specimens were slightly grinded in order for the face to be horizontal and parallel to the bottom face, and at a right angle with the specimen sides. This, however, was not done for Adobe specimens due to their weaknesses.

CHAPTER 5. EXPERIMENTAL DESIGN

Four 10mm linear variable differential transducers (LVDTs) were used to measure the deflections of the specimens during the test. The LVDTs were symmetrically fitted around the specimen by means of an aluminium frame designed for this purpose. The aluminium frame consisted of a top bracket, which held the LVDTs in position, and a bottom bracket used as datum. Each bracket had four blunt screws which tightened onto the side faces of the specimen (see Figure 5.2(b)). The frame was placed, using spacers, in such a way that the four LVDTs measured the deflections occurring at about half the height of the tested specimen over a gauge length of 50mm, as shown in Figure 5.2(c).

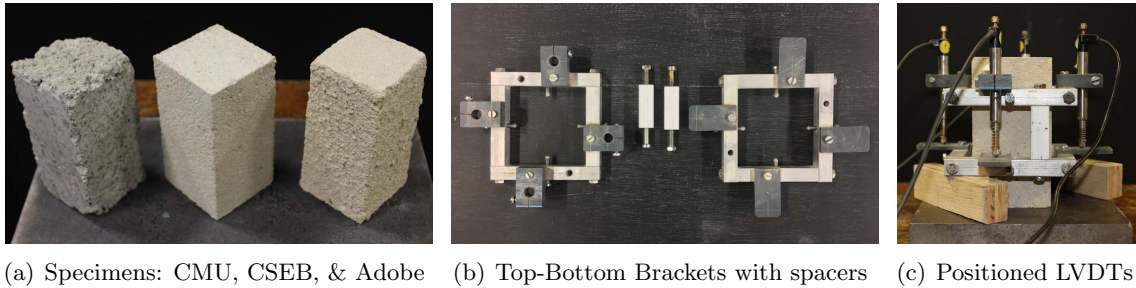


Figure 5.2: Modulus of Elasticity Specimens and Frames

With the LVDTs in position, the specimen was placed at the centre of the testing machine's actuator, in between steel platens and on top of an external 2MN load cell (LC) which recorded the applied load. The test data including the displacements measured by the LVDTs, the applied load readings from both the Instron testing machine and the 2MN LC, were recorded using an HBM Spider 8 data acquisition system. The test set-up with a typical specimen are shown in Figure 5.3.

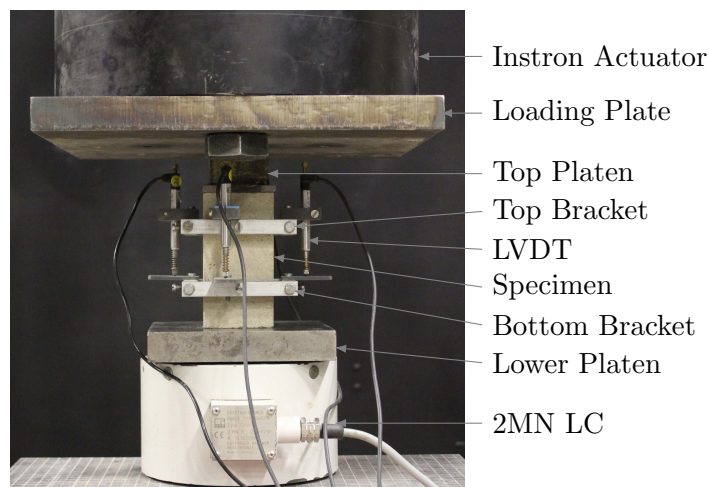


Figure 5.3: Modulus of Elasticity Test Set-up for Prismatic Specimens

The test was conducted following Method B as provided in the standard. A companion specimen, of similar shape and size as the test specimen, was used to determine the compressive strength required to determine the stress levels of loading cycles needed for the test. The strength of

CHAPTER 5. EXPERIMENTAL DESIGN

these specimens was so low that the loading rate of 0.6 ± 0.2 MPa/s provided in the standard needed to be reduced. For the CMU and CSEB specimens, the lower bound of the loading rate was reduced by a factor of 10 to 0.04 MPa/s which translated, for the testing machine and based on the specimen loading face area, to a loading rate of approximately 135 N/s. This new loading rate was still too high for the Adobe specimen because of the lower strength of these specimen. It was then decided to further decrease the loading rate by a factor of 10 to 0.004 MPa/s which translated to approximately 13.5 N/s.

A preload of 500N was adopted for CMU and CSEB specimens and 100N for Adobe specimens. The lower and upper load for the loading cycles were determined as specified in [BS EN 12390-13 \(2013\)](#). Once the test was completed, the specimen was tested to destruction in order to determine its compressive strength. With the data recorded from the tests, the stabilised secant modulus of elasticity was calculated as described in Section [4.1.2](#).

Prismatic specimens were created to determine the modulus of elasticity according to the orientation in which the masonry units are used within a masonry assemblage. However, due to the stone content in the AACB mixes, it was not possible to properly cut prismatic specimens. As these blocks were created by casting and not compaction, it was therefore decided for cylinders to be cast from the AACB mixes during the manufacturing process. The cylinder mould used produced specimens of a height of 200mm and a diameter of 100mm.

A Contest Grade A compression testing machine, which was not able to execute programmable loading cycles as recommended in [BS EN 12390-13 \(2013\)](#), but was able to apply loads at constant rate within the stress range of 0 to 40% ultimate compressive strength. [ASTM C469/C469M-14 \(2014\)](#) was then adopted and used to determine the chord modulus of elasticity of AACB. The actuator of the Contest machine has a bearing that compensates for any irregularity in the specimen and allows for a pure uniaxial compressive test to be conducted.

Three LVDTs, mounted on a frame consisting of two aluminium rings, were fitted around the cylindrical specimen and used to measure the deflections at about half the height of the tested specimen and over a gauge length of 70mm. [Figure 5.4](#) shows the aluminium frame, a cylindrical specimen, and the test set-up with a cylindrical specimen positioned on top of a 2MN LC.

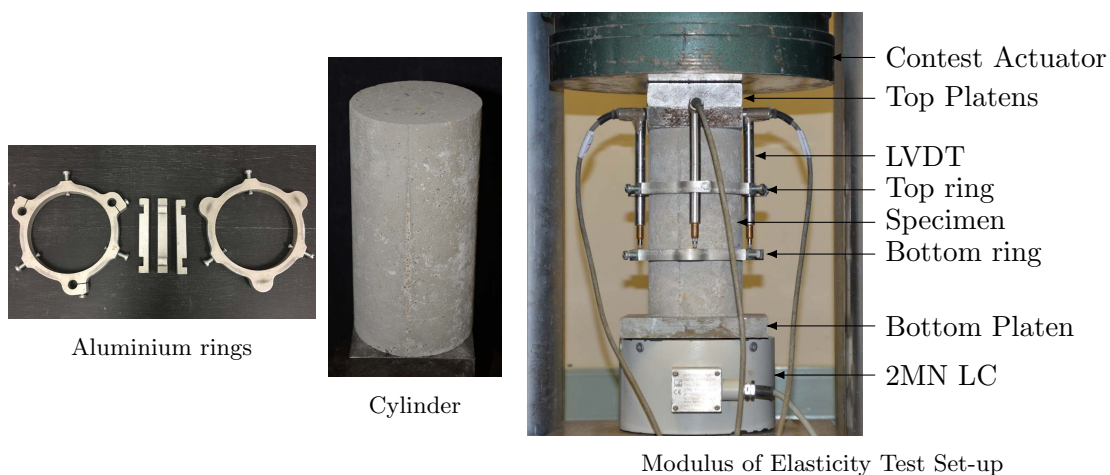


Figure 5.4: Set-up for Cylindrical Specimens

CHAPTER 5. EXPERIMENTAL DESIGN

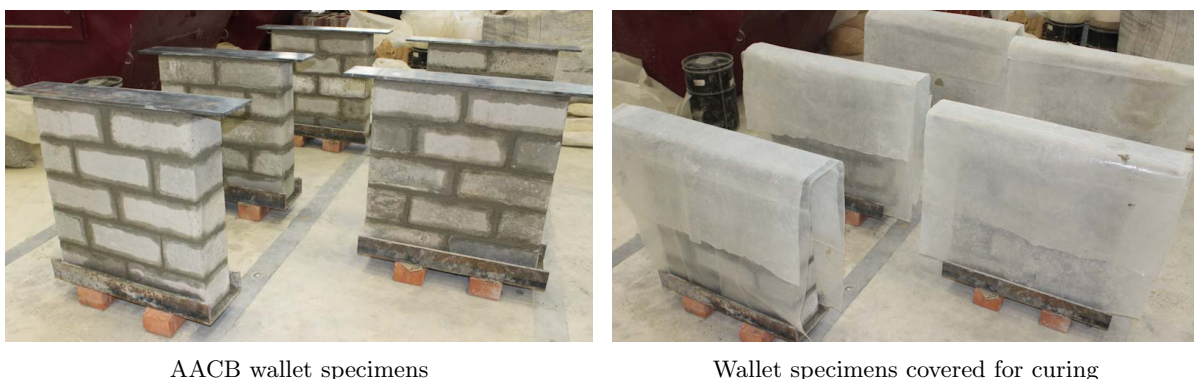
The compressive strength used for the stress limit was determined by testing three companion cylinders and by taking the average of the results. The load was then applied in three cycles by the Contest testing machine, with a loading rate of approximately 90 kN/min and was manually stopped and started between the stress range of 0 to 40% compressive stress.

The test data were also recorded using the HBM Spider 8 data acquisition system. For each specimen test, the stress-strain graph was plotted from the results and used to determine the chord modulus of elasticity as outlined in Section 4.1.2. It should be noted that cylinder specimens were also cast for all the four mortar types and their modulus of elasticity were determined in the same manner as for the AACB specimens. The compressive strength of each mortar cylinder specimen was approximated by reducing the respective cube strength by a factor of 0.8.

5.3 Tests on Masonry Wallets

The uniaxial compressive strength and the modulus of elasticity of masonry were investigated through experimental tests following the guidelines provided in [BS EN 1052-1 \(1999\)](#). The standard recommends that the dimensions of the masonry wallets be based on the unit dimensions. As represented in Figure 4.5, the masonry wallets were constructed with ten masonry units bonded together with mortar of joint thickness of 10mm. Based on the unit dimensions and recommendations from the guidelines, the masonry specimen had a length of approximately 590mm and a height of 610mm.

All the masonry wallets were built inside a steel channel section by a professional bricklayer. Care was taken to ensure uniformity between the specimens and that the top and bottom loading faces had flat horizontal surfaces and were parallel to each other and orthogonal with the main axis of the specimen. To provide similar boundary conditions between the top and bottom loading faces, 10mm steel plates were mortared at the top of the specimens which were also kept horizontal as shown in Figure 5.5. The specimens were cured for three days by covering them with polyethylene sheets and then kept uncovered until the day they were tested.



AACB wallet specimens

Wallet specimens covered for curing

Figure 5.5: Wallet Specimens

Due to the protracted block manufacturing process it was not practical to create wallets of exactly 28 day age. While the units within the wallets were not at 28 day age at the time of testing, all the wallets were tested at seven days after they were constructed. While the specimens were

CHAPTER 5. EXPERIMENTAL DESIGN

being constructed, a sample of mortar taken from the mason's board was cast into cubes and tested for compressive strength at the same period as the masonry specimen tests.

Five specimens were constructed for each masonry unit type and were subjected to compressive strength tests. The modulus of elasticity was determined on four of these specimens by positioning four 100mm LVDTs around the specimen. The LVDTs were positioned using LVDT mounts glued onto the two large faces of the specimen, and on each face, the distance between two LVDTs was 360mm with a gauge length of 210mm. These dimensions were adopted from those used by [Fourie \(2017\)](#) although slightly different from those suggested in the standard.

A 2MN Instron Materials Testing Machine was used to carry out the test, with a steel spreader beam attached to the Instron actuator. The masonry specimen was carefully positioned by means of an overhead crane on one side of the Instron testing machine, just below and in parallel with the spreader beam. The specimen was then placed unto small steel rods at the base of the apparatus, which acted like rollers and allowed the positioning of the specimen at the centre of the testing machine. Finally, the steel bars were carefully removed ensuring that both the top and bottom faces of the specimen were in contact with the apparatus.

The load was then applied at the top of the specimen with its magnitude increasing at a constant rate until failure. As the units were of different types with different strengths, the loading rates for the CMU, CSEB, Adobe and AACB were respectively 0.4 mm/min, 0.25 mm/min, 0.2 mm/min and 0.3 mm/min. These rates were selected to ensure each specimen failed between 15 to 30 minutes from the moment the loading was applied. Shown in Figure 5.6 is the test set-up with an AACB wallet specimen placed in the testing machine.

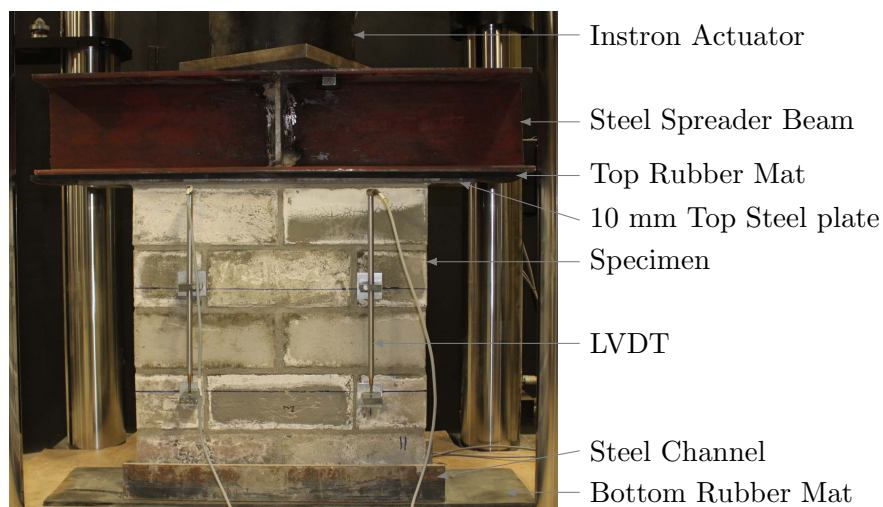


Figure 5.6: Masonry Wallet Test Set-up

Initially only one 10mm thick rubber mat was positioned between the top of the wallet and the steel spreader beam to ensure full contact. However, after testing CMU wallets, a second rubber mat was also placed at the bottom of the specimen (see Figure 5.6), providing similar boundary conditions. After the compressive strength test of the first specimen was completed, the maximum compressive load achieved was recorded. The remaining specimens to which were attached LVDTs were successively tested in the same manner as the first specimen. To prevent

CHAPTER 5. EXPERIMENTAL DESIGN

damaging the LVDTs, they were removed once the load being applied reached approximately 50% of the recorded maximum load.

The measured displacement at the four points of the specimen as well as the applied compressive load from the Instron testing machine, were recorded using the HBM Spider 8 data acquisition system. The masonry compressive strength as well as the modulus of elasticity were calculated as averages of the obtained results using the equations provided in Section 4.2.1.

5.4 Density test

The dry density test was conducted following the guidelines provided in [BS EN 772-13 \(2000\)](#). For each masonry type, six units were subsequently tested by placing them in a well ventilated oven kept at a constant temperature of 70°C and after their initial masses were recorded.

Every 24 hours, the units were taken out of the oven, left to cool for a few minutes before their masses were recorded. The process was repeated until a constant mass of each specimen was achieved. As defined in the standard, the constant mass is achieved when the mass loss between two subsequent weighing of the specimen, within a period of 24 hours, is lower than 0.2% of the total mass.

With a known volume of each specimen, the dry density was determined by dividing the achieved constant mass by the specimen volume. Taking an average of the six specimens, the dry density of a given masonry type was thus determined.

5.5 In-plane Shear-Compression Test

This section presents the designed set-up for the in-plane shear-compression test carried out on the CMU and AMUs URM walls. The objective was to design a test set-up that would use materials already available in the laboratory and which, once built, will necessitate as little adjustments as possible.

As a test set-up for in-plane shear wall test is not currently provided in design standards, a review of literature, presented in Chapter 2, was necessary in order to understand the nature of the test set-up and to learn from existing designs suggested by various researchers.

Experimental shear wall tests have previously been conducted on small walls at Stellenbosch University, as described in Section 2.7.4. However, the walls tested for this research study were larger than the dimensions of the walls for which the existing test set-up had been created and other devices needed to be used for the application of loads. A new test set-up was therefore necessary. From the existing set-up, the column was kept and used as a reaction and support member for the Enerpac hydraulic jack applying the horizontal force.

The general outcomes for the new test set-up were as follow;

- The wall dimensions were determined such that they were representative of walls of a typical Category 1 building, with the maximum length being 6m, and according to the amount of time available to manufacture enough blocks for one wall;

CHAPTER 5. EXPERIMENTAL DESIGN

- Based on the testing equipment available in the laboratory, the pre-compression force was to be applied by the Instron testing machine through a stiff spreader beam, and the horizontal force by an Enerpac hydraulic jack;
- To avoid damage on the wall specimens, they were to be built under the test set-up and tested at 7 days of age;
- Although different types of failure modes may occur during a shear wall test, especially for a single storey building, diagonal shear failure on walls was sought, as this type of failure would indicate a lower displacement capacity compared to other failure modes.

In order to achieve these outcomes, few questions needed to be answered. Some of these questions were in relation to the exact dimensions of wall specimens, the reaction elements (structural frame) for the testing machine applying the vertical and horizontal forces, the size and length of the spreader beam, the type of foundation for the wall, the connection between the wall and the spreader beam, and the prevention of the out of plane movements of the spreader beam.

5.5.1 Wall Specimens

Masonry walls are built by joining masonry units, using mortar, in a determinate geometric pattern. This assembly forms a heterogeneous material which is used in various ways such as structural elements, space subdivision, thermal insulators, protection against fire and weather, and acoustic insulators (Hendry *et al.*, 1997).

As structural elements, masonry walls are designed and built to resist service loads and minimize, throughout their lifetime, deflection, cracking and collapse. The walls are built on stiff foundations which transfer to the ground the loads applied on the wall. A detailed explanation of the design of masonry structures is not pursued in the present study, however various literatures, such as Hendry *et al.* (1997), can be consulted.

In practice, different arrangements between masonry units and mortar joints can be adopted, as illustrated in Figure 5.7. Masonry structures in South Africa, including Category 1 buildings are typically built in the stretcher bond pattern. This pattern is therefore adopted for the walls built in this experimental study.

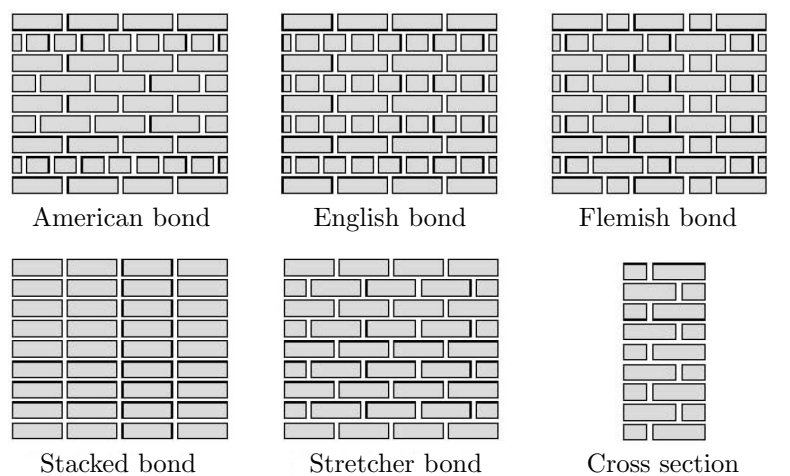


Figure 5.7: Masonry Bonds Adopted in Practice (Pelà, 2009)

CHAPTER 5. EXPERIMENTAL DESIGN

Due to the limited time available for the block manufacturing and the number of experimental tests required for this study, the length (l_w) of the walls was to be 1.8m. With an aspect ratio of 1.2 (l_w/h), the height (h) was therefore 1.5m. With these dimensions, it was sought to construct a wall that would be sufficiently squat to result in diagonal shear failure mode during the shear-compression wall test. Both bed and head mortar joints in the walls were about 10mm thick, the wall had 6 units in length and 12 units in height, the wall dimensions were then, $1800\pm 5 \times 1500\pm 5 \times 140$ mm, as shown in Figure 5.8.

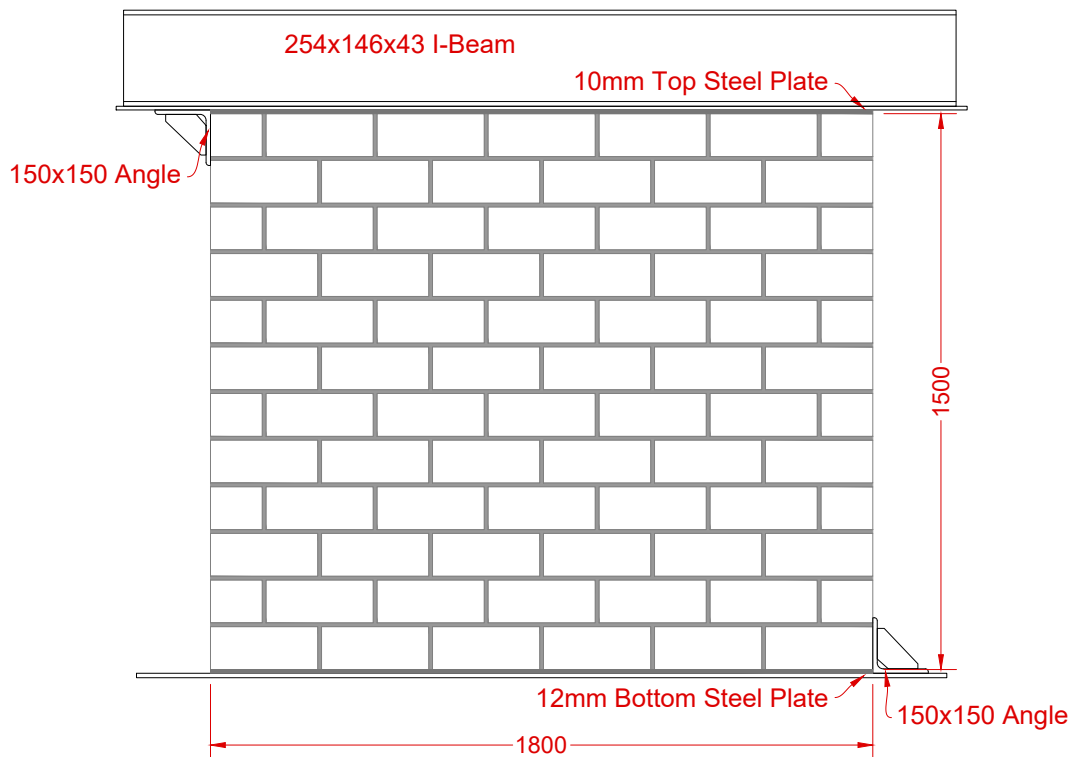


Figure 5.8: Dimensions of Wall Specimen

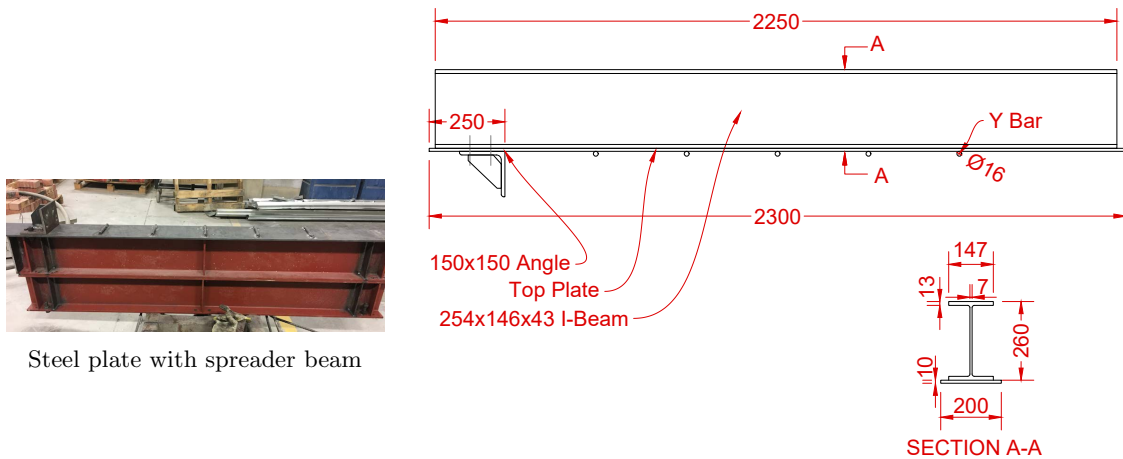
The laboratory strong floor was used as the foundation of the wall. As shown in Figure 5.9, a 12mm thick steel plate was connected to the strong floor, with four M30 high tensile studs, through connecting holes in the floor, spaced in a 920mm x 920mm grid. As the diameter of holes in the floor was larger than the high tensile studs, steel bushes were used to reduce, to a minimum, horizontal movements of the plates which may happen while performing the test.

With a strong mortar (mix shown under “All Units” in Table 3.7), the wall was built on the steel plate which had 16mm diameter Y bars welded onto it. The Y bars were spaced at 300mm which added mechanical friction on the steel plate and the wall interface, ensuring that failure will not occur at the interface. A 150x150 steel angle, bolted to the steel plate, prevented horizontal movement at the bottom of the wall.

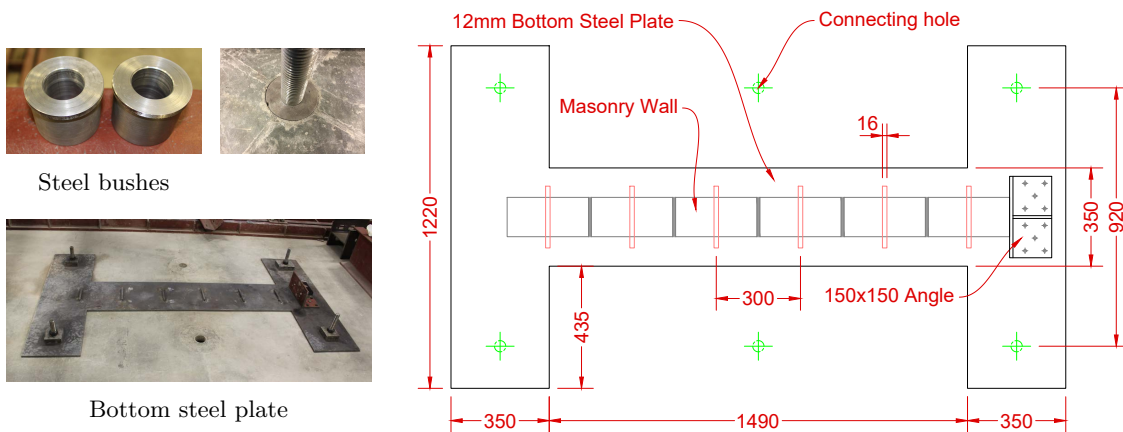
With the Y-bars welded onto the plate, a few CMUs and Adobe blocks were created with a 20mm groove cut (see Figure 5.10) during the compaction process to allow for the bars to go through the grooves and maintain the 10mm mortar thickness at the bottom of the wall. It was difficult, however, to create CSEBs and AACBs with grooves. For this reason, a thicker mortar was used for the walls built with these blocks.

CHAPTER 5. EXPERIMENTAL DESIGN

At the top of the wall, a 10mm steel plate, connected to the spreader beam, was mortared to the wall. In the same manner as the bottom plate, the top plate had 16mm Y bars welded onto the plate (see Figure 5.9) and a stronger mortar was used as mentioned earlier. The top steel plate was attached to one 254x146x43 I-section beam throughout the whole duration of the experimental study. A 150x150 steel angle, bolted to the steel plate and I-section beam, contribution to the transfer of the horizontal load from the beam to the top of the wall. The connecting bolts were regularly checked to ensure that the plate and the beam were tightly connected.



Dimensions of top steel plate and I-beam



Dimensions of bottom steel plate

Figure 5.9: Top and Bottom Steel Plates

The walls were built by a skilled bricklayer who maintained the same quality and consistency in the mortar thickness for all the specimens. Figure 5.10 shows a typical construction of a wall specimen. The masonry units were taken directly from their curing locations and were not soaked in water before building the wall. CMUs, however, were wet as they were taken directly from the curing tanks.

CHAPTER 5. EXPERIMENTAL DESIGN

The wall specimens were built one at a time and tested at seven days of age. For each wall, cube and cylinder mortar samples were cast with the mortar taken from the pan mixer. These were used to carry out the compressive strength and modulus of elasticity tests for the mortar. Half blocks were cut with a saw cutting machine to be used for the construction of the wall. This, however, was difficult for AACBs because of the presence of 13mm stones in them. For this specimen, half blocks were cast in the wooden moulds during the manufacturing process. Once built, the wall was left to set for two to three days before placing, on a mortar layer, the top steel plate with the beam. The beam was positioned on top of the wall by means of an overhead crane, which was also used to level the beam. Once levelled, the beam was left attached to the overhead crane for two days to allow the top mortar joint to set, then the second beam was placed on top of the first beam. After each test, the beams were removed one after the other using the overhead crane.



Figure 5.10: Typical Construction of a Wall Specimen

For each unit material type, two walls were built and tested. Hence a total of 8 walls were investigated by subjecting each of them to a shear-compression test. The test results presented in this study will further contribute to the on-going studies on AMUs.

5.5.2 Test Set-up and Procedure

The test set-up was built from structural steel elements available in the laboratory. A structural frame, built with two 254x254x89 H-section columns and two C381x102 beams, was used as supporting and reacting frame for the Instron actuator, attached vertically to the channel beams, and the Enerpac hydraulic jack, connected horizontally to a shorter 254x254x89 H-section column, which was bolted to one column, and two PC 180x70 providing lateral support to the column.

The channel beams were connected to the columns with angle cleats and the whole frame was post-tensioned to the 500mm thick strong floor of the laboratory. All connections and structural elements were checked to ensure that no structural failure would occur if the Instron actuator was to be used to its maximum capacity.

CHAPTER 5. EXPERIMENTAL DESIGN

The vertical Instron testing machine, which has a maximum capacity of $\pm 500\text{kN}$ and 100mm stroke, was used to apply the pre-compression force onto the wall specimen through two 254x146x43 I-section beams, bolted together. The two beams acted as one single deep beam ($\pm 510\text{mm}$) hence forth referred to as spreader beam, and ensured that the applied pre-compression force was distributed evenly at the top of the wall. A bridge bearing (see Figure 5.11(a)), positioned between the Instron and the spreader beam, was used to allow horizontal movement of the beam during the test, to ensure that the horizontal load would not go through the Instron and to provide a frictionless connection in the horizontal direction.

The test set-up also comprised of two lateral support frames which were connected, and could also be moved along a railing system attached to the strong floor. A sliding system - consisting of four small steel plates, each with a roller, and attached to the lateral support frames on each sides of the spreader beam - was designed to prevent any out-of-plane movements of the spreader beam. The sliding system served as a guide to the spreader beam through steel angles bolted to the flange, as shown in Figure 5.11(b). Vertical roller supports, also connected to lateral support frames, were positioned at about 15mm below the spreader beam and steel plate (shown in Figure 5.11(d)). Their purpose was to provide support to the spreader beam in case of unexpected failure. However, during each test and as a safety measure, the spreader beam was loosely attached to the overhead crane on the hooks at each ends of the spreader beam (Figure 5.11(c)).

The application of the horizontal force was achieved with an Enerpac hydraulic jack of 60Tons capacity, reacting on the supporting frame column and located at about 1675mm from the laboratory strong floor. A LC with a capacity of 50 t (tonne) was attached to the hydraulic jack which was operated with a manual hand pump and applied the force to the top of the wall through a stiffener (see Figure 5.11(d)) welded to the spreader beam and the steel angle bolted to the top steel plate and the beam.

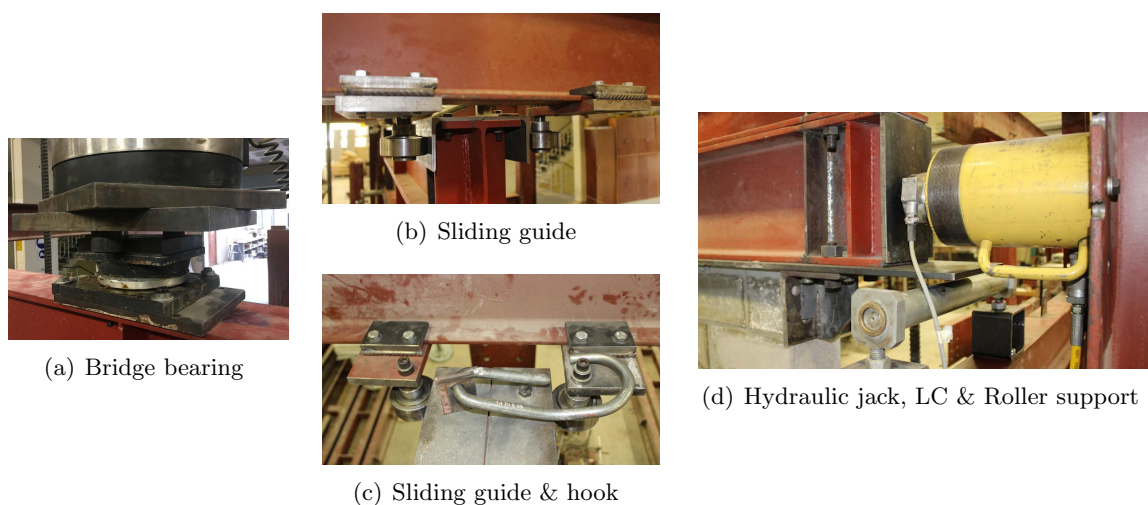


Figure 5.11: Various Elements of the Test Set-up

Figure 5.12 shows the drawing of the designed test set-up where the wall specimen, the loading system, and the lateral steel support frames can be seen.

CHAPTER 5. EXPERIMENTAL DESIGN

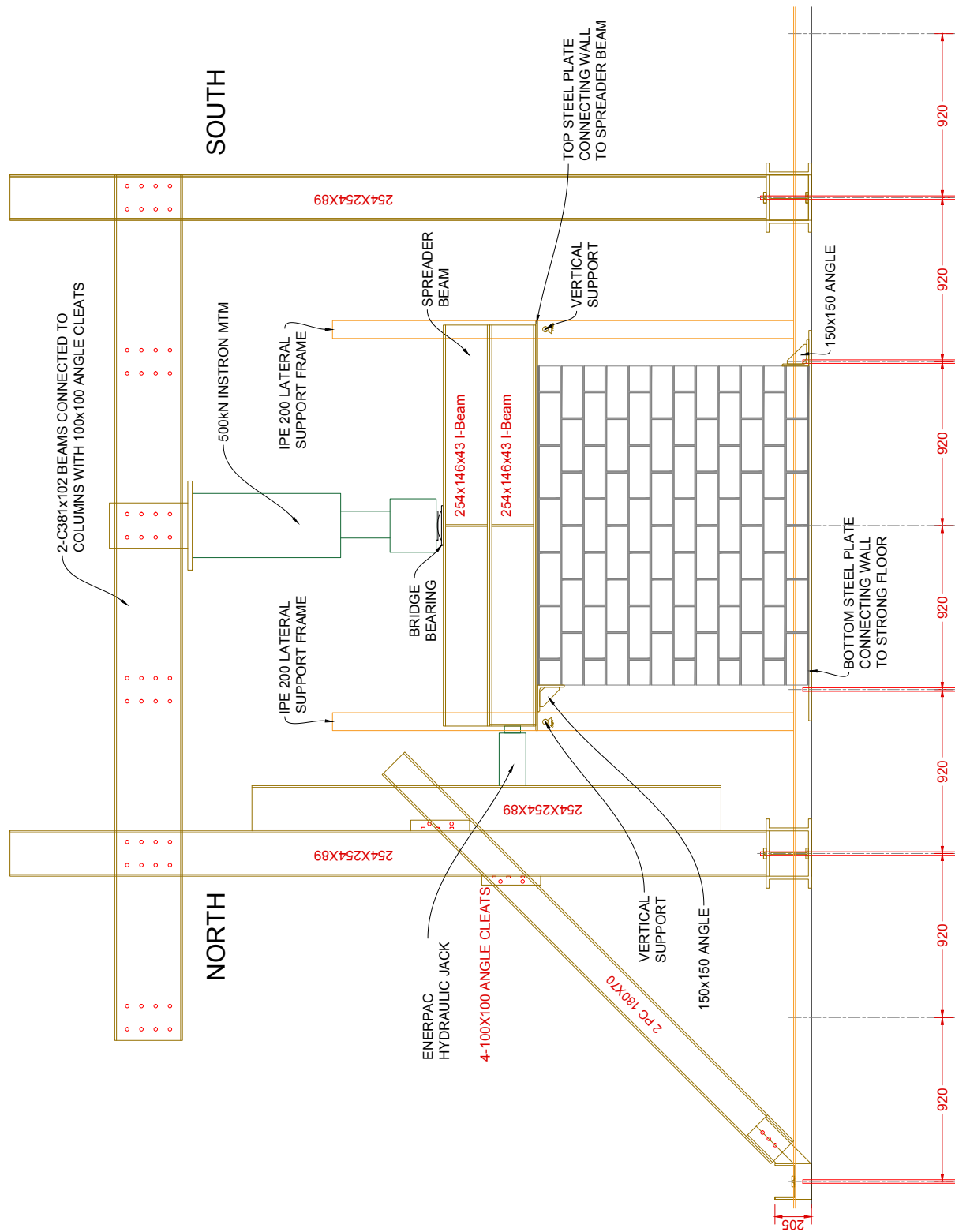


Figure 5.12: Drawing of Test Set-up A (all dimensions in mm)

CHAPTER 5. EXPERIMENTAL DESIGN

The set-up was constructed by the researcher, mainly using steel structural elements available in the laboratory. Safety gear was worn at all times when working in the structural laboratory and when putting in position all the structural elements of the set-up.

A test was first performed on a wall referred to as “mock wall”, constructed with 220x100x75 mm³ imperial bricks. Sourced from a local brick supplier, the imperial bricks had a compressive strength of about 26.47MPa. The test thus performed aimed at investigating the behaviour of the test set-up before testing the walls constructed with the blocks manufactured for this study, and was a way by which the boundary conditions of the system were determined.

The testing programme consisted of applying a pre-compression force using the vertical Instron actuator. The magnitude of the force was determined such that the compressive stress induced on the wall was 15% of the determined compressive strength of the masonry wallet. The force was then maintained constant during the test, as the horizontal force was being applied by the Enerpac hydraulic jack.

For the mock wall test, the applied pre-compression force was 160kN. The wall was able to resist a significant amount of horizontal force and resulted in flexural failure mode and overturning of the wall specimen. The results of this test, which are not presented nor discussed in this study, indicated that a few adjustments to the test set-up were needed to obtain a diagonal shear failure of the wall specimen. Images of the mock wall before and after the test are shown in Figure 5.13. As indicated in Figure 5.12, “NORTH” represents the side of the set-up where the Enerpac hydraulic jack is located.

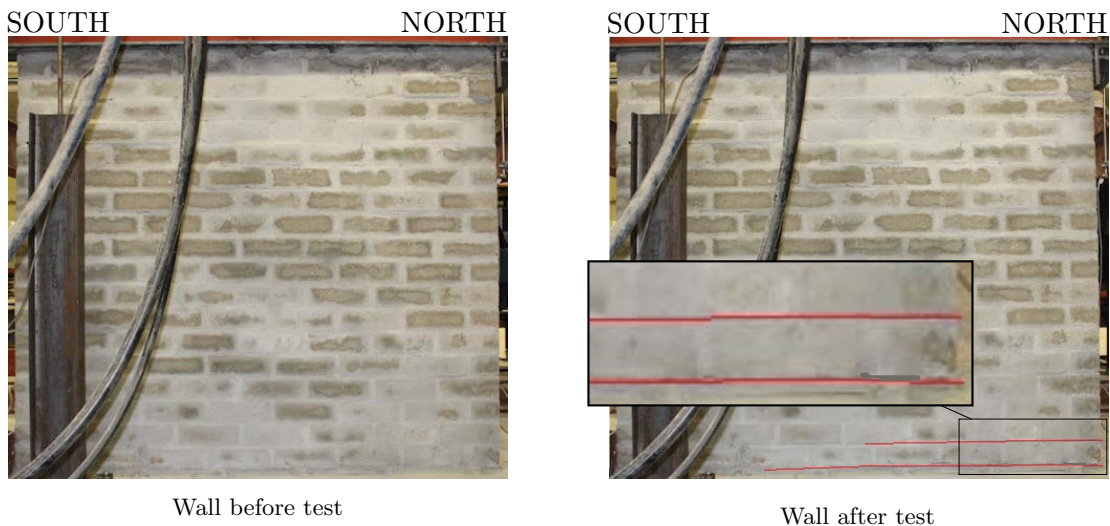


Figure 5.13: First Mock Wall Test

Although overturning of walls can occur in a single-storey building during an earthquake, it was understood that this failure is likely to occur in the experimental test and with the set-up configuration because of the dilatant behaviour of masonry. It was decided then that the set-up configuration, here forth referred to as “Test set-up A”, would be used to test four wall specimens (one of each unit type) and then be adjusted in such a manner to maintain the horizontality of the spreader beam.

CHAPTER 5. EXPERIMENTAL DESIGN

The main change of the test set-up was replacing, from the north side of the set-up, two M30 high tensile studs, connecting the bottom steel plate to the strong floor, with two long 36mm-diameter high tensile steel bars. The bars, connected directly from the bottom of the strong floor, kept the bottom steel plate attached to the floor and were long enough to have a height, extruding from the floor, of approximately 2650mm. Two 150x150 angle sections, 1000mm long, welded together to form a short channel section like beam (Figure 5.14), were placed on top of the spreader beam and were used to provide a fixed configuration of the spreader beam. The increase in rotation of the wall during testing, from the north side, was prevented by the additional lateral beam. This resulted in an increase of the tensile force in the high tensile steel bars, which was monitored by means of a 2MN LC. The lateral beam was connected through the two high tensile steel bars and its position could be adjusted with high tensile nuts. The LC, positioned under the lateral beam, was resting on a second bridge bearing connected to the spreader beam, as shown in Figure 5.14.

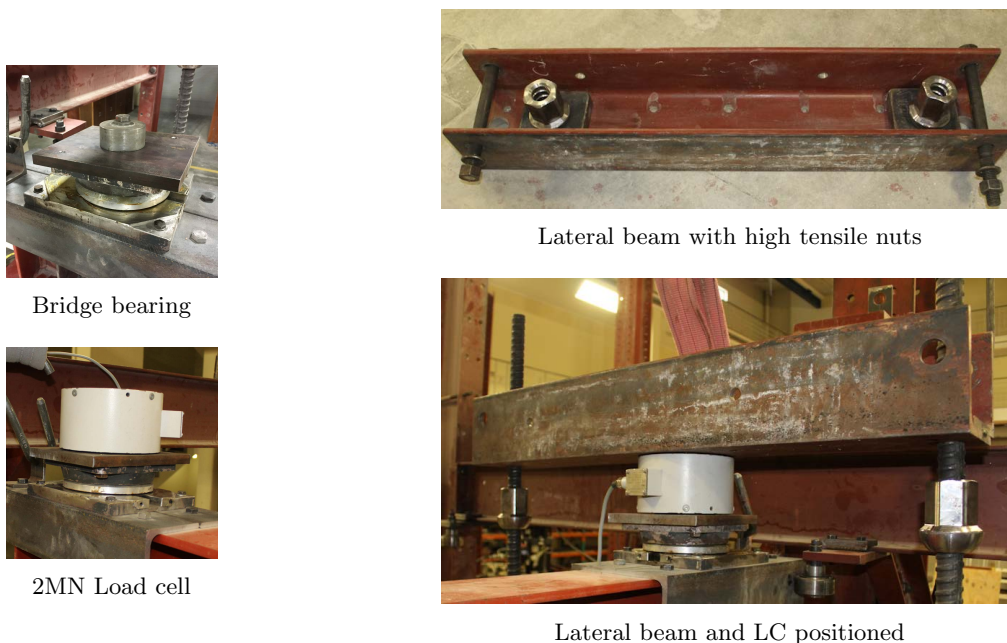


Figure 5.14: Components of Test Set-up B

A second mock wall test was then performed with the new configuration. A new test programme was adopted which consisted of applying the pre-compression force and, once reached, the displacement of the Instron actuator was kept constant throughout the test. The same pre-compression force of 160kN was applied to the second mock wall built with the same type of imperial bricks. Once the force was reached, the Instron actuator was switched from a force to a displacement control configuration. The nuts on the lateral beam were adjusted to lower the beam to the new position of the spreader beam, after which the horizontal force was applied.

The test resulted in a diagonal shear failure of the wall specimen, as shown in Figure 5.15. As this was the failure mode sought to be achieved with the designed test set-up, it was decided that the other four wall specimens would be tested with the new configuration of the test set-up which is referred to as “Test set-up B”.

CHAPTER 5. EXPERIMENTAL DESIGN



Figure 5.15: Second Mock Wall Test

From the obtained results of both mock wall tests, it can be concluded that Test set-up A configuration resulted in a fixed-free or cantilever boundary condition as the in-plane vertical displacement of the spreader beam was not controlled. However, with Test set-up B configuration, the vertical displacement could be controlled resulting in little rotation induced at the top of the wall. Figure 5.16 shows the test set-up with a wall specimen and Figure 5.17, the drawing of Test set-up B.



Figure 5.16: Test Set-up with Wall Specimen

CHAPTER 5. EXPERIMENTAL DESIGN

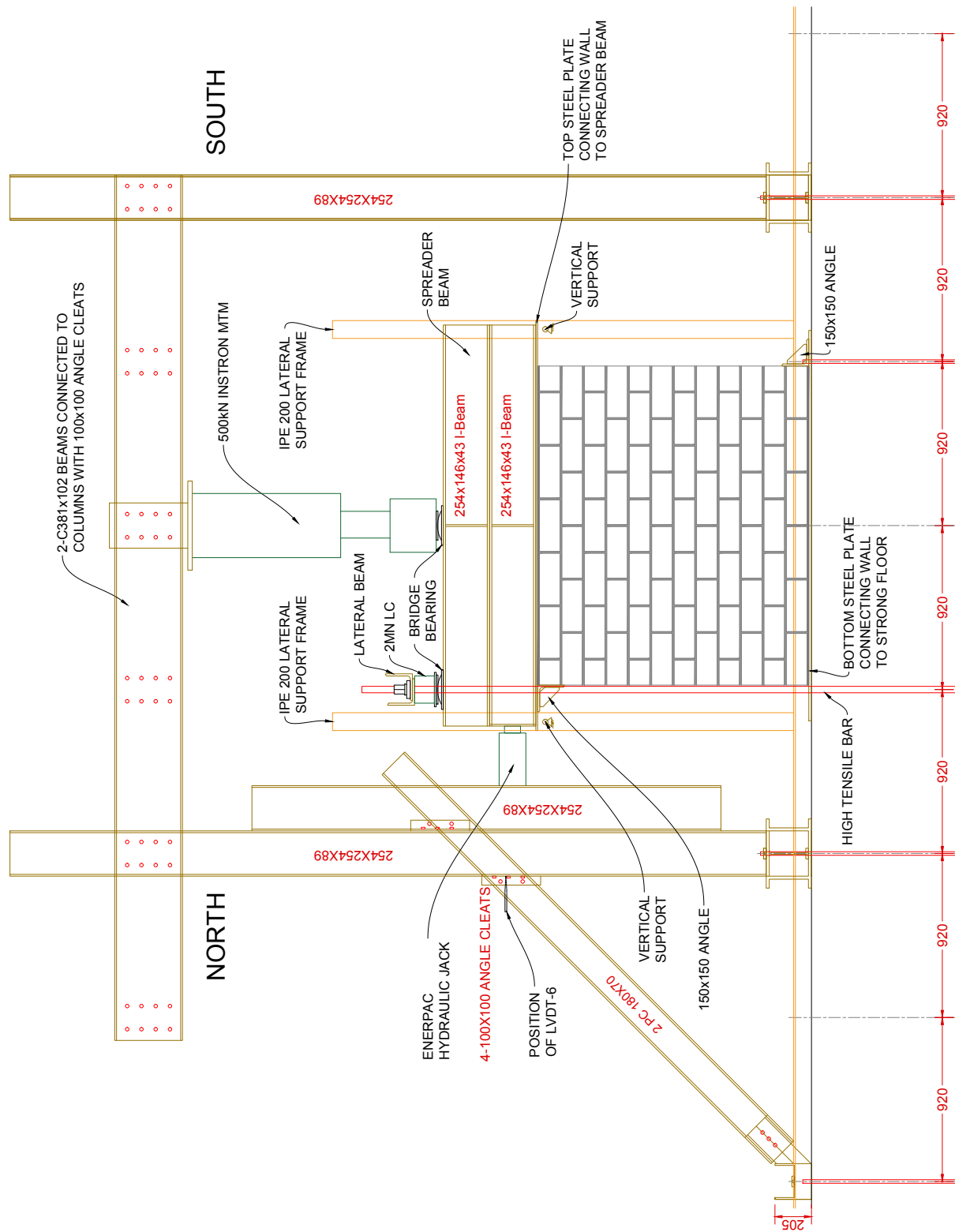


Figure 5.17: Drawing of Test Set-up B (all dimensions in mm)

5.5.3 Measurements and Data Collection

Throughout the test, the displacements and applied loads were measured by means of LVDTs and LCs respectively. The data was captured in a computer using the Spider 8 data acquisition system. The data from the Instron were also collected through the same system.

As previously mentioned, two LCs were used to monitor the magnitude of the horizontal force (50 t LC) and the increasing vertical force (2MN LC) resisted by two high tensile bars with a lateral beam positioned through the bars. Five LVDTs positioned independently from the set-up frames measured the horizontal and vertical displacements of the wall in relation to the floor. The positions of these LVDTs are shown in Figure 5.18.

The horizontal displacements were measured by three LVDTs, referred to as LVDT-1, -3 and -5;

- LVDT-1 was a 100mm LVDT positioned at the top of the wall and north of the test set-up. It provided the main horizontal shear displacement of the wall. LVDT-1 was in direct contact with the steel angle bolted to the top steel plate on a smooth Perspex surface.
- LVDT-3 was a 50mm LVDT positioned at the bottom of the wall and south of the test set-up. It was in contact with the steel angle connected to the bottom steel plate and monitored the movement of the steel angle as the wall pushed against it due to the horizontal force applied. The displacements provided by LVDT-3 gave an indication of the wall movement with respect to the floor. Although very minimal, these displacement readings were subtracted from LVDT-1 readings to obtain the actual displacement of the wall.
- LVDT-5 was a 50mm LVDT positioned south of the test set-up, on the spreader beam just above the wall. Readings from LVDT-5 were similar to LVDT-1.

The vertical displacements were measured by two LVDTs, referred to as LVDT-2 and -4

- LVDT-2 was a 100mm LVDT positioned at the top of the wall and north of the test set-up. It was in direct contact with the steel angle at the top of the wall, on a smooth Perspex surface. This LVDT provided the main upward vertical displacement of the spreader beam. However, as the beam was in direct contact with the wall, the readings from LVDT-2 indicated the vertical displacement of wall specimen.
- LVDT-4 was another 100mm LVDT positioned south of the test set-up just below the top steel plate. The readings from LVDT-4 provided the downward vertical displacement of the spreader beam.

In addition to the five LVDTs mentioned above, it was observed that the supporting frame would move during the tests, especially in the cases of stronger walls. An additional LVDT, referred to as LVDT-6 and shown in Figure 5.17, was therefore added north of the set-up for the two AACB walls to measure the horizontal displacement of the column at a height of 1,720mm from the strong floor.

The test performed and the cracks induced in the wall were also documented with two high resolution digital cameras. With one camera, videos of the tests were recorded, and photographs

CHAPTER 5. EXPERIMENTAL DESIGN

were taken with the second camera. The two cameras were positioned on each side of the set-up facing the wall specimen.

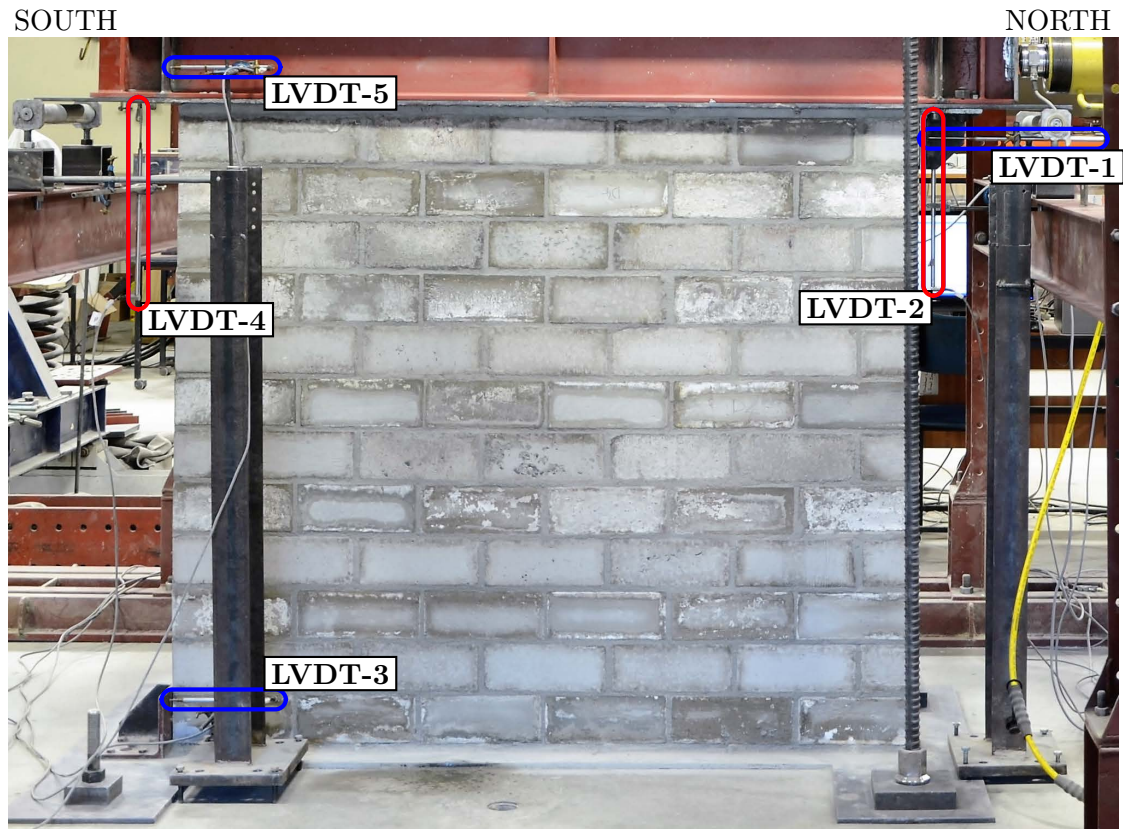


Figure 5.18: Close up View of Wall Indicating Locations of LVDTs

5.6 Conclusion

In this chapter, each of the tests carried out during this study is discussed in relation to its respective test set-up. The testing procedures followed when performing the tests and the approach taken in collecting the test measurements and data are also highlighted. Further, photographs and drawings have been included to provide visual representations of the various tests.

Different loading rates are used for the tests on masonry units, wallets and mortar specimens. A summary of the loading rates mentioned in this chapter is provided in Table A.1 (Appendix A).

An element to mention with regard to the design and construction of the in-plane shear-compression test set-up, is that it had many limiting factors, including the space and materials available in the laboratory, the human resources required to perform the tests, and due to the magnitude of the test set-up, the physical capacity of the researcher.

Chapter 6

Results and Discussion

This experimental study aimed at investigating the in-plane shear behaviour of CMU and AMU walls. The tests were conducted at various stages of the experimental programme and at different masonry ages, using the test set-ups and following the testing procedures presented in Chapter 5. The results from all the tests performed on masonry units, wallets, and walls, are presented in this chapter. Discussions on the obtained results and the stability of the test set-up are also provided.

6.1 Masonry Unit Test Results

6.1.1 Compressive Strength

The compressive strength of a masonry unit, a common mechanical property required in the design of masonry structures, is typically determined by conducting experimental tests according to guidelines provided in various standards such as the one discussed in Section 5.1.

For each unit type investigated in this study, the compressive strength tests were conducted at three different periods. The first tests determined the strength gained 28 days after the units were manufactured. The second and the third tests were aimed at determining the strength of the units just after performing the first (Wall#1) and the second (Wall#2) wall tests respectively. For the strength test at 28 days, eight units were individually selected from the units manufactured on different days, then the tests were carried out over a period of eight days. For the strength test carried out after each wall test, the units tested were randomly selected from the remaining batch of units. In this case, seven units were selected after each wall test and were tested all at once.

An important aspect to mention with regard to the unit test, especially for CMUs and CSEBs, is that the loading face of the specimen needed to be grinded before each test to ensure that it is horizontal and parallel to the bottom face of the unit. However, due to the nature and weakness of Adobe blocks, these were not grinded. As for the AACBs, they were not grinded either because each unit was cast in a wooden mould and the loading face was in contact with the wooden sides of the mould and perpendicular to the casting direction.

CHAPTER 6. RESULTS AND DISCUSSION

The number of units tested provided a reliable overall estimate of the strength of the manufactured units. As the tests were performed at different periods, this allowed a comparison of strength gain between the units. The age of the units tested after 28 days were not the same between the specimens from one unit type as well as the other unit types. For a given masonry unit type, the age at time of testing was then estimated based on an average of the age of all masonry units. This is because the units could not be manufactured all at once.

The compressive strength test results for the four masonry types are presented in Figure 6.1. The calculated average compressive strengths are represented in the graph by the columns, and the error bars provide the variability of the compressive strength among the tested specimens, based on the standard deviation. For Wall#1 and Wall#2 the average unit age, in days, is provided in brackets above each column.

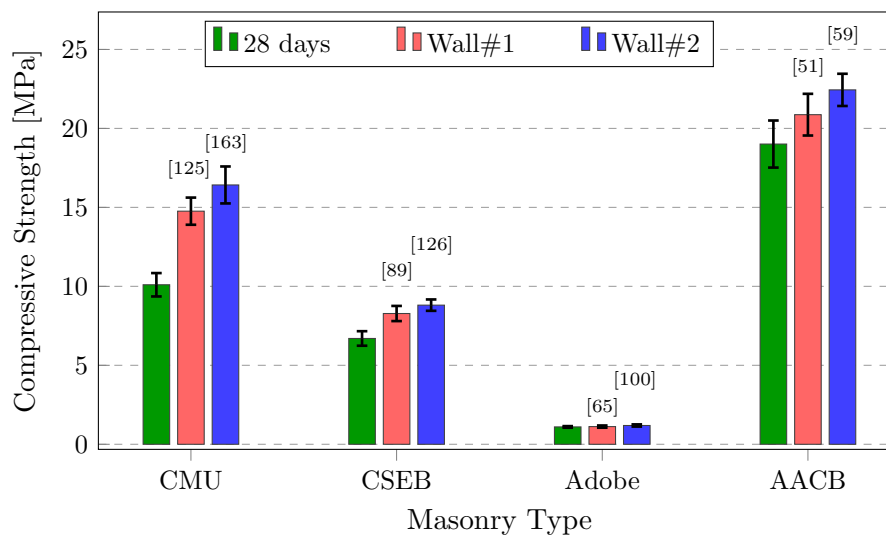


Figure 6.1: Unit Compressive Strength Results

For each masonry type, the obtained results clearly show the strength gained over time, beside the ones for Adobe blocks which present little strength gain. When comparing the strength of four masonry unit types at 28 days, AACBs showed a much higher strength, followed by CMUs, CSEBs, and Adobe blocks which were the weakest.

It should be noted that the compressive strength of the masonry units can be modified by optimising the mix designs, however this was not the purpose of this study. The aim here was to achieve similar unit strengths to those attained in previous studies (e.g. Fourie, 2017). The mix designs for AMUs aimed at providing three types of masonry units with as wide a spectrum of mechanical properties as possible (i.e. strength and stiffness), to result in structural responses over a wide spectrum.

Table 6.1 provides numerical values of the mean compressive strengths shown in Figure 6.1 together with the coefficient of variation (COV) associated with the mean strengths, as well as an average unit age at the time the test was performed. The COV, expressed as a ratio of the standard deviation to the mean, is provided to indicate the variability of the test results for a given masonry type.

CHAPTER 6. RESULTS AND DISCUSSION

Table 6.1: Unit Compressive Strength Results with COV

Masonry	28 days		Wall#1			Wall#2		
Unit	f_u [MPa]	(COV)	f_u [MPa]	(COV)	Age [days]	f_u [MPa]	(COV)	Age [days]
CMU	10.10	7.3 %	14.76	5.8 %	125	16.42	7.1 %	163
CSEB	6.70	6.9 %	8.28	5.8 %	89	8.81	4.1 %	126
Adobe	1.10	4.8 %	1.12	6.1 %	65	1.19	5.8 %	100
AACB	19.01	7.8 %	20.87	6.3 %	51	22.44	4.5 %	59

A general observation is that all COV values are less than 10%, a good indication of quality control in the manufacturing process. A decrease in COV values between the tests at 28 days, Wall#1 and Wall#2 is noticeable for CSEBs and AACBs, indicating that as the strength is gained over time, the variability within one group of units reduces.

Compressive Strength Discussion

Table 6.1 shows that the tests carried out after the 28 days tests were done with units at different ages. As indicated before, the age shown in the table represents an average of the age of the units at the time of testing. CMUs were the first units manufactured and the subsequent compressive strength tests, performed after the 28 days test, occurred much later in the experimental programme. As for AACBs, they were the last set of units manufactured closer to the time their respective wall tests occurred.

For the CMU and CSEB specimens, the time difference between the first and second wall test was almost the same (38 and 37 days respectively). The compressive strength gain of these units between the two tests was 11.2% for CMU and 6.4% for CSEB. The strength gain of these masonry units can be attributed to the cement hydration process.

With about 35 days difference between the first and second Adobe wall tests, no significant compressive strength gain of Adobe blocks was observed, as compared to CMU and CSEB specimens. This is attributed to the fact that the final compressive strength of Adobe blocks is reached as the units are dried. No hydration process, similar to that which happens for CMU and CSEB, takes place.

The geopolymerisation process contributes to strength gain in AACBs. The obtained results show relatively good strength gain over the period of the experimental programme. However, it can be noticed that there was a rapid strength gain occurring within 8 days (7.5% increase) between the Wall#1 and Wall#2 tests than there was within 23 days (9.8% increase) between the 28 days and Wall#1 tests. This may be related to the fact that the units tested were randomly selected from the batch, introducing possible variabilities between the actual ages of the units.

Efforts were made however, to ensure that the first wall was built with the first set of manufactured units, and specimens for the unit compressive strength test were taken from the same batch. Due to the time constraint, the experimental programme was not designed in such a way for the compressive strength tests to be performed at predetermined units age, for better comparison of strength gain between the four masonry unit types.

CHAPTER 6. RESULTS AND DISCUSSION

However, the test results provided an indication of the unit compressive strength within a given wall. With all the masonry units having the same dimensions, the compressive strength tests were successfully conducted with fewer complications. The tests were performed following the guidelines provided in [BS EN 772-1 \(2011\)](#), and the test set-up presented in Section 5.1 which had also been used in previous studies at Stellenbosch University, allowed for the obtention of compressive strength results acceptable for the purpose of this study. Table A.2 in Section A.2 ([Appendix A](#)) shows the compressive strength of all the masonry units tested.

6.1.2 Modulus of Elasticity

As outlined in Section 5.2, the modulus of elasticity tests were performed according to [BS EN 12390-13 \(2013\)](#) for prismatic specimens (CMU, CSEB and Adobe), and according to [ASTM C469/C469M-14 \(2014\)](#) for cylindrical specimens (AACB). The difference in specimens as well as their respective dimensions and the testing descriptions are also outlined in Section 5.2.

Based on the difference in the geometry of the testing specimens, the use of two different testing machines, and the adoption of two testing standards, the modulus of elasticity was determined differently for the two specimens. For prismatic specimens, it was determined as the stabilised secant modulus of elasticity based on [BS EN 12390-13 \(2013\)](#), while, for cylindrical specimens, it was determined as the chord modulus of elasticity based on [ASTM C469/C469M-14 \(2014\)](#).

The tested specimens were selected in a similar way as those for the compressive strength test described in Section 6.1.1, and they were tested at three different periods - at 28 days, and after the first and second wall tests. Based on the adopted standards, the modulus of elasticity of each masonry unit type was determined as described in Section 4.1.2.

For each masonry type and testing time, the results of the modulus of elasticity are presented in Figure 6.2 as the average modulus of elasticity shown by the columns, with the error bars providing the variability in the results based on the standard deviation. The average unit age at the time of Wall#1 and Wall#2 tests is provided in brackets above each column.

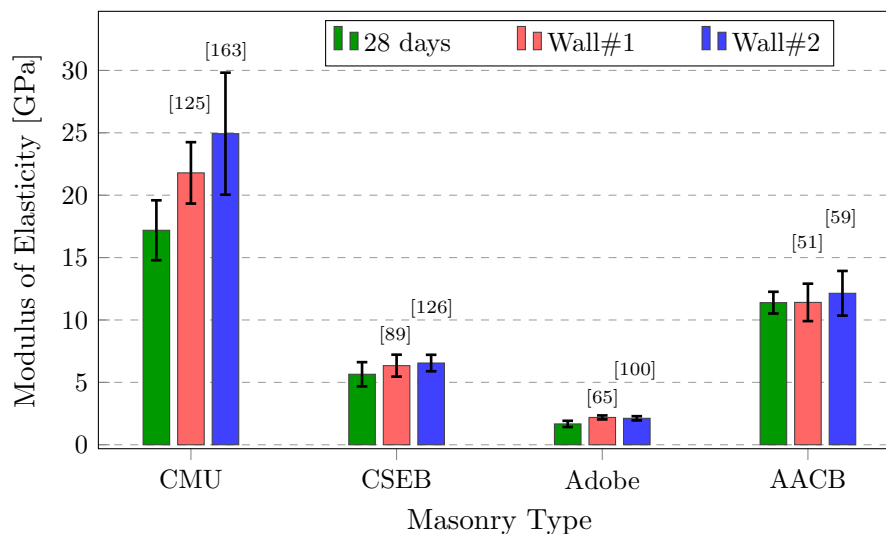


Figure 6.2: Unit Modulus of Elasticity Results

CHAPTER 6. RESULTS AND DISCUSSION

Looking at the results of the tests at 28 days in Figure 6.2, it can be observed that CMU specimens showed a higher modulus of elasticity compared to the other three masonry unit types. The AACB specimens were second highest followed by the CSEB and Adobe specimens. Although the increase of the modulus of elasticity among the units over time cannot be compared directly, due to the difference in age at the time of testing, CMU specimens show much higher gain in stiffness over time, however with a much higher COV value.

Although each masonry unit type exhibited an increased value of the modulus of elasticity over time, they all have higher COV values as compared to the results obtained for the compressive strength tests. This is discussed further in a later section.

The numerical values of the modulus of elasticity shown in Figure 6.2 are presented in Table 6.2 together with the COV values associated with the mean modulus of elasticity results, as well as an average unit age at the time the test was performed.

Table 6.2: Unit Modulus of Elasticity Results with COV

Masonry	28 days		Wall#1			Wall#2		
Unit	E_u [GPa]	(COV)	E_u [GPa]	(COV)	Age [days]	E_u [GPa]	(COV)	Age [days]
CMU	17.19	13.9 %	21.79	11.3 %	125	24.93	19.6 %	163
CSEB	5.65	17.2 %	6.34	13.9 %	89	6.55	10.0 %	126
Adobe	1.67	14.7 %	2.19	7.3 %	65	2.12	8.0 %	100
AACB	11.39	7.7 %	11.41	13.2 %	51	12.14	14.7 %	59

Modulus of Elasticity Discussion

The AACB modulus of elasticity obtained at 28 days was similar to the result obtained by [Fourie \(2017\)](#). However, the results for CMU, CSEB and Adobe were slightly lower than those obtained by [Fourie](#). This may be attributed to the difference in geometry of the specimens. [Fourie](#) performed tests on cylindrical specimens and in this study, the tests for CMU, CSEB and Adobe were performed on prismatic specimens.

[Domone and Illston \(2010\)](#) provide a table indicating the range of the modulus of elasticity for common masonry construction materials. The modulus of elasticity results obtained for CMU specimens fall within the range of “dense concrete: 10-25 GPa”.

Comparing the results of both the compressive strength and modulus of elasticity at 28 days for AACB and CMU specimens, it can be seen that AACBs were much stronger but less stiff than CMUs. Similar results have been reported in literature (e.g. [Barnard, 2014](#); [Lee and Lee, 2013](#)) where AAC mixes containing an addition of fly ash and slag in their mixes, resulted in lower modulus of elasticity with higher compressive strength.

A rapid gain in stiffness for the AACB was also observed between Wall#1 and Wall#2 test results, as was the case for the AACB compressive strength test results presented in Section 6.1.1. However, higher COV values were obtained from the results, suggesting that the stiffness gain was not the same for the specimens and that the method adopted in selecting the test specimens

CHAPTER 6. RESULTS AND DISCUSSION

as described in Section 6.1.1, when discussing the rapid strength gain of AACB specimens, may also be attributed to the rapid stiffness gain.

The modulus of elasticity tests were performed on both prismatic and cylindrical specimens. The compressive strength of specimens was needed in order to determine the stress limits required for the modulus of elasticity tests. For the eight tests performed at 28 days on prismatic specimens, eight companion specimens (one for each modulus of elasticity test) were tested to destruction, the results of which were the adopted compressive strength. As for the tests performed after the two wall tests, compressive strength tests were performed on three companion specimens and the mean of the three test results was adopted as the compressive strength required. A similar approach in calculating the mean of the compressive strength of three companion specimens was adopted for the cylindrical specimens for the 28 days test, and Wall#1 and Wall#2 tests.

Sources of Errors in the Experiment

The prismatic specimens needed to be cut from the masonry units in their bedface orientation, mainly due to the fact that this is generally the orientation in which masonry units are used in a masonry assemblage such as wallets and walls. Difficulties were encountered in this process mostly because of the nature and constituent materials of the three masonry units (CMU, CSEB, and Adobe). The cutting process may have also affected the specimen properties for each of the three masonry units respectively, and as the specimens were cut from different masonry units, this may have resulted in high variability between the test results.

A common difficulty was getting the dimensions required for the prismatic specimen (height of 116mm and width of 58mm). While efforts were made to get the exact dimensions, small measurement errors were inevitable and may have contributed to the variabilities in the test results. CSEB specimens, however, were easier to cut from the units, mainly because of the high compaction achieved in the manufacturing process and the use of a finer sand (Philippi sand) in their mixes.

In the case of CMU mixes, the use of crusher dust made it difficult to cut the specimens to the exact dimensions. Although the internal surface of the unit showed good compaction, some particles of the specimen would peel off during the cutting process, especially at the corners, because of the angular particle shape of crusher dust. The top loading face of both the CMU and CSEB specimens needed to be grinded before performing the modulus of elasticity test.

The weak nature of Adobe specimens made the cutting process harder and care needed to be taken while cutting and testing these specimens. As no binder was used in the designed mixes, the internal structure and bond between aggregates were very weak. The only constituent of the mix holding the materials together was the fine clay soil that was used. However, large Malmesbury sand particles would peel off the specimen surfaces if they were not handled gently.

Adobe specimens presented rougher surfaces as opposed to CMU and CSEB specimens (see Figure 5.2(a)). In addition to the weakness of the specimens, it was difficult to place and hold in position the LVDT brackets. Efforts needed to be made in handling the specimens with great

CHAPTER 6. RESULTS AND DISCUSSION

care and performing the test at a slower pace. The reduction in the variability values between the two wall tests and the test at 28 days may be attributed to the added efforts.

Another difficulty in performing the test was related to the testing equipment. It was necessary to check before each test that the LVDTs were working perfectly and, when required, the faulty LVDT was replaced. The use of a large capacity LC (2MN) in the test set-up (see Figure 5.3) may have introduced errors in the recorded results due to the low strength of specimens. In some cases, although the 2MN Instron testing machine was able to maintain the stress limits (preload and upper load stresses) for 10 seconds in each of the three loading cycles, the variation in the LC readings were larger for the load being applied, or in other cases, the load readings were less than the actual Instron readings.

The Instron output readings were also recorded using the HBM Spider 8 data acquisition system. However, it was realised that, for various tests, the readings were not correct because of technical reasons, hence making it difficult to use the recorded data.

For some prismatic specimens, the recorded data showed negative values of one or two LVDTs, indicating that bending stresses were induced in the specimen even after grinding the loading face of the specimen. However, this was not observed with the cylindrical specimens due to the use of the Contest Grade A compression testing machine, where the top bearing catered for any irregularities of the loading face.

The overall test was much easier to perform in comparison to the test on prismatic specimens, especially Adobe specimens, as no cutting was required. Placing the LVDT supports (aluminium rings) around the specimen and positioning the specimen in the testing machine was much easier.

It was not possible to have a programmable loading cycle using the Contest machine. The loading and unloading cycles for each tested specimen were done manually between the stress range of 0 to 40% compressive stress as recommended in the standards. With the mean compressive strength obtained from the three tested companion specimens, the 40% compressive stress turned out to be about 40kN as the upper load. The loading and unloading cycles applied on the Contest machine were then from 0 to 40kN.

It was noticed that the load on the Contest machine would increase rapidly from 0 to about 17kN after which the load would increase at a steady loading rate of 90 kN/min. From the recorded data, the stress-strain responses were plotted on a graph for the loads and displacements associated with the range where the loading rate was stable. Equation (4.6) provided in Section 4.1.2 was slightly modified so that, once the results were plotted as a stress-strain curve, a best fit straight line of the plotted results would give the chord modulus of elasticity.

For all the tests performed on the prismatic and cylindrical specimens, once the three loading cycles were performed, completing one test on the specimen, the loading cycles were repeated two more times on the same specimen after it was rotated 90 degrees with respect to the testing machine, contributing to minimising the hysteresis effects. With three tests performed on one specimen, the modulus of elasticity of the specimen was then determined by taking an average of the three test results. The stress-strain curves for the specimens tested at 28 days are illustrated in the figures provided in Section A.3 of Appendix A.

CHAPTER 6. RESULTS AND DISCUSSION

6.1.3 Density

The dry density test was performed once all the masonry units were manufactured. Six specimens were randomly selected from each masonry unit type. The test was performed as described in Section 5.4, by drying the six specimens in a well ventilated oven maintained at a temperature of 70°C, and determining their respective constant masses.

The dry density of each specimen was determined as illustrated in Section 4.3.1. From the results obtained for each of the six specimens, an average dry density was calculated and the results for the four masonry types are shown in Figure 6.3 together with the error bars representing the standard deviation.

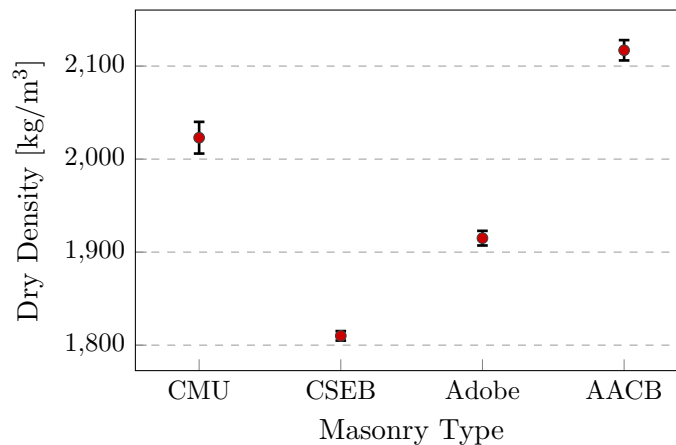


Figure 6.3: Dry Density Results

From the results in Figure 6.3, it can be observed that AACB specimens had the highest dry density, followed by the CMU, Adobe and CSEB specimens. Although the initial mass of wet AAC mixture cast in the wooden moulds was not determined, as compared to the other three masonry types, the high content of fine aggregate and the vibrating process in the AACB manufacturing resulted in a decrease of air voids and spaces between constituent materials. This may have contributed to the high density as mentioned by Barnard (2014), who found that the density of AAC mixes increased with an increase in the fine aggregate content.

CMU, CSEB, as well as Adobe specimens were manufactured using dry mixes and following the same procedure. Their respective masses were predetermined based on the compaction efforts. The CSEB and Adobe water content in their respective mixes (see Tables 3.4 and 3.5) were almost similar however, the CMU mixes had less water content (Table 3.3) and did not have much finer aggregate content. Even with less water content, the CMU mixture was not as dry as the CSEB and Adobe mixes. Further, the higher quantity of material used in the compaction process resulted in the units having higher densities than the CSEBs and Adobe blocks.

The CSEBs and Adobe blocks were manufactured by compacting similar quantities of wet mixtures. However, the Adobe mix had finer aggregate and a higher water content which contributed to the reduction of air voids during the compaction process and, as a result, the dry density result of Adobe specimens was higher than the CSEB results. Table 6.3 shows the numerical values of dry density results presented in Figure 6.3 together with the COV.

CHAPTER 6. RESULTS AND DISCUSSION

The relatively low COV values obtained from the dry density tests suggested that there was little variation between the mixes during the manufacturing process for the different masonry types. The obtained results fall in the range of values in Table 4.1, where the various density ranges of different masonry units are presented.

Table 6.3: Dry Density Results with COV

Unit Type	CMU	CSEB	Adobe	AACB
Dry Density [kg/m ³]	2023	1810	1915	2117
(COV)	0.8 %	0.3 %	0.4 %	0.5 %

It is worth mentioning that Venkatarama Reddy (2012) found that, despite the amount of cement in the mix and the creation process of the block, the density of CSEB blocks, which he referred to as stabilised soil blocks, has a direct influence on the compressive strength of the block, that is a rise of the block density will result in an increase of the compressive strength.

6.2 Masonry Wallet Test Results

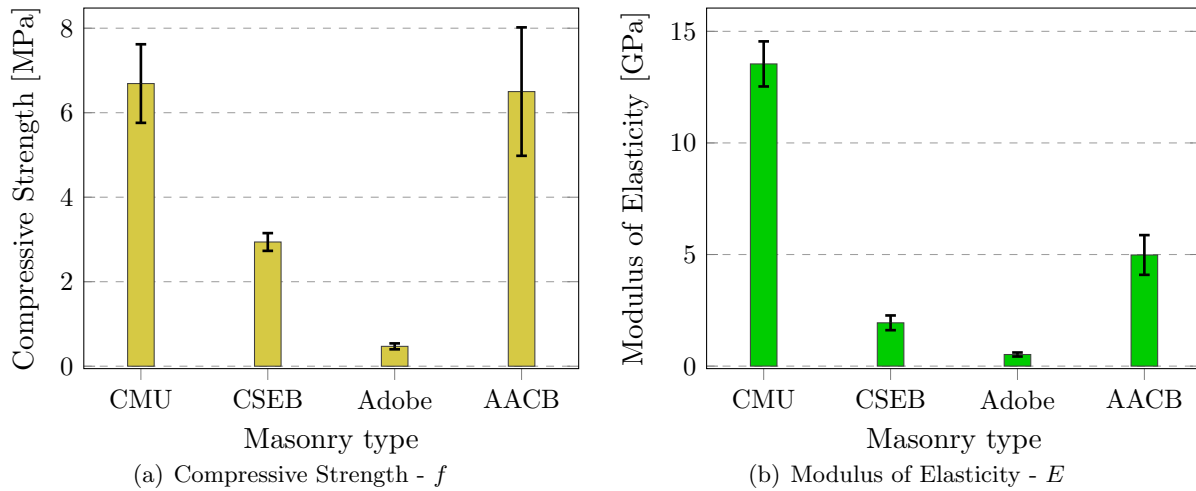
The masonry wallet tests were performed following the guidelines provided in BS EN 1052-1 (1999). The wallet specimens, built by a professional bricklayer, had a length of approximately 590mm and a height of 610mm. The tests were conducted as described in Section 5.3, and from the test results, the compressive strength and the modulus of elasticity were determined.

For each masonry type, five specimens were tested to destruction to determine their respective compressive strengths, and four LVDTs were positioned around four of these specimens to measure the deflection occurring at the four LVDT positions over a gauge length of 210mm. The LVDT measurements together with the compressive strength results were used to calculate the modulus of elasticity of the four specimens. Equations provided in Section 4.2.1 were used for the calculations. From the obtained test results, an average compressive strength and modulus of elasticity were calculated. The final results are shown in Figure 6.4 with the standard deviation represented by the error bars.

The compressive strength results shown in Figure 6.4(a) denote that the CMUs had the highest strength, followed by AACBs being slightly weaker, then CSEBs, and finally Adobe specimens being the weakest. Although the tests were not performed at the same masonry units age for all specimens and the compressive strength of AACB specimens were higher than the other three masonry unit types as described in Section 6.1.1, the compressive strength of AACB wallet were expected to be higher than the CMUs. However, this was not the case from the obtained results and the bar representing the standard deviation showing a large spread of the five AACB Specimen results and the calculated average.

The modulus of elasticity results represented in Figure 6.4(b) indicate a higher modulus of elasticity for CMU specimens followed by the AACB, CSEB and Adobe specimens respectively. When comparing the modulus of elasticity results between the wallet and unit specimens shown in Figure 6.2 in Section 6.1.2, similar trends are observed with CMUs being stiffer.

CHAPTER 6. RESULTS AND DISCUSSION

**Figure 6.4:** Masonry Wallet Results

However, there was a concern with the wallet modulus of elasticity results of the AMUs as these were much lower and not within the range of those obtained by [Fourie \(2017\)](#). This concern will shortly be elaborated on further.

Numerical values of the results for the compressive strength as well as the modulus of elasticity illustrated in Figure 6.4 are presented in Table 6.4 together with the COV values. Mortar taken from the mason's board were cast in cubes and tested at the same period as the wallet tests. Three mortar cube specimens were tested to determine their compressive strength, as highlighted in Section 5.1, the results of which are also provided in Table 6.4 as mortar characteristic, together with COV values.

Table 6.4: Masonry Wallet Results with COV and Mortar Characteristic

Wallet Specimen	CMU		CSEB		Adobe		AACB	
	Mean	(COV)	Mean	(COV)	Mean	(COV)	Mean	(COV)
Strength - f [MPa]	6.69	13.8 %	2.94	7.2 %	0.47	14.5 %	6.50	23.3 %
E. Mod. - E [GPa]	13.54	7.4 %	1.94	17.1 %	0.52	17.8 %	4.98	16.3 %
Mortar characteristic								
Strength - f_m [MPa]	19.65	11.36 %	8.28	0.94 %	2.68	10.65 %	19.20	3.53 %

Wallet Results Discussion

Results in Table 6.4 show high COV values for the four masonry wallet types. As previously highlighted from the results in Figure 6.4(a), the large spread of the AACB wallet compressive strength results is reflected in Table 6.4 by the high COV value. This variability may be attributed to the use of a steel channel section in which the wallets were built. Due to multiple use of these steel elements in other test set-ups, some of them may have not been straight anymore with the webs at right angle to the flange. This may have caused, for some of the specimens, to not be in

CHAPTER 6. RESULTS AND DISCUSSION

full contact with the testing machine causing load concentration on one side of the specimen, hence affecting the final result.

After testing the first set of CMU wallets, it was noticed that the failure mode on some of the specimens was characterized by crushing of the top course of units with a few vertical cracks from the top second course of units to the third. For these specimens, a rubber mat was positioned at the top interface with the loading beam attached to the testing machine, while the steel channel at the bottom of the specimen was in direct contact with the testing apparatus. The failure mode just mentioned was attributed to the difference in boundary conditions at the top and bottom of the specimens. It was then decided that a steel plate would be mortared at the top of the specimen, and keeping the top rubber mat, a second rubber mat was positioned at the bottom of the specimen.

The failure mode recorded for the subsequent specimens was characterised by vertical cracks from the top to the bottom of the specimen and parallel to the loading direction. These crack patterns were observed from the sides as well as the large faces of the specimens as shown in Figure 6.5. Similar crack patterns were observed by [Fourie \(2017\)](#) and other researchers (e.g. [Wu *et al.*, 2013](#); [Sassoni *et al.*, 2014](#)).

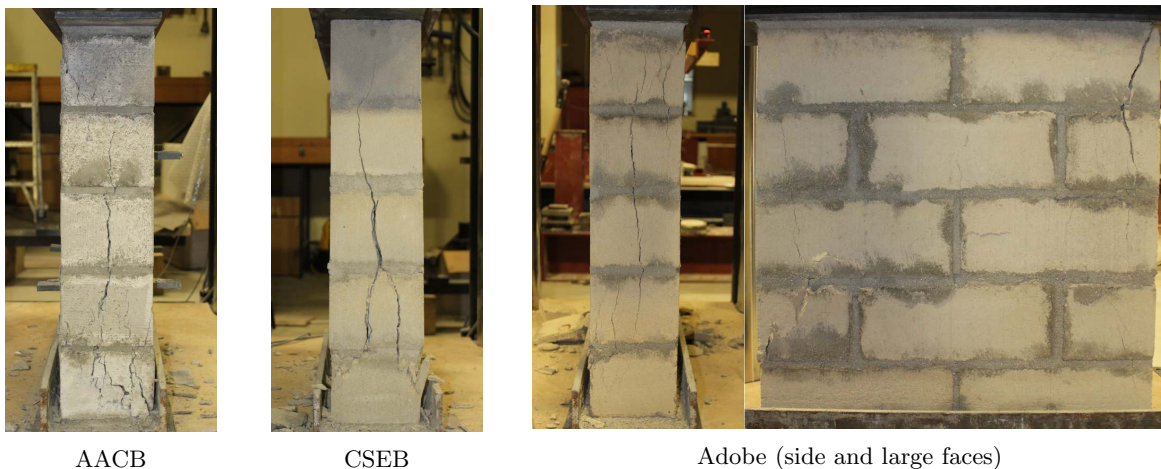


Figure 6.5: Vertical Cracks on Wallet Specimens

Another difficulty was related to the LVDT mounts used to position LVDTs onto the specimens. It was necessary to ensure that they were glued at a right angle with the large faces of the specimens and that they provided the exact gauge length for the deflection measurements. Due to the weakness of Adobe specimens and the presence of finer material on the faces, it was found that the LVDT mount would detach from the face of the specimen as soon as the LVDT was in position. To solve this, and to ensure that the LVDT mounts were positioned at the right gauge length, the gluing area was increased by using square steel sheets of about 1mm thick and about 40mm side dimensions. LVDT mounts were first glued at a right angle on the steel sheet which were then glued onto the specimens. This had shown to be more resistant in maintaining the position of the LVDT mounts and led to tests being performed successfully.

CHAPTER 6. RESULTS AND DISCUSSION

The mortar compressive strengths for the four masonry types are also shown in Table 6.4. An attempt was made to design four different mortar mixes that would have similar compressive strengths as the respective masonry units. This process is outlined in Section 3.3. However, the mortar strengths in Table 6.4 were not similar to the masonry unit compressive strengths at 28 days shown in Figure 6.1 and Table 6.1. But it was necessary to maintain the same mortar mixes for the wallet and wall tests for consistency throughout the experimental study, and additionally, the actual strengths of masonry units were not determined at the time the wallets were tested, it was then decided to keep the same mortar mix proportion throughout the experimental programme.

Typical stress-strain responses of the tested wallet specimens are provided in Figure B.1 (Appendix B). From an overall look at the wallet test, it can be concluded that the difficulties related to how the tests were conducted may have also contributed to the variability reflected in the test results. However, these results were important for the present study, as the pre-compression levels applied on the wall specimens for shear-compression tests were 15% of the wallet compressive strengths. For each unit type, the exact values of the pre-compression levels are presented in the subsequent sections.

6.3 Masonry Wall Test Results

The CMU and AMU masonry walls were tested in the laboratory by subjecting them to a shear-compression loading programme. The applied compressive forces were determined as 15% of the compressive strength of each masonry wallet type presented in Section 6.2 and were kept constant throughout the tests. The shear force, applied at the top of each wall specimen, was a quasi-static monotonic load. The loading application rate was not determined as a manually controlled hydraulic jack was used to apply the horizontal force.

The outcome of the tests was captured with photographs, written descriptions, and the data acquisition system. The experimental results are readily available to be used as validation for the numerical modelling. However, as the validation was not performed in this study, the test results are presented by means of photographs, descriptions of the resulting failure modes, and graphical representations of the experimental data (experimental curve) which also include an idealised bilinear envelope of the results.

As described in Section 2.6.3, the limit states considered for an idealised bilinear envelope are highlighted in the test results. These include the crack limit, and the maximum and ultimate resistance, which are represented as follow;

- The crack limit, by the resistance- H_{cr} , determined using Equation (2.3), and the corresponding displacement- d_{cr} , determined based on the test results and obtained value of H_{cr} ;
- The maximum resistance, by the maximum lateral load- H_{max} resisted by the wall together with the corresponding horizontal displacement- $d_{H_{max}}$ at the top of the wall; and
- The ultimate resistance, by the ultimate load- H_u calculated using Equation (2.5). The displacement- d_e at which H_u occurs is calculated with Equation (2.6), although not

CHAPTER 6. RESULTS AND DISCUSSION

indicated in the graphical representation of the test results.

Whenever the strength degradation reached 20% of the obtained maximum resistance, the corresponding ultimate displacement d_u was determined and indicated on the graph.

It should be mentioned that the wall tests carried out focussed on the pre-peak behaviour of the wall specimens. The tests were conducted until the maximum lateral resistance of the wall was attained or the top horizontal displacement reached about 10mm, thereafter the application of the horizontal force was stopped.

The effective stiffness K_e , calculated using Equation (2.2), determines the force-displacement behaviour of the masonry wall. This parameter is important for both the force based and displacement based seismic design methods Wilding and Beyer (2016). It was also determined and presented for the wall tests performed.

The drift capacity δ expressing the deformation capacity of the tested wall was also determined for the displacement at the peak resistance and, where applicable, the ultimate drift capacity δ_u , which is related to the horizontal displacement at 20% strength degradation of the peak resistance, was also determined.

After each wall test, the characteristics of the masonry wall constituents were determined. The masonry unit properties, which were presented and discussed in Section 6.1.1, are reproduced as part of the wall results together with the mortar properties. A COV was calculated for the tests performed on the mortar cubes and cylinders. COV values are presented with the mortar results to show the variabilities between mortar used for two walls constructed with the same type of masonry unit. The mortar results were not discussed in depth but the test results indicate that, for future studies, further mixes need to be designed and trial mixes performed to produce a mortar that will have the same strength as the respective masonry unit for a given wall specimen.

For each wall test performed, two figures are provided. One figure shows a photograph and a drawing of the crack patterns in the wall, and the second figure contains two plots representing the test result data. The left plot shows a graph of the vertical uplift versus the applied horizontal force of the north side of the wall specimen, which was recorded with LVDT-2 (see Figure 5.18). The second plot on the right, shows a graph of the absolute horizontal displacement measured at the top of the wall versus the applied horizontal force. The resulted idealised bilinear envelope for the specimen under consideration is also presented on the second plot.

The absolute top horizontal displacement, used for the second graph of the results, refers to the displacement recorded by LVDT-1 subtracting the displacement recorded by LVDT-3 (see Figure 5.18). However, it was not possible to plot an idealised bilinear envelope for the CMU walls due to the outcome of the tests. For all the wall specimens, the displacement readings recorded with all five LVDTs are provided in Figures C.1, C.2, C.3 and C.4 in Appendix C.

6.3.1 CMU Walls

The first and second CMU wall specimens tested with the Test set-up A and Test set-up B are respectively referred to as CMU-W-A and CMU-W-B. The two different test set-ups are described in Section 5.5.2. For both walls, the applied pre-compression level, corresponding to

CHAPTER 6. RESULTS AND DISCUSSION

15% of the CMU wallet compressive strength, was about 1MPa, which was achieved by applying a force of 253kN at the top of the wall specimen. The masonry unit and mortar properties are shown in Table 6.5, from which it can be seen that, for both walls, the compressive strength of mortar was higher than the unit strengths.

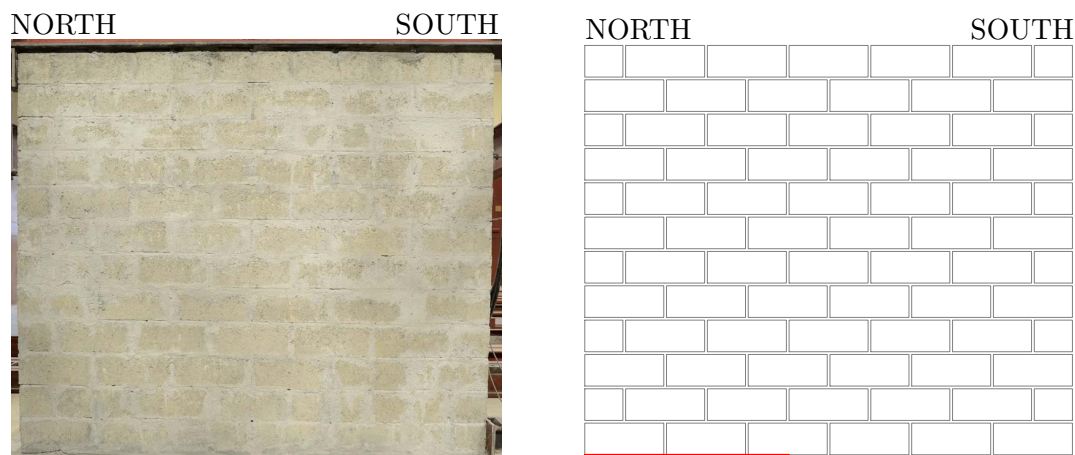
Table 6.5: CMU walls - Unit and Mortar Properties

WALL	UNIT		MORTAR			
	f_u	E_u	f_m	E_m		
	[MPa]	[GPa]	[MPa]	(COV)	[GPa]	(COV)
CMU-W-A	14.76	21.79	19.90	11.00 %	13.45	16.50 %
CMU-W-B	16.42	24.93	18.24	1.37 %	14.35	11.70 %

The mortar mix proportions used for both walls were similar and are presented in Table 3.7 in Section 3.3. As it can be seen in Table 6.5, the achieved compressive strength of mortar was higher than the unit compressive strength. The mortar mix was similar to the mix used to construct CMU wallets. Even with the strength gain of units, the objective of obtaining a mortar with similar strength as the unit was not achieved. Trial mixes for mortar would be required for future studies to design a mix that will achieve similar strength as the masonry unit. However, the mortar strength will need to be determined based on the time of testing and the masonry unit at the time, taking into account the strength gain.

CMU-W-A

The obtained failure mode was flexural failure. Tension cracks appeared at the toe of the specimen along the mortar joint between the wall and the bottom steel plate. The specimen showed a high lateral resistance and, as the applied horizontal force increased, the tension crack slowly extended towards the centre of the specimen resulting in high rotation at the top of the specimen. The crack patterns and graphical representation of the test results are shown in Figure 6.6 and Figure 6.7.

**Figure 6.6:** CMU-W-A: Crack Patterns

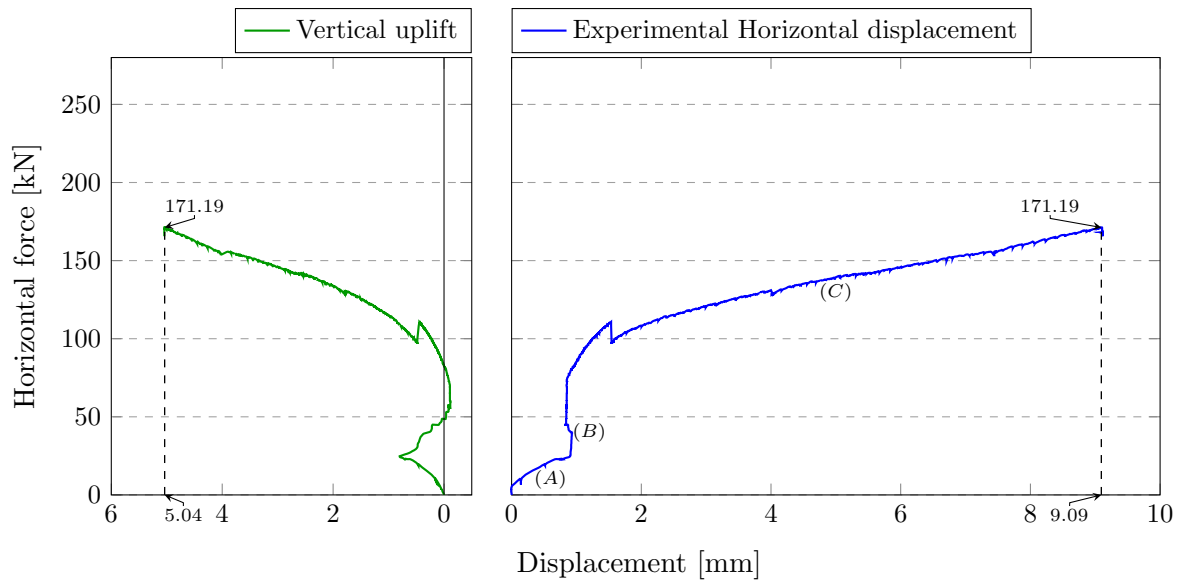


Figure 6.7: CMU-W-A: Test Results

Both the vertical uplift (plotted in green) and the horizontal displacement at the top of the wall (plotted in blue) are shown in Figure 6.7. From the graph showing the horizontal displacement, it can be seen that there are three distinctive slopes indicated by (A), (B), and (C). Comparing the horizontal displacement graph with the vertical uplift graph, the change between slope (A) and (B) indicates that the application of the horizontal force started before the full pre-compression force was applied. This unfortunately affected the test results.

Furthermore, the combination of vertical and horizontal displacements caused a rotation of the spreader beam. Due to high friction at the surface contact of the Enerpac hydraulic jack and the spreader beam (see Figure 5.11(d)), which did not allow free vertical movements of the spreader beam, a rotation of the hydraulic jack together with the spreader beam was observed, resulting in a sway movement of the reaction frame.

The test was then stopped at a shear resistance of 171.19kN, which was attained at a horizontal displacement of 9.09mm, corresponding to a drift capacity of 0.61%. In Figure 6.7, the slope (C) indicates a constant increase in the wall resistance as the lateral force was being applied. Typical for walls with flexural failure, if the test was not stopped, this trend would have continued until crushing of the toe bricks in the compressed zone.

CMU-W-B

The second CMU wall, CMU-W-B, behaved in a similar way to CMU-W-A. However, the initial tension crack was formed at the mortar joint between the first and the second course of masonry units. The wall exhibited high lateral resistance and the tension crack did not extend as fast as the crack formed with CMU-W-A specimen.

Although high tensile rods were used, it was noticed that significant rotation of the spreader beam still occurred. It was realised that an important step while performing the shear-compression

CHAPTER 6. RESULTS AND DISCUSSION

test with Test set-up B was to tighten the high tensile nuts on the lateral beam (see Figure 5.14), and slightly pre-tension the high tensile steel bars. As this was not done before starting the test, the rotation of the spreader beam was not prevented.

Another observation of the test was related to the middle bridge bearing. This element, placed at the top centre of the spreader beam and below the Instron actuator, allowed for the horizontal movement of the beam once the compressive force was applied. However, as the bottom bearing plate was centrally bolted on top of the beam, the large horizontal displacement, together with the sway movement of the reaction frame resulting from the test, had caused the bearing guide to reach its limit. Due to these reasons, the test had to be stopped. However at that moment, diagonal shear cracks had developed in staircase shape through the mortar joint as shown in Figure 6.8. The obtained results are graphically presented in Figure 6.9.

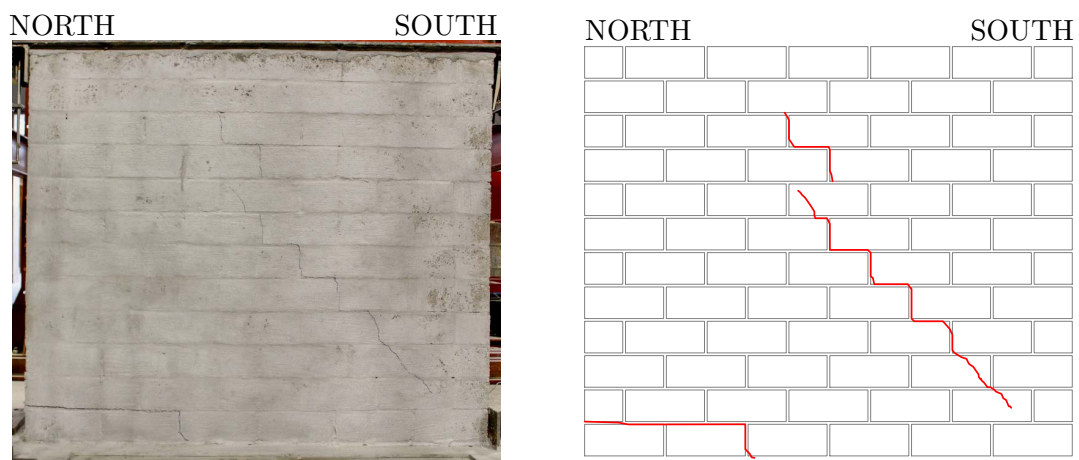


Figure 6.8: CMU-W-B: Crack Patterns

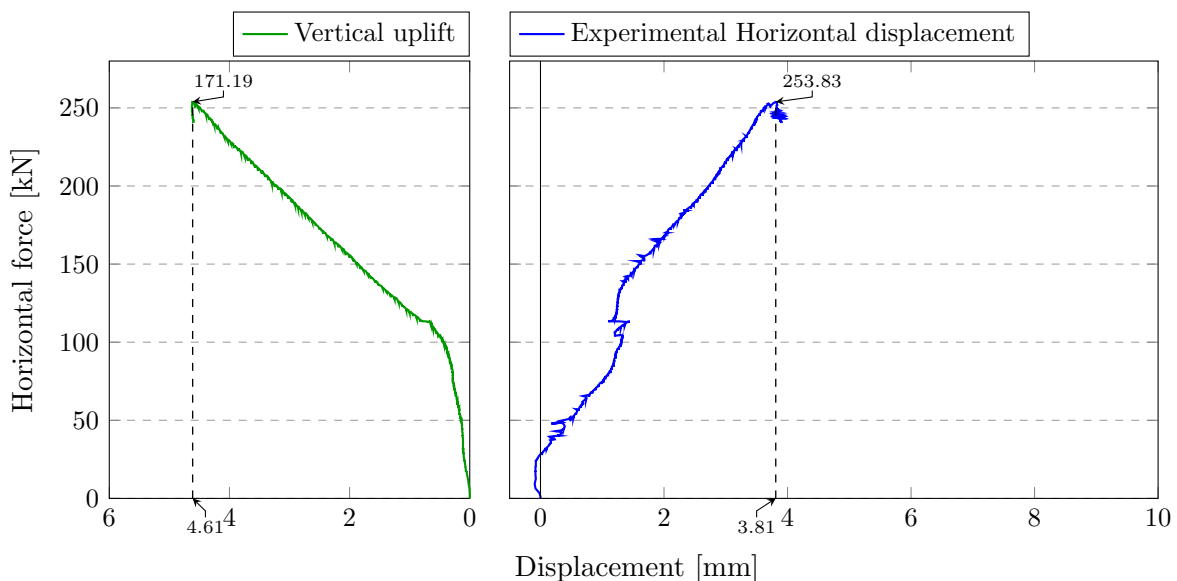


Figure 6.9: CMU-W-B: Test Results

CHAPTER 6. RESULTS AND DISCUSSION

From the wall behaviour it can be concluded that the specimen had already reached the crack limit by the time the test was stopped. The maximum lateral resistance reached after the test was stopped was 253.83kN with a horizontal displacement of 3.81mm and 0.25% drift capacity. The shape of the plotted graph in Figure 6.9 indicates that, for a certain period of time, mostly vertical uplift occurred during the test as the horizontal displacement remained almost constant.

The obtained results for CMU wall specimens are summarised in Table 6.6. The maximum values of lateral resistance H_{max} do not necessarily indicate the lateral capacity of the walls, but represent the load attained before the tests were stopped. The respective horizontal displacements and drift capacities at these lateral resistances are also provided.

Table 6.6: CMU walls - Results from Experimental Curves

Wall Specimen	H_{max} [kN]	$d_{H_{max}}$ [mm]	δ [%]
CMU-W-A	171.19	9.09	0.61
CMU-W-B	253.83	3.81	0.25

6.3.2 CSEB Walls

The two CSEB wall specimens are referred to as CSEB-W-A, tested with Test set-up A, and CSEB-W-B, tested with Test set-up B. The applied pre-compression level was about 0.44MPa, corresponding to a force of 111kN applied by the vertical Instron at the top of the wall. The properties of the wall constituents (units and mortar) were determined immediately after each wall test. These are presented in Table 6.7. For both specimens, the mortar compressive strength achieved at the time of testing was about 85% of the unit strength.

Table 6.7: CSEB walls - Unit and Mortar Properties

WALL	UNIT		MORTAR			
	f_u	E_u	f_m		E_m	
	[MPa]	[GPa]	[MPa]	(COV)	[GPa]	(COV)
CSEB-W-A	8.28	6.34	7.03	2.53 %	6.13	6.40 %
CSEB-W-B	8.81	6.55	7.55	3.58 %	6.91	2.10 %

CSEB-W-A

As the horizontal force was being applied, initial cracks formed at mid height of the specimen. These cracks continued extending diagonally and in opposite direction toward the top and bottom of the specimen. The length of the cracks increased further because of the horizontal movement of the top first and second course of units, as horizontal cracks had formed through the joints between the first and second course, and between the second and third course of masonry units from the northern side of the specimen.

CHAPTER 6. RESULTS AND DISCUSSION

As shown in Figure 6.10, CSEB-W-A was characterised by diagonal shear failure, with the shear cracks developed through the units and mortar joints. The test results are graphically presented in Figure 6.11.

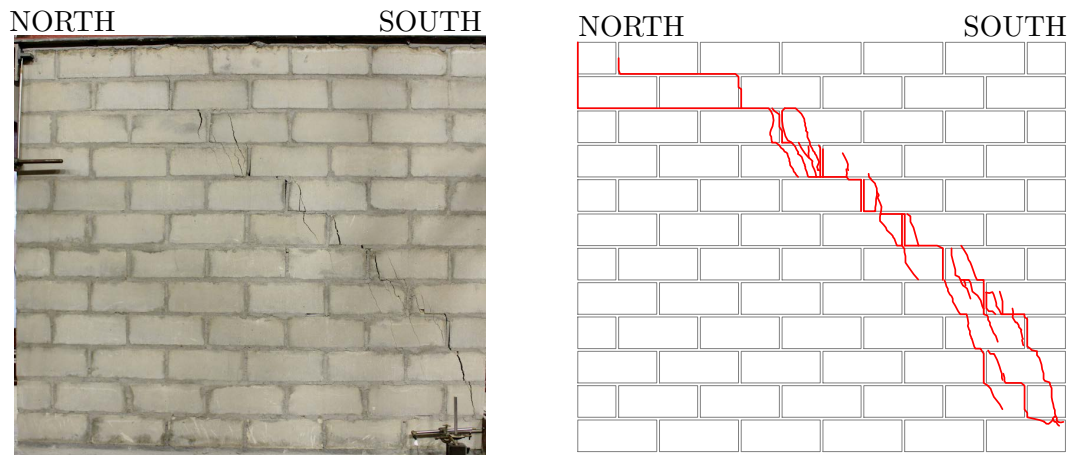


Figure 6.10: CSEB-W-A: Crack Patterns

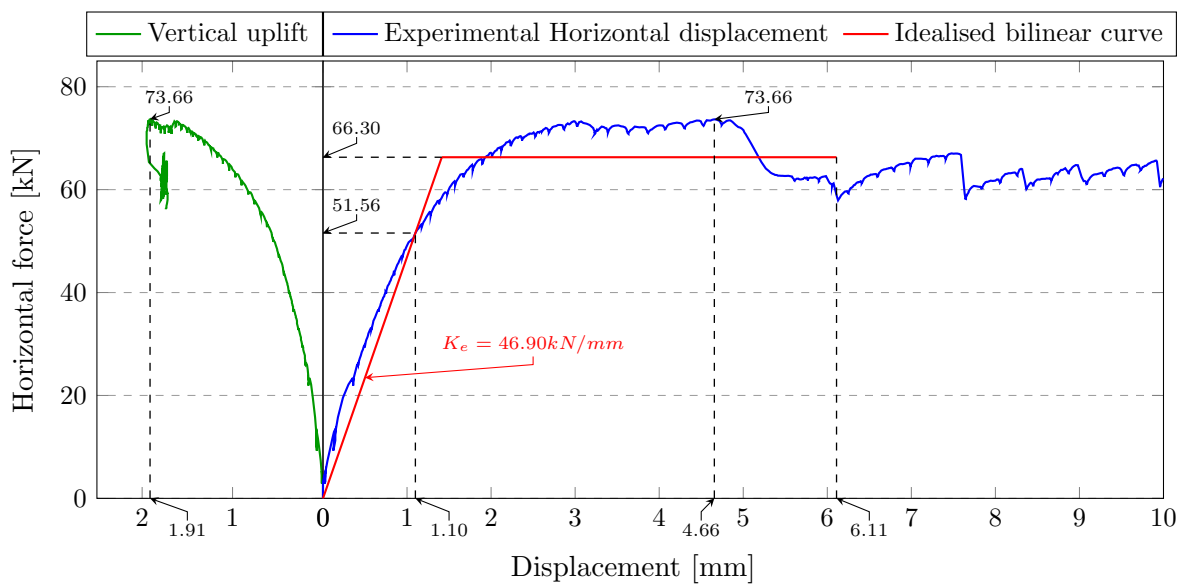


Figure 6.11: CSEB-W-A: Test Results

The maximum lateral shear resistance of 73.66kN was attained after a horizontal displacement of 4.66mm which corresponds to a drift ratio of 0.31%. The application of the horizontal force stopped after the horizontal displacement reached 10mm. The resistance at crack limit was found to be 51.56kN which was reached after a displacement of 1.10mm. The effective stiffness was then calculated to be 46.90 kN/mm. With the obtained results, the idealised bilinear curve was plotted as shown in Figure 6.11. The ultimate resistance of CSEB-W-A was found to be 66.30kN and its corresponding displacement was 1.41mm. A 20% drop of the maximum lateral resistance occurred at the ultimate displacement of 6.11mm, which corresponds to a drift ratio of 0.41%. At the maximum lateral resistance, the vertical uplift recorded was 1.91mm.

CHAPTER 6. RESULTS AND DISCUSSION

CSEB-W-B

Cracks in the CSEB-W-B specimen developed in the same manner as in the CSEB-W-A specimen. Initial visible cracks were formed around the centre of the specimen and gradually extended toward the two opposite corners of the specimen. A horizontal movement of the two top courses of masonry units also occurred. As shown in Figure 6.12, the failure was characterised by a diagonal shear. The cracks developed mostly as staircase-shaped cracks through the mortar joints, and cracks through the unit developed further toward the southern side of the specimen. The graphical representation of the test results is shown in Figure 6.13.

The test continued until the horizontal displacement was near 10mm. After the diagonal shear cracks had formed in the specimen, the applied horizontal force remained almost constant while the horizontal displacement increased. The staircase-shaped cracks divided the wall specimen in two parts, and the south side of the wall was able to slide through the mortar joints. This movement increased horizontally the length of the diagonal shear cracks.

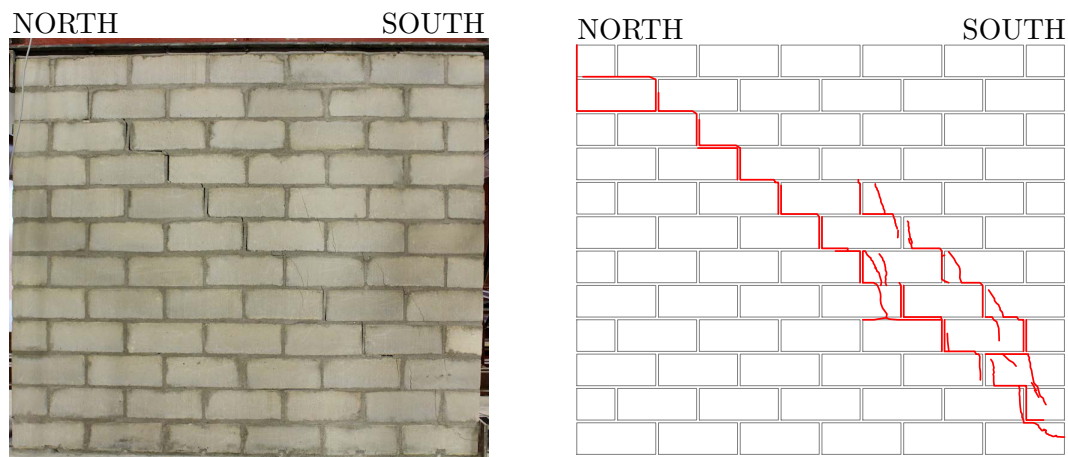


Figure 6.12: CSEB-W-B: Crack Patterns

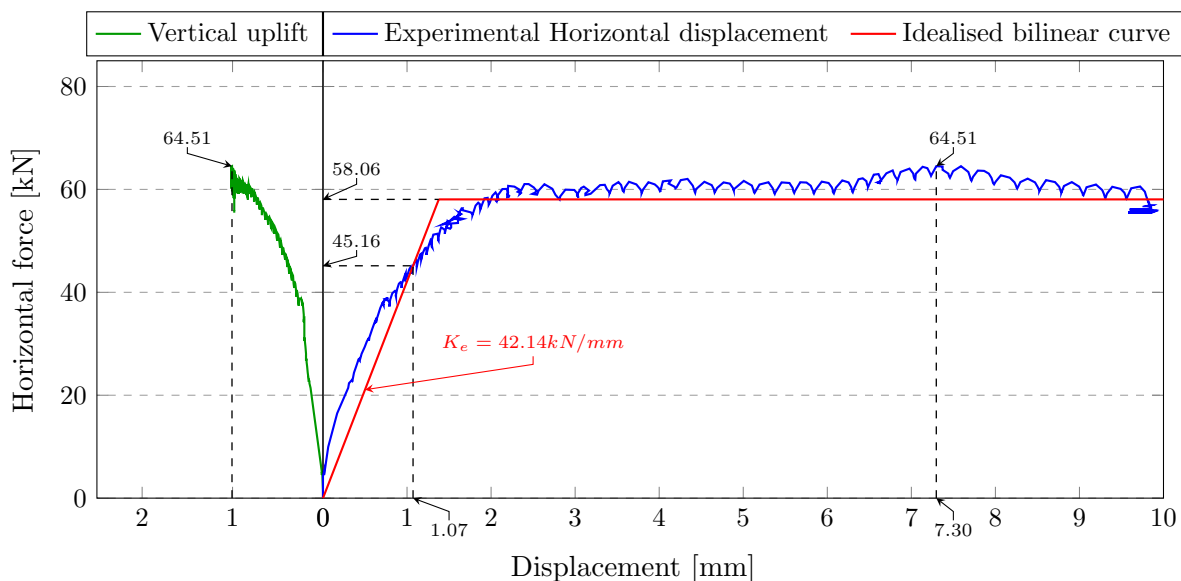


Figure 6.13: CSEB-W-B: Test Results

CHAPTER 6. RESULTS AND DISCUSSION

As the two parts remained in contact with each other, the constant horizontal force maintained can be attributed to the friction at the joints interface, which was caused by the applied vertical pressure. The use of high tensile bars contributed to a reduction in the rotation of the spreader beam.

The maximum lateral resistance of CSEB-W-B was 64.51kN attained at a horizontal displacement of 7.30mm, corresponding to a drift capacity of 0.49%. The resistance at crack limit was 45.16kN with a displacement of 1.07mm. The calculated effective stiffness was 42.14 kN/mm, and the ultimate resistance was found to be 58.06kN with a corresponding displacement of 1.38mm. The ultimate displacement was not determined as the load remained constant until the test was stopped. The test results for both CSEB wall specimens as idealised in Figure 6.11 and Figure 6.13 are summarized in Table 6.8.

Table 6.8: CSEB walls - Results from Experimental and Idealised Curves

Wall Specimen	H_{cr} [kN]	d_{cr} [mm]	K_e [kN/mm]	H_u [kN]	d_e [mm]	H_{max} [kN]	$d_{H_{max}}$ [mm]	δ [%]	d_u [mm]	δ_u [%]
CSEB-W-A	51.56	1.10	46.90	66.30	1.41	73.66	4.66	0.31	6.11	0.41
CSEB-W-B	45.16	1.07	42.14	58.06	1.38	64.51	7.30	0.49	-	-

The difference in the test results were clearly influenced by the two test set-up configurations. The vertical uplift was reduced considerably from 1.91mm (shown in Figure 6.11) to 1mm (shown in Figure 6.13), and the vertical force recorded by the 2MN LC at the maximum horizontal force was 22.56kN. In Table 6.8, a reduction in the effective stiffness, ultimate and maximum resistance can be noticed. A higher drift capacity can be attributed to the observed failure mode characterised by large horizontal displacement as indicated earlier.

6.3.3 Adobe Walls

The Adobe wall tested with Test set-up A was referred to as Adobe-W-A and the one tested with Test set-up B, Adobe-W-B. The pre-compression level was 0.071MPa, corresponding to a force of 18kN. The properties of the masonry units and mortar determined after each wall test are presented in Table 6.9. The obtained mortar results indicated that the compressive strength of mortar was greater than the strength of the masonry units.

Table 6.9: Adobe walls - Unit and Mortar Properties

WALL	UNIT		MORTAR			
	f_u	E_u	f_m	E_m		
	[MPa]	[GPa]	[MPa]	(COV)	[GPa]	(COV)
Adobe-W-A	1.12	2.19	2.42	8.71 %	1.65	5.00 %
Adobe-W-B	1.19	2.12	2.48	18.50 %	1.77	4.77 %

CHAPTER 6. RESULTS AND DISCUSSION

Adobe-W-A

The first Adobe wall specimen, Adobe-W-A, failed in a similar manner to the CSEB-W-A specimen, with cracks extending diagonally towards the north side-upper and south side-lower corners of the specimen. The first crack developed due to an uplift of the specimen at the bottom course of masonry units. As the horizontal load increased, a slight movement of the third top course of units was observed which led to a crack within the specimen, and ultimately a diagonal shear crack was formed. The crack pattern is shown in Figure 6.14, and the test results in Figure 6.15.

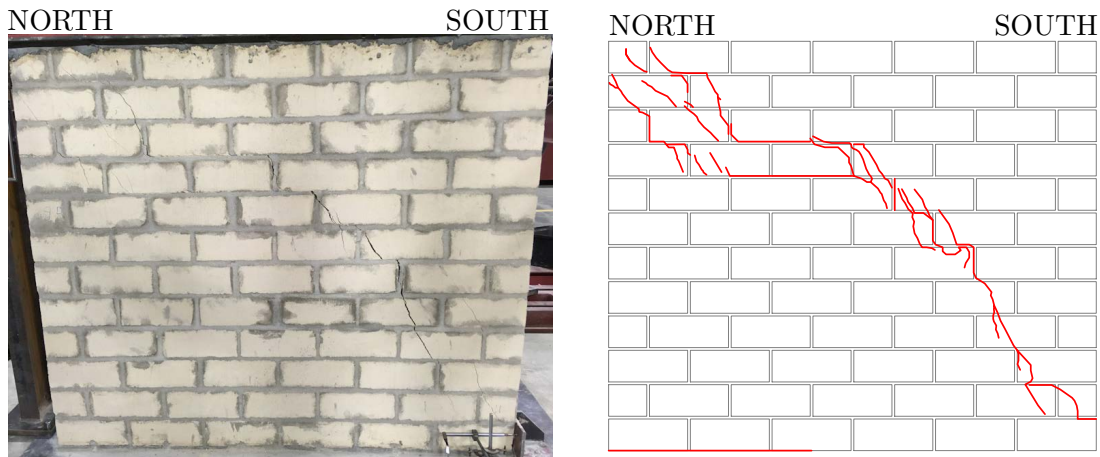


Figure 6.14: Adobe-W-A: Crack Patterns

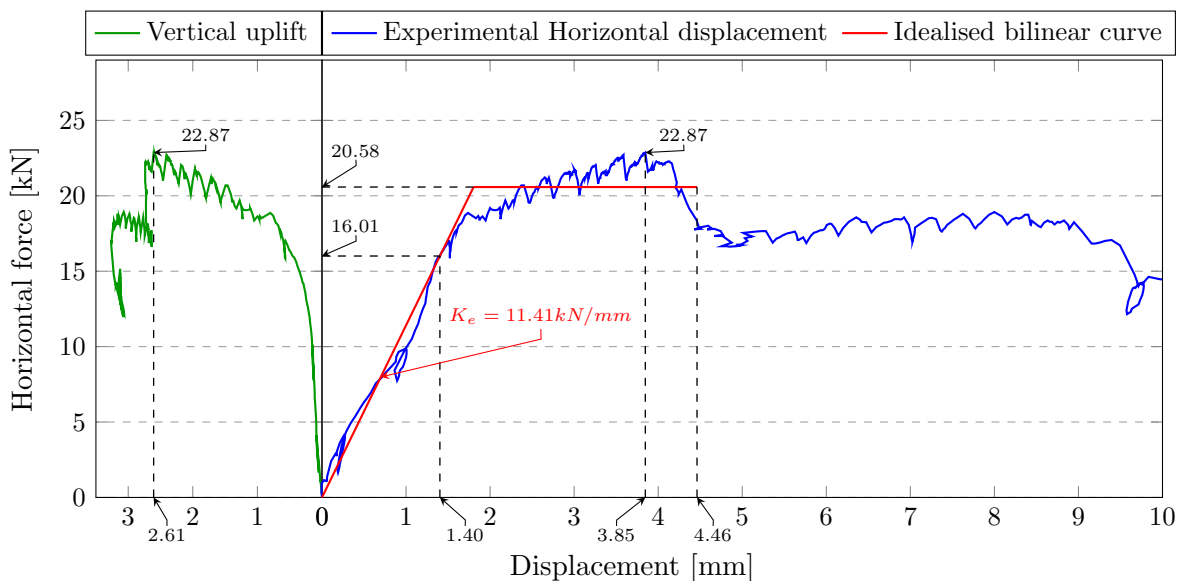


Figure 6.15: Adobe-W-A: Test Results

The maximum lateral resistance of the wall was achieved at a load of 22.87kN, with a horizontal displacement of 3.85mm, corresponding to a drift capacity of 0.26%. The application of the horizontal force was stopped after the displacement had reached 10mm. The resistance at crack limit was 16.01kN with a displacement of 1.40mm.

CHAPTER 6. RESULTS AND DISCUSSION

The effective stiffness calculated was 11.41 kN/mm and the ultimate resistance with the corresponding displacement was 20.58kN and 1.80mm. After the maximum lateral force was reached, a reduction in the specimen capacity was observed, and the ultimate displacement was then determined to be 4.46mm, corresponding to an ultimate drift capacity of 0.30%.

Adobe-W-B

A diagonal shear crack failure characterised the final behaviour of Adobe-W-B after completion of the test. The cracks developed through the masonry units as well as mortar joints, and were located in the middle of the specimen, running from the top second course to the bottom second course of masonry, as shown in Figure 6.16. The experimental results are shown in Figure 6.17.

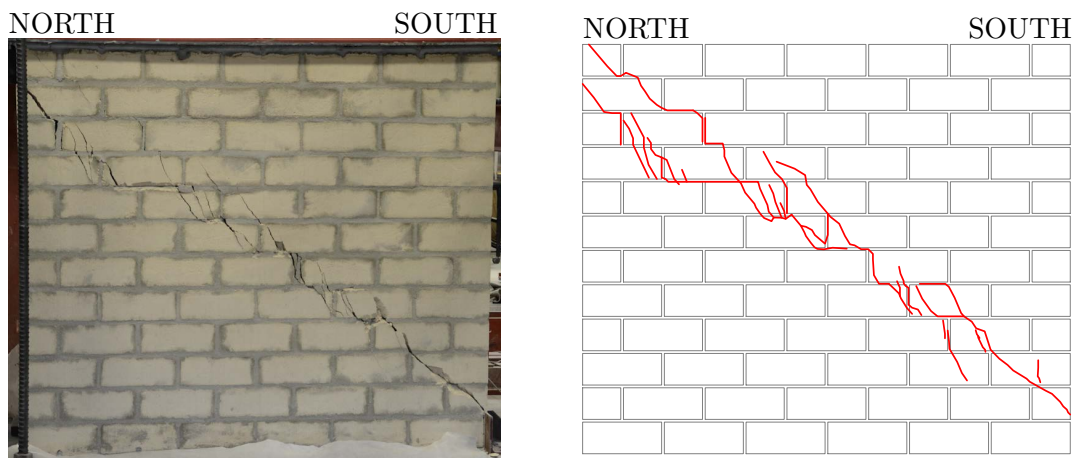


Figure 6.16: Adobe-W-B: Crack Patterns

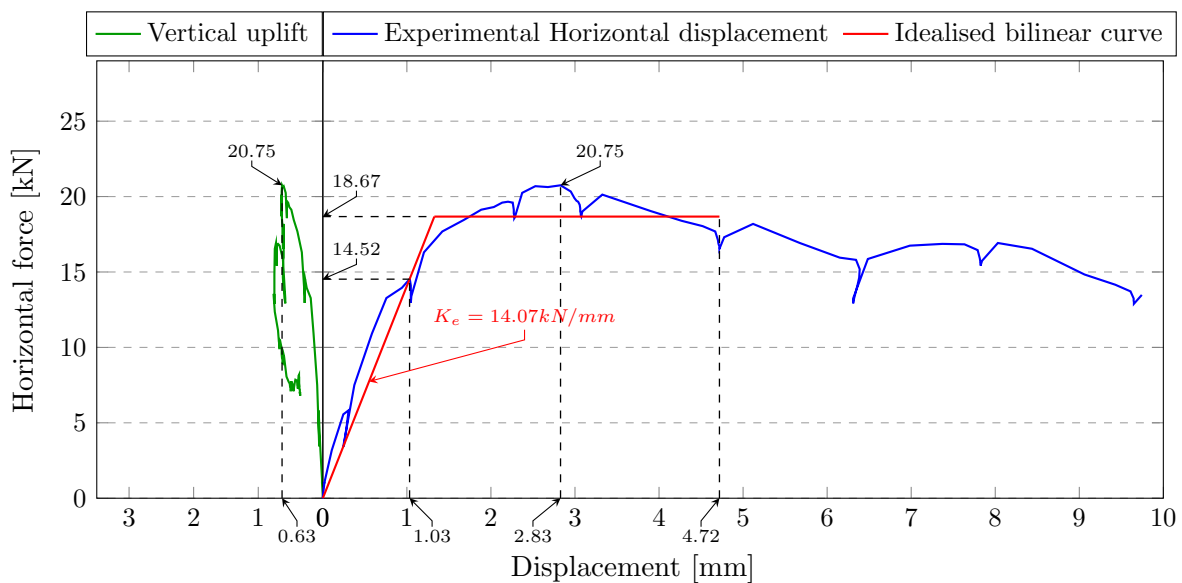


Figure 6.17: Adobe-W-B: Test Results

CHAPTER 6. RESULTS AND DISCUSSION

The specimen failed at a maximum lateral resistance of 20.75kN, reached after a horizontal displacement of 2.83mm, which corresponds to a drift capacity of 0.19%. The resistance at crack limit was 14.52kN with a displacement of 1.03mm and the calculated effective stiffness was 14.07 kN/mm. The ultimate resistance was found to be 18.67kN, corresponding to a displacement of 1.33mm. The ultimate displacement was 4.72mm, corresponding to an ultimate drift capacity of 0.31%. The test results of both Adobe wall specimens are summarised in Table 6.10.

Similar trends can be observed between the CSEB and Adobe wall results. The shift of the diagonal crack towards the middle of the specimen was observed for Adobe-W-B. Further, a reduction in the maximum and ultimate lateral resistance as well as their respective horizontal displacement between the two Adobe walls can be seen from the tests results. Adobe-W-B showed, however, an increase in the effective stiffness, whereas the opposite was observed with the CSEB specimens.

Table 6.10: Adobe walls - Results from Experimental and Idealised Curves

Wall Specimen	H_{cr} [kN]	d_{cr} [mm]	K_e [kN/mm]	H_u [kN]	d_e [mm]	H_{max} [kN]	$d_{H_{max}}$ [mm]	δ [%]	d_u [mm]	δ_u [%]
Adobe-W-A	16.01	1.40	11.41	20.58	1.80	22.87	3.85	0.26	4.46	0.30
Adobe-W-B	14.52	1.03	14.07	18.67	1.33	20.75	2.83	0.19	4.72	0.31

It can be seen in Figure 6.15 and Figure 6.17 that there was a significant reduction in the vertical uplift between the two tests. The reading from the 2MN LC at the maximum horizontal force reached during the Adobe-W-B test indicated a force of 14.76kN.

6.3.4 AACB Walls

The two AACB wall specimens were the last walls tested in this experimental study. The applied pre-compression level was determined similarly to the other wall specimens and had a magnitude of 0.97MPa, corresponding to a force of 246kN. The walls were referred to as AACB-W-A and AACB-W-B, the meaning of which is based on the test set-up configurations. The constituent material properties are given in Table 6.11.

It should be noted that the time at which the AACB walls were tested differed from the other walls types as the AACB-W-B specimen was tested before AACB-W-A. This is reflected in the unit compressive strength of AACB-W-A being greater than the AACB-W-B unit compressive strength.

Table 6.11: AACB walls - Unit and Mortar Properties

WALL	UNIT		MORTAR			
	f_u	E_u	f_m		E_m	
	[MPa]	[GPa]	[MPa]	(COV)	[GPa]	(COV)
AACB-W-A	22.44	12.14	19.03	3.16 %	13.21	2.90 %
AACB-W-B	20.87	11.41	19.44	3.76 %	13.45	1.30 %

CHAPTER 6. RESULTS AND DISCUSSION

AACB-W-A

The behaviour of AACB-W-A, during the test, was characterised by an initial uplift of the wall as a horizontal crack formed at the bottom mortar joint. A second crack formed in a staircase shape, starting from the unit on the sixth course of masonry down to the second course. Slight rotation of the wall was observed as the horizontal and vertical displacement increased. The third crack formed after a horizontal movement occurred of the two top courses of masonry which had ultimately caused a diagonal shear crack through the mortar joints as well as through the units around the bottom compressive area of the wall. The crack pattern and test results are shown in Figure 6.18 and Figure 6.19 respectively.

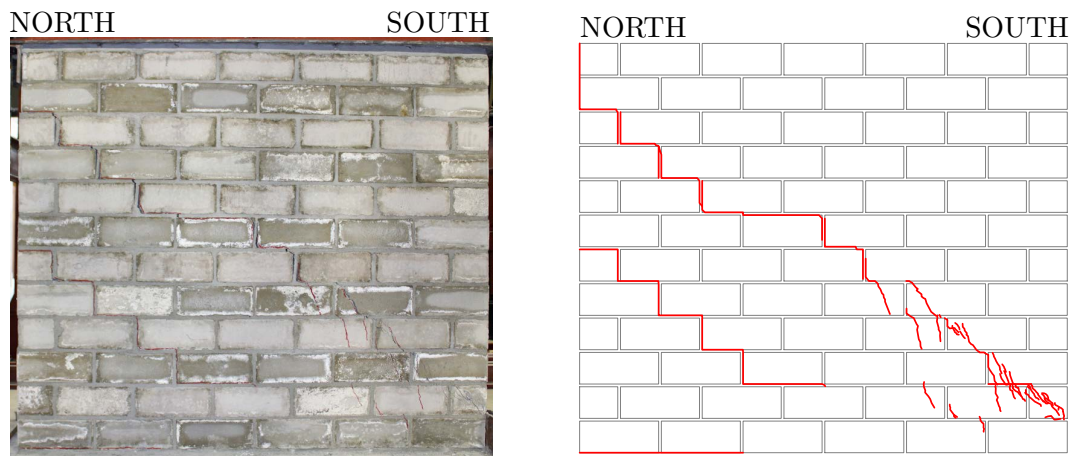


Figure 6.18: AACB-W-A: Crack Patterns

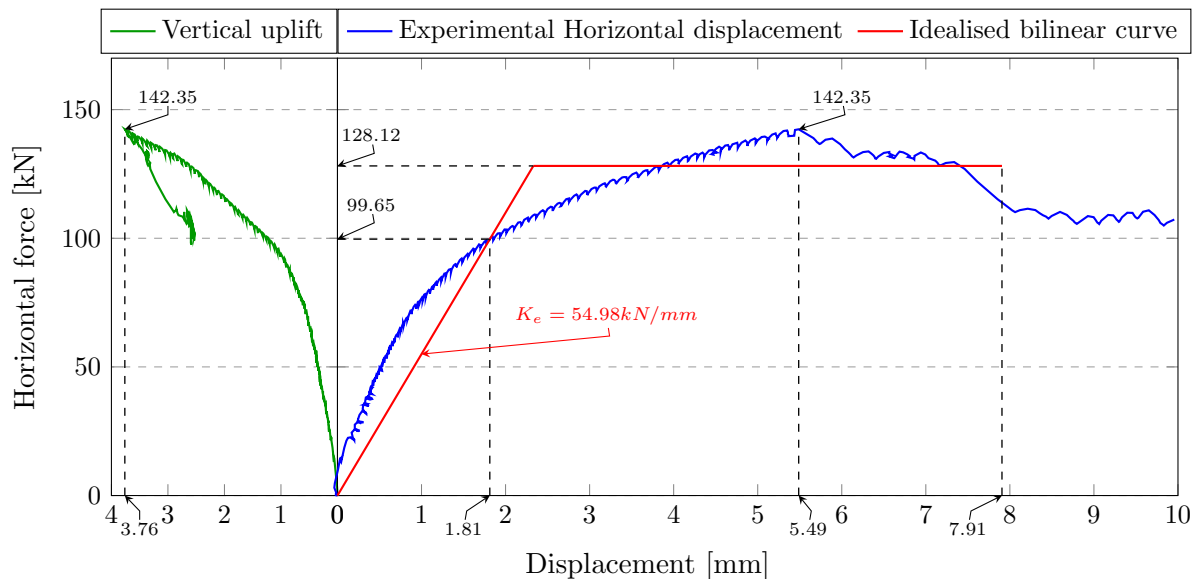


Figure 6.19: AACB-W-A: Test Results

A maximum lateral resistance of 142.35kN was reached at a horizontal displacement of 5.49mm, which corresponds to a drift capacity of 0.37%. At the crack limit, the lateral resistance was

CHAPTER 6. RESULTS AND DISCUSSION

99.65kN and the horizontal displacement was 1.81mm. The effective stiffness was calculated to be 54.98 kN/mm. The ultimate resistance was 128.12kN, at a horizontal displacement of 2.33mm. The ultimate displacement corresponding to 20% strength degradation was 7.91mm, which corresponds to an ultimate drift capacity of 0.53%.

AACB-W-B

AACB-W-B was characterised by a diagonal shear failure. The shear cracks developed in similar ways as for the CSEB walls, with the crack starting from the centre of the specimen and gradually extending towards the opposite corners. The cracks formed through the units as well as the mortar joint. As the vertical uplift was minimised, no bottom horizontal cracks were induced. The final crack patterns are shown in Figure 6.20 and the graphical representation of the test results are shown in Figure 6.21.

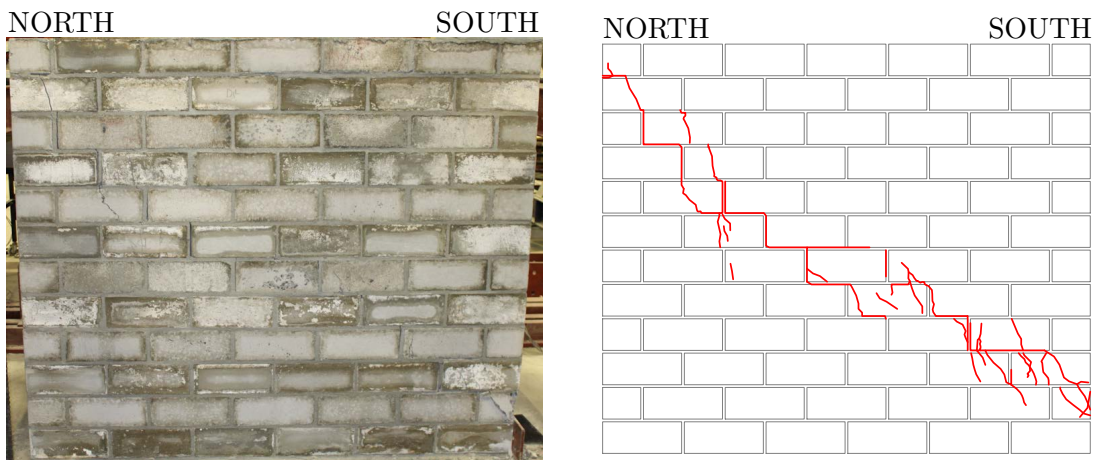


Figure 6.20: AACB-W-B: Crack Patterns

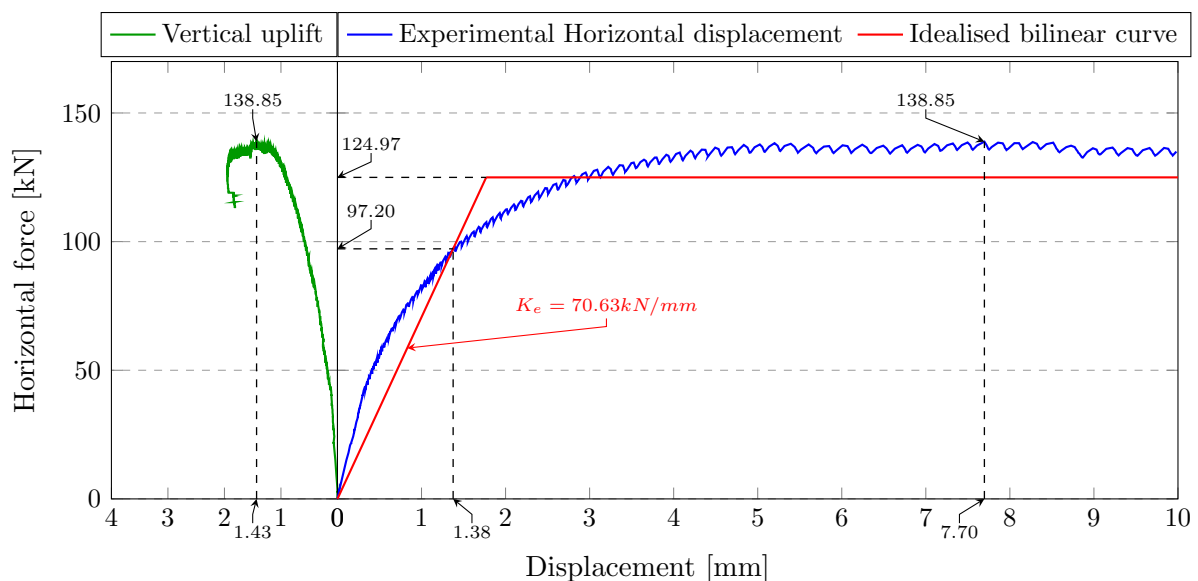


Figure 6.21: AACB-W-B: Test Results

CHAPTER 6. RESULTS AND DISCUSSION

The specimen resisted a maximum lateral force of 138.85kN at a horizontal displacement of 7.70mm which corresponds to a drift capacity of 0.51%. The lateral resistance at crack limit was 97.20kN with a horizontal displacement of 1.38mm. The effective stiffness of the wall was calculated to be 70.63 kN/mm. The ultimate resistance was found to be 124.97kN, with a corresponding horizontal displacement of 1.77mm. As no strength degradation was observed in the post peak range and before the test was stopped, the ultimate displacement was not determined.

Comparing the results shown in both Figure 6.19 and Figure 6.21, a considerable reduction in the vertical uplift can be observed, an indication that the test set-up was able to achieve its purpose. The test results for both AACB-W-A and AACB-W-B are summarised in Table 6.12.

Table 6.12: AACB walls - Results from Experimental and Idealised Curves

Wall Specimen	H_{cr} [kN]	d_{cr} [mm]	K_e [kN/mm]	H_u [kN]	d_e [mm]	H_{max} [kN]	$d_{H_{max}}$ [mm]	δ [%]	d_u [mm]	δ_u [%]
AACB-W-A	99.65	1.81	54.98	128.12	2.33	142.35	5.49	0.37	7.91	0.53
AACB-W-B	97.20	1.38	70.63	124.97	1.77	138.85	7.70	0.51	-	-

The test results show a decrease in the ultimate and maximum lateral resistance between the two wall specimen. However, AACB-W-B shows an increase in the effective stiffness, similar to the Adobe-W-B specimen. At the maximum lateral load, the force reading from the 2MN LC was 78.36kN.

6.3.5 Discussion on the Shear-compression Test

Shear-compression tests on AMU walls were successfully conducted using both test set-up configurations. The CMU wall test outcomes provided insights on how to improve the subsequent tests. With CMU-W-A, it was realised that the application of the horizontal force should only begin after the full pre-compression force was applied, this was carefully monitored for all the subsequent tests. Another realisation was with regard to the movement of the supporting frame resulting from the wall resistance as well as the rotation of the spreader beam which caused the rotation of the hydraulic jack and ultimately causing sway movement of the frame.

With CMU-W-B, it was realised that the vertical uplift of the specimen was not fully restrained by the lateral beam as the high tensile nuts, connecting the lateral beam to the high tensile bars and maintaining it in position on top of the spreader beam, were not fastened after the compressive force was applied. This resulted in a configuration where the vertical uplift was not restrained. However, the test results shown in Figure 6.22, which represent the vertical displacements on both the north and south sides of the specimen, plotted against the increasing vertical force which was monitored by the 2MN LC.

The upwards displacement was recorded as positive reading by LVDT-2, located north of the specimen, and the downwards displacement was recorded as negative reading by LVDT-4 which was located south of the specimen.

CHAPTER 6. RESULTS AND DISCUSSION

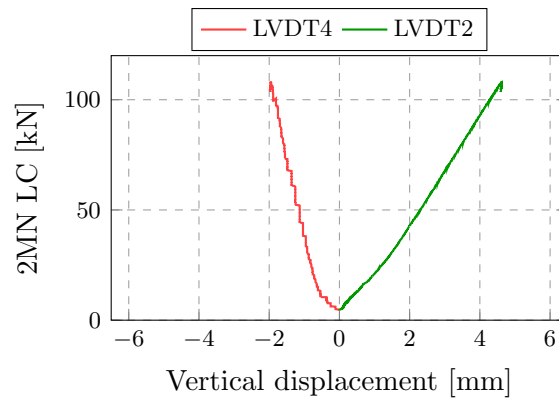


Figure 6.22: CMU-W-B: 2MN LC Force vs Vertical Displacement

As it can be seen in Figure 6.22, larger vertical displacements were recorded with LVDT-2 than LVDT-4. Although the fixed configuration provided by the high tensile bars in Test Set-up B was still able to slightly reduce the vertical uplift, the graphs in Figure 6.22 give an indication of how much rotation occurred with Test Set-up A. The initial reading in the LC was simply the weight of the lateral beam. After seeing how the wall behaved from the test results, it was clear that the high tensile nuts needed to be tightened and that the tensile bars required to be slightly pre-tensioned as soon as the full pre-compression force was applied.

This was done with the three AMU walls tested using Test set-up B. Shown in Figure 6.23, the vertical displacements of the three AMU walls were plotted against the increasing vertical force in the 2MN LC. It should be noted that the vertical axis label, 2MN LC [kN], is the same for all three graphs, even though the magnitude of the force differs.

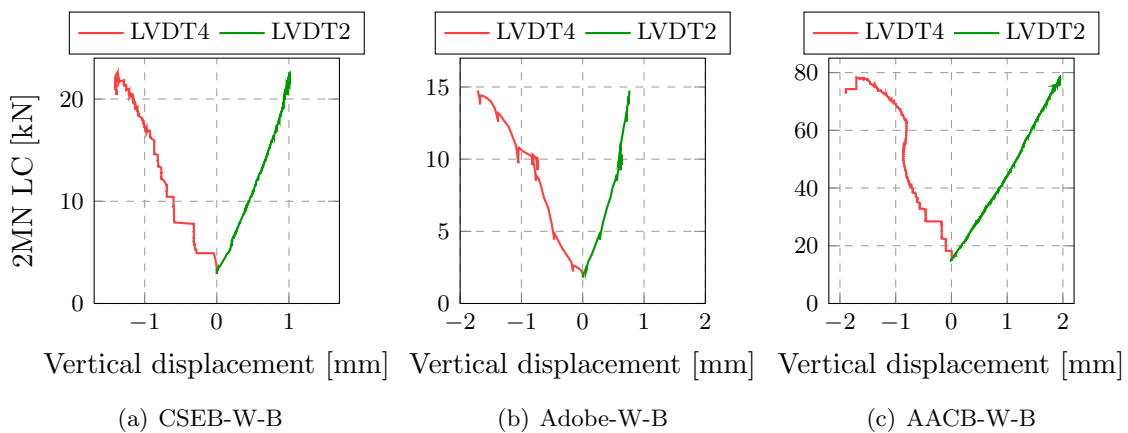


Figure 6.23: 2MN LC force vs Vertical Displacement

The three graphs show similar trends, with a reduction in the vertical displacement recorded by LVDT-2. This indicated that the use of high tensile bars with the lateral beam in Test set-up B to reduce the rotation of the spreader beam was achieved. The high tensile bars were slightly pre-tensioned before starting each test. The magnitude of the initial LC readings was 3kN, 1.8kN, and 15kN for CSEB-W-B, Adobe-W-B, and AACB-W-B respectively.

CHAPTER 6. RESULTS AND DISCUSSION

Shown in Figure 6.24 are the force-displacement responses of all the wall specimens. Although the tests performed on both CMU walls were not completed successfully, their force-displacement responses show higher stiffness compared to the AMU wall specimens.

The behaviour of the masonry wall specimens indicate a relation between each wall and its constituents. At the material level, CMU specimens showed higher strength and stiffness as highlighted in Section 6.1.2. Similar findings are also reflected at the structure level with the wall test results. As it was sought, the wall tests on AMUs resulted in structural responses over a wide spectrum, with the AACB walls showing higher lateral capacities and stiffnesses followed by the CSEB walls and Adobe walls.

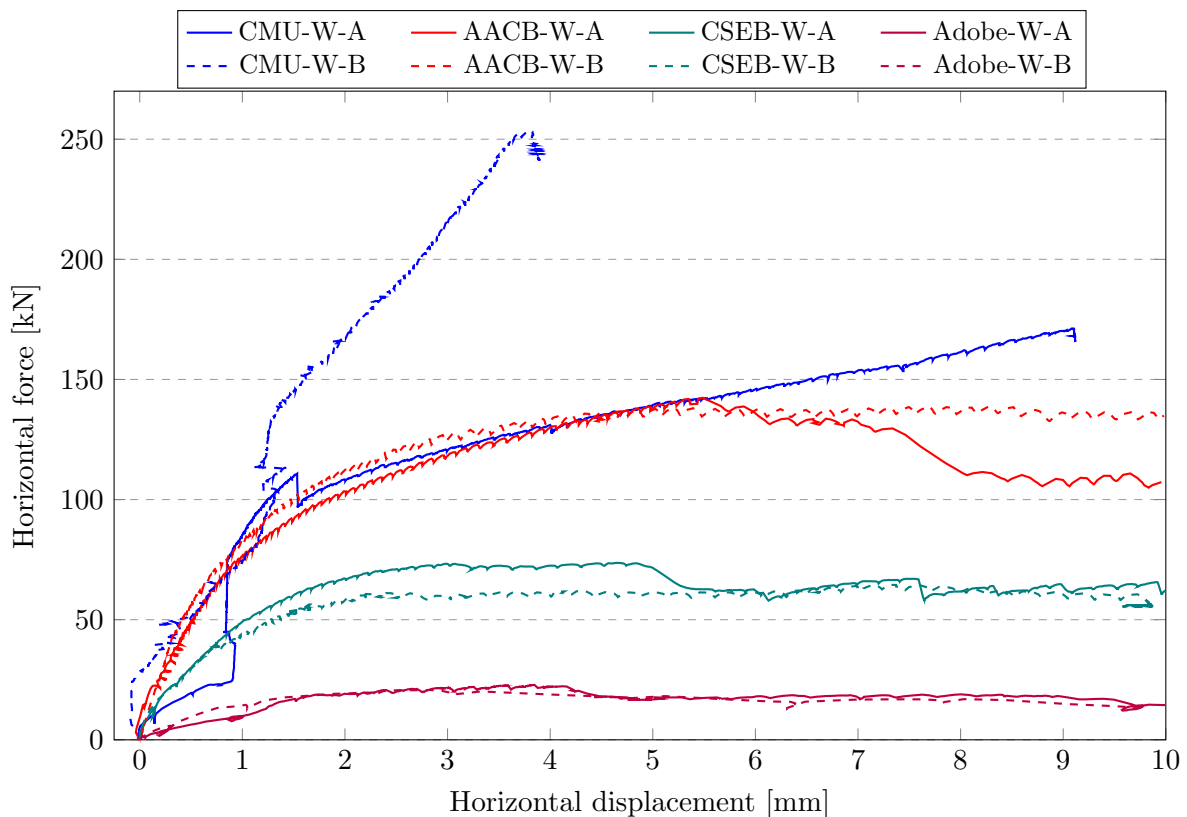


Figure 6.24: Masonry Wall Test Results

For each wall tested, the drift capacity δ and the ultimate drift capacity δ_u were determined for the respective horizontal displacements. Assuming that the Limit State of Significant Damage (LSSD) is reached at the maximum lateral resistance, and the Limit State of Near Collapse (LSNC) at 20% strength degradation, a comparison between the test results and the values provided in Table 2.1 from BS EN 1998-3 (2005), is shown in Table 6.13. Due to the difference in boundary conditions (BC) between Test set-up A and Test set-up B, the drift capacity values for BS EN 1998-3 are calculated using values of shear span h_0 equal to h for Test set-up A and $0.5h$ for Test set-up B for the flexural failure mode.

With the exception of CSEB-W-B and AACB-W-B, the obtained results are lower than the values provided in the code for conventional material walls. The values of the drift capacity vary

CHAPTER 6. RESULTS AND DISCUSSION

largely between the 3 AMUs, with Adobe walls having the lowest value, followed by CSEB and AACB walls. Although [BS EN 1998-3 \(2005\)](#) does not take into account the difference in BC for the shear failure mode, the effect of the difference in boundary conditions is clearly visible, with an increase in the drift capacity between the results for Test set-up A and Test set-up B for CSEB and AACB walls. However, the opposite result is observed for Adobe walls.

Table 6.13: Drift Capacity Comparison

Wall Specimen	Drift Capacity [%]				Failure Mode
	LSSD		LSNC		
	Results	BS EN 1998-3	Results	BS EN 1998-3	
CMU-W-A	0.61	0.67		0.89	Flexural
CMU-W-B	0.25	0.33		0.44	Flexural
CSEB-W-A	0.31	0.40	0.41	0.53	Shear
CSEB-W-B	0.49	0.40	-	0.53	Shear
Adobe-W-A	0.26	0.40	0.30	0.53	Shear
Adobe-W-B	0.19	0.40	0.31	0.53	Shear
AACB-W-A	0.37	0.40	0.53	0.53	Shear
AACB-W-B	0.51	0.40	-	0.53	Shear

In representing the idealized bilinear envelope, the factors of 0.7 and 0.9 were respectively used to determine the crack limit and ultimate resistances of the wall specimens. However, it should be noted that these values were determined based on experimental tests performed on URM walls constructed with conventional masonry units. For future studies, additional shear-compression tests on AMU walls will contribute in gathering necessary data to determine the factors that can be used for idealized bilinear envelope of AMU walls.

With Test set-up B, the control of the Instron testing machine changed from force control, to a displacement control configuration. The test started by applying the pre-compression force and once the magnitude of the force is reached, the position of the Instron actuator was maintained throughout the test. The test results indicated that a slight reduction in the compressive force gradually occurred as the horizontal force was applied. The load decreased at a faster rate until the crack limit was reached, after that the load either increased again at a slower rate until the maximum lateral resistance of the wall was reached (Adobe-W-B and AACB-WB) or the load continued reducing at a slower rate (CSEB-W-B).

The load reduction was about 14%, 20%, and 11% of the initial load for CSEB-W-B, Adobe-W-B, and AACB-W-B specimen respectively. This however did not seem to have affected the final test results as the position of the spreader beam was maintained, leading to a shift of the diagonal shear cracks towards the middle of the specimens. The test results indicating the load readings in the Instron testing machine and the 2MN LC together with the applied horizontal force are provided in [Figure C.5](#) in [Appendix C](#). The load readings in the 2MN LC indicate the tensile force in the two high tensile bars.

CHAPTER 6. RESULTS AND DISCUSSION

Due to the observed movement of the supporting frame, the connecting bolts needed to be checked, and halfway through the experimental programme, all the bolts were loosened then retightened to ensure that the test set-up was back in its original position. The movement of the supporting frame was monitored during both the AACB wall tests. An additional LVDT, referred to as LVDT-6 was positioned north of the test set-up at the hydraulic jack reacting column and at a height of 1720mm above the laboratory floor. The measured displacements were plotted against the horizontal force and are shown in Figure 6.25.

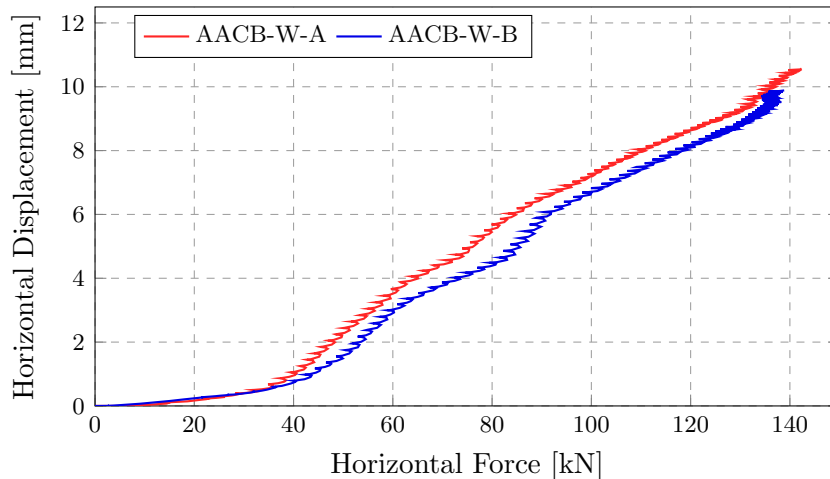


Figure 6.25: LVDT-6 Readings (AACB-W-A & AACB-W-B)

As it can be seen in the figure, significant movement of the supporting frame occurred during the tests. Slow displacement occurred at low horizontal forces (0 to 40kN) thereafter the displacement occurred at a faster rate until the test was stopped. The causes of this movement can be attributed to many factors, including the rotation of the spreader beam causing the rotation of the hydraulic jack, induced movement due to the application of the horizontal force, the bolted connections of most of the steel elements (beams and columns) using angle cleats, and the overall size of the test set-up.

Minimising the rotation of the spreader beam in Test set-up B had contributed to reducing, though only slightly, the movement of the supporting frame - for a given force after 40kN, the displacement readings for AACB-W-A were higher than the AACB-W-B readings.

From these observations it is clear that the test set-up will need to be stiffened more for future studies. Various options could be considered based on the materials available in the laboratory. However, having a reaction wall would significantly contribute to a stiffer test set-up.

Although significant movement of the supporting frame was observed, the influence this had on the test results for a given wall was considered minimal as all the displacement of the wall specimens were measured using LVDTs fixed on separate supporting elements which were not in contact with the test set-up. The LC attached to the Enerpac hydraulic jack provided the actual readings of the applied load. The results presented in the section were from these recorded

CHAPTER 6. RESULTS AND DISCUSSION

readings. For each wall tested, the strong mortar used at top and bottom of the specimen which had a compressive strength of more than 50MPa, had also contributed to avoiding any failure at those mortar joints. the strong mortar mix is shown under “All Units” in Table 3.7.

The difference in the results from the two test set-up configurations indicated that with Test set-up A, where fixed-free boundary conditions were provided to the wall, higher lateral capacity of wall specimens was observed as compared to the results from Test set-up B. With the configuration in Test set-up B, which provided fixed boundary conditions with a mixed control approach of the vertical movement (force and displacement), a reduction in the shear span was observed as it can be seen in the figures showing the crack patterns mostly located in the centre of the specimens. These findings are similar to some of those provided by [Petry and Beyer \(2014\)](#) as highlighted in Section 2.6.

6.4 Conclusion

This chapter presented and discussed the results obtained from the various tests performed in this experimental study. The tests were conducted in the laboratory of Stellenbosch University and were performed on masonry units, wallets, and walls. The unit tests were conducted on CMU and AMUs to determine their respective compressive strength and modulus of elasticity, as well as the densities.

The characteristics of masonry were determined by performing tests on the masonry wallets. During this test, both the compressive strength and modulus of elasticity of the wallets were determined. The compressive strength of masonry wallets was required for the test performed on the walls.

Shear-compressive tests, with monotonic horizontal force applied at the top of the wall specimen, were performed on eight masonry walls, with two walls made of each of the four masonry units, namely CMU, CSEB, Adobe and AACB. Difficulties were encountered while performing tests on CMU walls. However the learnings from these tests were applied to the AMU walls which resulted in tests being completed successfully.

Chapter 7

Conclusion

The aim of the experimental study presented in this document was to determine the in-plane structural response of unreinforced masonry (URM) walls constructed with alternative masonry units (AMUs). This is part of a larger study project underway at Stellenbosch University which focuses on the development of AMUs to be used as construction materials for low-income housing in South Africa.

As seismic standards have been introduced in South Africa and certain areas in the country identified to be at risk of low to moderate seismic actions, structural buildings such as URM buildings are required to be designed for seismic actions. Experimentally, the effect of seismic actions is usually investigated by subjecting the structural wall through similar load conditions as to those experienced within the structural building during an earthquake. To this end, different tests are performed in a laboratory setting, some of which are conducted through testing devices, designed and constructed in the laboratory, which apply lateral and vertical loading or displacements in various ways.

This was the case for this experimental study. Investigating the in-plane structural response of AMU walls was the means by which the capacity of AMU walls to resist lateral forces induced by seismic actions was determined. The obtained results form part of the mechanical performances of AMUs, which will further be used for validation of numerical models being developed, and ultimately contribute to the development of AMUs as construction materials.

Three objectives guided this study. The first objective consisted in manufacturing the masonry units being investigated, namely the concrete masonry units (CMUs) - considered a benchmark for the larger study project - the compressed stabilized earth blocks (CSEBs), the Adobe blocks, and the alkali-activated concrete blocks (AACBs). Characterisation tests were also conducted on these masonry units as part of the first objective.

The second objective was the design and construction of the test set-up which was used to perform the shear-compression test on masonry walls. Determinant factors with this objective were related to the limitations in the laboratory. However, using effectively the materials and equipment available, a test set-up was designed and constructed which allowed for the achievement of the third objective, consisting in the performance of in-plane shear-compression tests on masonry

CHAPTER 7. CONCLUSION

walls constructed with CMUs and AMUs respectively. The observations and conclusions made with regard to the three objectives of this study are provided hereafter.

7.1 Block Manufacturing

The block manufacturing process was set up in such a way that the blocks were created with a high degree of quality control. This aimed at reducing variabilities in the properties of the blocks. The following conclusions could be made with regard to manufacturing the blocks.

- The mix proportions for each unit type were adopted from previous studies; however it was necessary to investigate the constituent material properties for the mixes as these would differ from one batch to another and ultimately required adjustments to be made to the mix design.
- CMUs, CSEBs, and Adobe blocks were created by compacting their respective mixtures in a manual earth block press. A lot of effort was particularly required during the creation of CMUs due to the nature of the mixture, and care needed to be taken while removing the unit from the block press to ensure that no deformation was induced to the unit.
- CSEBs and Adobe blocks were manufactured with much more ease as these blocks held their shape well after compaction. A new CSEB mix design was proposed by adjusting the water content based on the constituent materials available.
- The study showed that good quality Adobe blocks could be created using the block press. If needed, the mass of the mixture placed in the block press chamber could be increased to improve the properties of these blocks (i.e. density, compressive strength, etc.). However, due to the nature of the mixture, the block press chamber should regularly be cleaned during the manufacturing process.
- AACBs were created by casting the wet mixture into wooden moulds. Due to the use of sodium hydroxide and sodium silicate in the mix, it was important to handle these products with great care and avoid skin contact with the mixture.
- Once each AACB was demoulded, the wooden moulds needed to be cleaned and prepared for the next set of blocks. This task was particularly time consuming, protracting the manufacturing process.
- The manufactured AACB had a powdery substance with crystal-like shapes forming on the surface of the units. The cause was not investigated in this study, and it is suggested that further investigation be carried out in future studies.

7.2 Characterisation and In-plane Shear-compression Tests

The characterisation tests performed in this study on masonry units include the compressive strength and modulus of elasticity tests, as well as the density tests. For the masonry wallets, the compressive strength as well as the modulus of elasticity of each of the masonry types were also

CHAPTER 7. CONCLUSION

determined together with the in-plane shear-compression tests on masonry walls. The following observations were made in relation to the obtained results.

7.2.1 Characterisation Tests

- The compressive strength tests were performed at different periods of the experimental programme. For each of the four masonry types (CMUs, CSEBs, Adobe and AACBs) investigated, a strength gain was observed over time, although very little for the Adobe specimens. Between the four masonry types, the AACB ones showed the highest compressive strength, followed by the CMU, CSEB and Adobe specimens.
- Little variabilities were observed for the compressive strength tests, with all the COV values less than 10%. Care needed to be taken to ensure that the loading faces of each specimen were horizontal and parallel to each other. This was achieved by grinding the specimens.
- The modulus of elasticity tests were also performed at different periods of the experimental programme. While an increase in the stiffness was observed over time, this occurred to different degrees based on the age differences at the time of testing. For instance, large stiffness gain was observed with CMU specimens, as the age difference between two consecutive tests (i.e. 28 days and Wall#1) was significant.
- The results of the modulus of elasticity of specimens tested at 28 days were similar to those obtained in previous studies and were related to values presented in literature. However, large variabilities depicted by large COV values were observed from the test results.
- The results from the density tests were within the range of values reported in literature. Low COV values were obtained, which suggested that there were little variations between the different mixes of a given masonry unit. Further, a high quality control in the manufacturing process was observed.
- The compressive strength and modulus of elasticity of the masonry were obtained by performing uniaxial compressive tests on wallets. The compressive strength results were almost similar to the results obtained by [Fourie \(2017\)](#). However, there were concerns with the modulus of elasticity results as they were low compared to the results from [Fourie](#). This was attributed to the difficulty encountered during the test performance. However, the observed failure mode of the AMU specimens - where rubber mats were used at the top and bottom loading faces - was characterised by vertical cracks from the top to the bottom of the specimen, and parallel to the loading direction.

7.2.2 In-plane Shear-compression Tests

- A pre-compression level, corresponding to 15% of the masonry wallet compressive strength was applied at the top of the wall specimen. A horizontal monotonic force was slowly applied at the top of the wall.
- The applied force and resulting displacement were monitored and recorded throughout the tests. Good results were obtained for the shear-compression tests on AMU walls. The

CHAPTER 7. CONCLUSION

results and behaviour of the CMU wall contributed to providing insights in how the tests needed to be conducted.

- The use of test set-ups with different boundary conditions resulted in walls showing different lateral capacities, with higher capacity achieved when a fixed-free boundary conditions configuration is adopted.
- The crack patterns within the different walls also highlighted the difference between the two boundary conditions configuration. When the wall was tested with fixed boundary conditions, the diagonal shear crack was located in the centre of the specimen and extended from one top corner to the opposite bottom corner.
- The use of the lateral beam positioned with the two high tensile bars on the north side of the specimen proved to be successful in creating the fixed-fixed boundary conditions for the test set-up and contributed in reducing considerably the vertical uplift which occurred with the fixed-free boundary conditions.
- For the shear-compression tests, the horizontal force was applied until the maximum lateral resistance of the wall was achieved, or after a horizontal displacement of 10mm. The obtained results are presented graphically - showing the experimental results and an idealised bilinear envelope - and are summarized in a table for all the four masonry types.
- Comparing the test results of CMUs and AMUs, the force-displacement responses of CMU walls have shown higher lateral capacities than the AMU walls. However, the force-displacement responses of AMU walls provide a good indication of their in-plane structural responses. The obtained experimental results can be used in future studies and contribute to validating numerical models on AMUs.
- The results obtained for the drift capacity provide a wide range of the displacement capacity of AMUs based on their respective lateral capacities (strength and stiffness). It is suggested that additional tests be performed in future studies to investigate and determine the (ultimate) drift capacity for walls constructed with AMUs.

7.3 Observations on the Test Set-ups

The results presented in this study were achieved through a series of experimental tests performed in the laboratory at Stellenbosch University. The test set-ups used were either based on guidelines provided in different design standards, adopted from previous studies, or designed and constructed using the available materials. The following observations and conclusions were made with regards to the test set-up.

- The compressive strength tests on CMUs and AMUs were successfully conducted with an adopted test set-up, which was previously used to conduct similar test in the structure laboratory at Stellenbosch University. Little difficulties were encountered while performing the compressive strength tests.
- The modulus of elasticity tests were conducted on prismatic (CMU, CSEB, Adobe) and

CHAPTER 7. CONCLUSION

cylindrical (AACB) specimens. Two different testing machines were used to perform the tests. Difficulties were encountered with cutting the prismatic specimens from the masonry units, resulting in small errors in their respective dimensions. Other difficulties were related to performing the test. These include placing the LVDTs around the specimen and ensuring that all the test data were recorded correctly.

- Even though the loading face of some of the specimens was grinded, it seemed, from the recorded data, that for some specimens one of the LVDT readings were negative, indicating that this side of the specimen was in tension, whereas the other sides were in compression.
- The density test was conducted following the guidelines provided in [BS EN 772-13 \(2000\)](#). The test was successfully conducted without difficulties.
- The test set-up for the masonry wallets was adopted from the study presented by [Fourie \(2017\)](#). Although all the tests were conducted to completion, difficulties were encountered with the test set-up as well as the testing equipment. While the technical difficulties related to the tests were solved, it is suggested for future studies that the wallet be built on different elements from those used in this study (steel channel sections) to reduce the variability they may have caused.
- The wallet specimens were positioned in the Instron testing machine using an overhead crane and were then centered using the steel rods acting as rollers. To remove the rollers, a steel bar was used to lift a little one side of the specimen and, once these removed, the specimen was put back into its normal position, where it would be in contact with the apparatus. This process needed to be conducted with a lot of care in order to ensure no damage was made to the specimen.
- The set-up used to conduct the shear-compression test had fulfilled its purpose based on the test results obtained. However, rotation of the spreader beam was observed with Test set-up A. This was reduced by adding a lateral beam positioned using high tensile bars.
- Large horizontal displacements of the supporting frame were observed while the test was underway. This was an indication that the test set-up will need to be further stiffened.
- Due to the high friction at the surface contact between the Enerpac hydraulic jack and the spreader beam, the occurring rotation of the spreader beam during the performance of the test resulted in the rotation of the hydraulic jack, which ultimately contributed to the sway movement of the supporting frame.
- Precautions and safety measures were observed while performing the in-plane shear-compression tests, especially while placing the two I-beams on top of the specimen. Care needed to be taken to ensure that the specimen was not destroyed before it was tested. There was little to no movements of the bottom steel plate and the out of plane movement of the spreader beam was prevented.
- Due to the size of the test set-up, additional assistance was required, which contributed to the tests being completed successfully and within the scheduled period of the experimental programme.

7.4 Recommendations for Future Studies

Based on the insight and learnings gained in this experimental study, the following are presented as recommendations for future studies.

- It is suggested that a system be put in place for the block manufacturing, in such a way that large amount of blocks can be manufactured in a short duration. Additional assistance had proven to speed up the process. A block process with capacity of producing more than one block at a time would contribute in reducing the manufacturing time period.
- Unit modulus of elasticity tests could be conducted on prismatic specimens using a LC with smaller capacity and ways could be determined to reduce the large variability in the results presented in this study.
- For the wallet tests, it should be ensured that the specimens are built in between two flat and horizontal surfaces. If steel channel sections are used, it should be ensured that they are not used for other test set-up, to avoid any deformation of these elements.
- Using rubber mats at the top and bottom of the specimen had proven to contribute further in reducing any unevenness of the specimen loading faces.
- Due to the large movements observed in the test set-up, it is suggested that the stability of the test set-up be increased. One option could be by adding a third column to the south side of the test set-up and providing bracings between the new added column and the existing column. However, if a reaction wall can be built, it could be used as a reacting element for the test equipment applying the horizontal force. In this study, the Enerpac hydraulic jack was used.
- The connections between steel members were done using angle cleats. This may have also contributed to the movement of the reaction frame. It is thus suggested to rotate the columns in such a way that the connections are made directly between the steel members.
- It is suggested to provide a mechanism, similar to a bridge bearing, or smooth and frictionless surface contact between the spreader beam and the hydraulic jack, which will allow the movement of the spreader beam (i.e. rotation) without inducing any vertical movement of the hydraulic jack.
- A fixed-fixed boundary condition of the test set-up was sought to be achieved in this study by minimizing the rotation of the spreader beam. This aim was reached by using the lateral beam placed on top of the spreader beam and held in position through high tensile bars. To further improve the system, two Instron testing machines could be placed on each side of the spreader beam and be operated in a force or displacement controlled manner.
- The design of a proposed test set-up for in-plane shear-compression test is shown in Figure C.6 in [Appendix C](#). In this set-up, two braced columns act as a reaction frame for the apparatus (Enerpac hydraulic jack) applying the horizontal force and which is connected to the reaction frame and spreader beam by means of hinges.

CHAPTER 7. CONCLUSION

- The application of the horizontal force can be done by means of an Instron actuator with a known and constant loading rate, the results of which could be compared to the ones presented in this study, to determine the impact of manually applying the horizontal force.
- The behaviour factor, provided in design codes for linear elastic analysis of URM, takes into account the non-linear behaviour of these structures. However, the value of 1.5 may not be applicable for AMUs. With the results of experimental tests on AMUs such as those presented in this study, a basis for the calculations of the behaviour factor for AMUs may be established. Further experimental tests, as well as direct non-linear dynamic analysis are necessary to calculate the value of the behaviour factor for AMUs.
- Once the test set-up has been improved, the post-peak behaviour of the tested wall can be investigated together with the ductility behaviour of AMU walls.
- Bracings should be provided to the lateral supporting frames to reduce movements resulting due to their heights.

References

- Abdullah, M.M.A., Ibrahim, W.M.W. and Tahir, M.F.M. (2015). The properties and durability of fly ash-based geopolymeric masonry bricks. In: Pacheco-Torgal, F., Lourenço, P.B., Labrincha, J.A., Kumar, S. and Chindaprasirt, P. (eds.), *Eco-Efficient Masonry Bricks and Blocks*, pp. 273–287. Woodhead Publishing, Oxford. ISBN 978-1-78242-305-8.
Available at: <http://www.sciencedirect.com/science/article/pii/B9781782423058000127>
- ASTM C469/C469M-14 (2014). Standard Test Method for Static Modulus of Elasticity and Poisson's Ratio of Concrete in Compression. *ASTM International*, vol. 04, pp. 1–5.
- Ballerino, C.C. (2002). Building Materials & Engineering Design: Low-Income Housing Projects.
- Barnard, R. (2014). *Mechanical properties of fly ash/slag based geopolymer concrete with the addition of macro fibres*. Master's thesis, Stellenbosch University.
Available at: <http://scholar.sun.ac.za/handle/10019.1/95866>
- Benhelal, E., Zahedi, G., Shamsaei, E. and Bahadori, A. (2013). Global strategies and potentials to curb CO₂ emissions in cement industry. *Journal of cleaner production*, vol. 51, pp. 142–161. ISSN 09596526.
Available at: <http://dx.doi.org/10.1016/j.jclepro.2012.10.049>
- Beyer, K. and Petry, S. (2015). Size effects in drift capacities of URM walls. In: *Proceedings of the 12th North American Masonry Conference, Denver, Colorado: Masonry: Science, Craft, Art*.
- Bhattacharya, S., Nayak, S. and Dutta, S.C. (2014 January). A critical review of retrofitting methods for unreinforced masonry structures. *International Journal of Disaster Risk Reduction*, vol. 7, pp. 51–67. ISSN 2212-4209.
Available at: <http://dx.doi.org/10.1016/j.ijdr.2013.12.004>
- Brown, P.W. and Clifton, J.R. (1978). Adobe I: The Properties of Adobe. *Studies in Conservation*, vol. 23, no. 4, pp. 139–146.
Available at: <https://doi.org/10.1179/sic.1978.019>
- BS EN 1052-1 (1999 January). *Methods of test for masonry - Part 1: Determination of compressive strength*. British Standards Institution, London, United Kingdom. ISBN 0-580-30735-2.
- BS EN 12390-13 (2013 November). *Testing hardened concrete - Part 13: Determination of the secant modulus of elasticity in compression*. British Standards Institution, London, United Kingdom. ISBN 978-0-580-78114-8.
- BS EN 1998-3 (2005 July). *Eurocode 8: Design of structures for earthquake resistance - Part 3: Assessment and retrofitting of buildings*. British Standards Institution, London, United Kingdom. ISBN 978-0-580-83532-2.

- BS EN 772-1 (2011). *Methods of test for masonry units - Part 1: Determination of compressive strength*. British Standards Institution, London, United Kingdom. ISBN 978-0-580-84584-0.
- BS EN 772-13 (2000 August). *Methods of test for masonry units - Part 13: Determination of net and gross dry density of masonry units*. British Standards Institution, London, United Kingdom. ISBN 0-580-32725-6.
- Capozucca, R. and Sinha, B.P. (2004). Strength and Behaviour of Historic Masonry under Lateral Loading. *Proc. IBMaC, Amsterdam*, vol. 1, pp. 277–284.
- Davidovits, J. (2013). Geopolymer Cement. *A review. Geopolymer Institute, Technical papers*, vol. 21, pp. 1–11.
- de Almeida, J.A.P.P. (2012 July). *Mechanical characterization of traditional adobe masonry elements*. Master's thesis, University of Minho.
Available at: <http://hdl.handle.net/1822/20607>
- De Beer, L.R. (2016). *Developing and testing a sprayable overlay of Strain Hardening Cement-based Composite for retrofitting of unreinforced load bearing*. Master's thesis, Stellenbosch University.
Available at: <http://scholar.sun.ac.za/handle/10019.1/100318>
- De Villiers, W. and Boshoff, W. (2014). 3D modelling strategy for alternative masonry walling for South African low-cost housing. *9th International Masonry Conference*, pp. 1–9.
- Deboucha, S. and Hashim, R. (2011). A review on bricks and stabilized compressed earth blocks. *Scientific Research and Essays*, vol. 6, no. 3, pp. 499–506. ISSN 1992-2248.
- Domone, P. and Illston, J. (2010). *Construction Materials: Their Nature and Behaviour*. 4th edn. Spon Press. ISBN 9780203927571.
- Evonik Industries (2010 November). GPS Safety Summary, Sodium Hydroxide (NaOH). Technical information, Evonik Industries.
- Fourie, J. (2017). *Characterisation and Evaluation of the Mechanical Properties of Alternative Masonry Units*. Master's thesis, Stellenbosch University.
Available at: <http://scholar.sun.ac.za/handle/10019.1/100880>
- Garcia-Lodeiro, I., Palomo, A. and Fernández-Jiménez, A. (2015). An overview of the chemistry of alkali-activated cement-based binders. In: Pacheco-Torgal, F., Labrincha, J.A., Leonelli, C., Palomo, A. and Chindaprasirt, P. (eds.), *Handbook of Alkali-Activated Cements, Mortars and Concretes*, pp. 19–47. Woodhead Publishing, Oxford. ISBN 978-1-78242-276-1.
Available at: <http://www.sciencedirect.com/science/article/pii/B9781782422761500022>
- Haach, V.G., Vasconcelos, G. and Lourenço, P.B. (2009). Experimental analysis of reinforced concrete block masonry walls subjected to in-plane cyclic loading. *Journal of structural engineering*, vol. 136, no. 4, pp. 452–462.
- Hendry, A.W., Sinha, B.P. and Davies, S.R. (1997). *Design of Masonry Structures*. 3rd edn. E & FN SPON. ISBN 0419215603.
- Jablonski, N. (1996). Mix Design for Concrete Block – Proportioning Using the Fineness Modulus Method. *The Aberdeen Group*, pp. 1–4.

- Karimi, A.H., Karimi, M.S., Kheyroddin, A. and Shahkarami, A.A. (2016). Experimental and Numerical Study on Seismic Behavior of An Infilled Masonry Wall Compared to An Arched Masonry Wall. *Structures*, vol. 8, pp. 144–153. ISSN 2352-0124.
Available at: <http://www.sciencedirect.com/science/article/pii/S2352012416300807>
- Kaushik, H.B., Rai, D.C., Jain, S.K. and Asce, M. (2007 September). Stress-Strain Characteristics of Clay Brick Masonry under Uniaxial Compression. *Journal of materials in Civil Engineering*, vol. 19, no. 9, pp. 728–739.
- Kijko, A., Retief, S. and Graham, G. (2002). Seismic hazard and risk assessment for Tulbagh, South Africa: Part I – assessment of seismic hazard. *Natural Hazards*, vol. 26, no. 2, pp. 175–201.
- Laing, H. (2011). The “CMA House” Bringing detail and durability to affordable housing. In: *International housing & construction conference & exhibition 2011*, pp. 11–14.
- le Roux, F. (2014). *Structural, Economic and Environmental Feasibility of Plastic Load-Bearing Walling and Roofing Systems for Low-Income Housing*. Master’s thesis, Stellenbosch University.
Available at: <http://scholar.sun.ac.za/handle/10019.1/95939>
- Lee, N.K. and Lee, H.K. (2013). Setting and mechanical properties of alkali-activated fly ash/slag concrete manufactured at room temperature. *Construction and Building Materials*, vol. 47, pp. 1201–1209.
- Lourenço, P.B. (1998). Experimental and Numerical Issues in the Modelling of the Mechanical Behaviour of Masonry. *Structural Analysis of Historical Constructions II. CIMNE, Barcelona*, pp. 57–91.
- Malherbe, D. (2016). *The characterisation of compressed earth blocks stabilised with cement and agro-industrial residues*. Master’s thesis, Stellenbosch University.
Available at: <http://scholar.sun.ac.za/handle/10019.1/98356>
- Mohamad, A.-b.A.E. and Chen, Z. (2017). Experimental Studies on the Behavior of a Newly-Developed Type of Self-Insulating Concrete Masonry Shear Wall under in-Plane Cyclic Loading. *Applied Sciences*, vol. 7, no. 5, p. 463. ISSN 2076-3417.
Available at: <http://www.mdpi.com/2076-3417/7/5/463>
- Morel, J.C., Pkla, A. and Walker, P. (2007). Compressive strength testing of compressed earth blocks. *Construction and Building Materials*, vol. 21, no. 2, pp. 303–309. ISSN 09500618.
- Norton, J. (1986). *Building With Earth: A Handbook*. Intermediate Technology.
- Pacheco-Torgal, F. and Jalali, S. (2011). *Eco-efficient Construction and Building Materials*. Springer, London. ISBN 978-0-85729-891-1.
- Pacheco-Torgal, F., Lourenco, P.B., Labrincha, J., Chindaprasirt, P. and Kumar, S. (2014). *Eco-efficient Masonry Bricks and Blocks: Design, Properties and Durability*. Woodhead Publishing.
- Parisi, F. and Augenti, N. (2012). A Shear Response Surface for the Characterization of Unit-Mortar Interfaces. In: *Report of the 15 th International Brick and Block Masonry Conf.- Brazil*.
- Pelà, L. (2009). *Continuum Damage Model For Nonlinear Analysis Of Masonry Structures*. Ph.D. thesis, Università degli Studi di Ferrara.
Available at: <http://eprints.unife.it/87/>
- Petry, S. (2015). *Force-displacement response of unreinforced masonry walls for seismic design*. PhD Thesis, Ecole Polytechnique Federale de Lausanne.

- Petry, S. and Beyer, K. (2014). Influence of boundary conditions and size effect on the drift capacity of URM walls. *Engineering Structures*, vol. 65, pp. 76–88.
Available at: <http://dx.doi.org/10.1016/j.engstruct.2014.01.048>
- Reddy, B.V. and Jagadish, K. (2003). Embodied energy of common and alternative building materials and technologies. *Energy and Buildings*, vol. 35, no. 2, pp. 129–137.
- Rigassi, V. (1985). Compressed Earth Blocks : Manual of Production. *Deutsches Zentrum fur Entwicklungstechnologien-GATE*, p. 143.
- Salmanpour, A.H. (2017). *Displacement Capacity of Structural Masonry*. PhD Thesis, ETH Zurich.
- Salmanpour, A.H. and Mojsilović, N. (2015). Simulation of boundary conditions for testing of masonry shear walls. In: *AIP Conference Proceedings*, vol. 1702, pp. 1–4. AIP Publishing. ISBN 9780735413498. ISSN 15517616.
- Salmanpour, A.H., Mojsilović, N. and Schwartz, J. (2012). Deformation Capacity of Structural Masonry: A Review of Theoretical Research. In: *15th World Conference on Earthquake Engineering, Lisbon, Portugal, Paper No. WCEE2012-2145*, pp. Paper No. WCEE2012–2145.
- Salmanpour, A.H., Mojsilović, N. and Schwartz, J. (2013). Deformation capacity of unreinforced masonry walls subjected to in-plane loading: a state-of-the-art review. *International Journal of Advanced Structural Engineering*, vol. 5, no. 1, p. 22. ISSN 2008-6695.
Available at: <https://link.springer.com/article/10.1186/2008-6695-5-22>
- SANS 10160-1 (2011). *Basis of structural design and actions for buildings and industrial structures, Part 1: Basis of structural design*. 1st edn. South African Bureau of Standards, Pretoria. ISBN 978-0-626-26428-4.
- SANS 10160-4 (2011). *Basis of structural design and actions for buildings and industrial structures, Part 4: Seismic actions and general requirements for buildings*. 1st edn. South African Bureau of Standards, Pretoria. ISBN 978-0-626-26431-4.
- SANS 10164-1 (1989). *The structural use of masonry, Part 1: Unreinforced masonry walling*. South African Bureau of Standards, Pretoria. ISBN 0-626-11256-7.
- SANS 10400-A (2016). *The Application of National Building Regulations, Part A: General principles and requirements*. 3rd edn. South African Bureau of Standards, Pretoria. ISBN 978-0-626-30399-0.
- SANS 201 (2008). *Sieve analysis, fines content and dust content of aggregates*. 2nd edn. South African Bureau of Standards, Pretoria. ISBN 978-0-626-30212-2.
- SANS 3001-GR30 (2015). *Civil engineering test methods, Part GR30: Determination of the maximum dry density and optimum moisture content*. 1st edn. South African Bureau of Standards, Pretoria. ISBN 978-0-626-31234-3.
- SANS 5844 (2014). *Particle and relative densities of aggregates*. 2nd edn. South African Bureau of Standards, Pretoria. ISBN 978-0-626-30857-5.
- SANS 5863 (2006). *Concrete tests - Compressive strength of hardened concrete*. 2nd edn. South African Bureau of Standards, Pretoria. ISBN 978-0-626-27125-1.
- Sassoni, E., Mazzotti, C. and Pagliai, G. (2014). Comparison between experimental methods for evaluating the compressive strength of existing masonry buildings. *Construction and Building Materials*, vol. 68, pp. 206–219.

- Schmidt, M. (nd). Tensile and shear characterisation of alternative masonry. Unpublished masters thesis.
- Statistics South Africa (2012). *General Household Survey*. Statistics South Africa.
- Tarback, E.J. and Lutgens, F.K. (2011). *Earth : an introduction to physical geology*. 10th edn. Pearson Prentice Hall, Upper Saddle River, N.J. ISBN 9780321699039.
- The Clay Brick Association of SA (2018). Top Projects - Affordable and Density Housing. Available at: <http://www.claybrick.org.za/gallery/7>
- Theart, P.J. (2014). *Development of a multi-criteria assessment tool to choose between housing systems for the low cost housing market*. Master's thesis, Stellenbosch University. Available at: <http://scholar.sun.ac.za/handle/10019.1/95844>
- Tomažević, M. (1999). *Earthquake-resistant design of masonry buildings*. Series on innovation in structures and construction ; v. 1. World Scientific, London. ISBN 1860940668.
- Tomažević, M. (2000 December). Some Aspects of Experimental Testing of Seismic Behavior of Masonry Walls and Models of Masonry Buildings. *ISET Journal of earthquake Technology*, vol. 37, no. 4, pp. 101–117.
- Tomlinson, M., Jeffery, A., Cronje, F., Moloi, L., Dimant, T., Kane-berman, J. and Folgore-mcLellan, C. (2015). South Africa's Housing Conundrum. *Liberty: The Policy Bulletin of the Institute of Race Relations*, vol. 20, no. 4, pp. 1–7. Available at: <https://irr.org.za/reports/atLiberty/liberty-2013-south-africas-housing-conundrum>
- Van Der Kolf, T. (2014). *The Seismic Analysis of a Typical South African Unreinforced Masonry Structure*. Master's thesis, Stellenbosch University. Available at: <http://scholar.sun.ac.za/handle/10019.1/86588>
- van Zijl, G.P.A.G. (2004). Modeling Masonry Shear-Compression: Role of Dilatancy Highlighted. *Journal of Engineering Mechanics*, vol. 130, no. 11, pp. 1289–1296. ISSN 0733-9399.
- Venkatarama Reddy, B.V. (2012). Stabilised soil blocks for structural masonry in earth construction. In: Hall, M.R., Lindsay, R. and Krayenhoff, M. (eds.), *Modern Earth Buildings*, no. 13 in Woodhead Publishing Series in Energy, pp. 324–363. Woodhead Publishing. ISBN 978-0-85709-026-3. Available at: <http://www.sciencedirect.com/science/article/pii/B9780857090263500137>
- Voon, K. and Ingham, J. (2006). Experimental in-plane shear strength investigation of reinforced concrete masonry walls. *Journal of structural engineering*, vol. 132, no. 3, pp. 400–408.
- WBCSD (2009). Cement Industry Energy and CO₂ Performance: Getting the Numbers Right. In: *The Cement Sustainability Initiative*.
- Wilding, B.V. and Beyer, K. (2016). Effective stiffness of unreinforced brick masonry walls. *Brick and Block Masonry – Trends, Innovations and Challenges*, pp. 1993–2001. Available at: <https://infoscience.epfl.ch/record/219014>
- Wilding, B.V., Dolatshahi, K.M. and Beyer, K. (2018). Shear-compression tests of URM walls: Various setups and their influence on experimental results. *Engineering Structures*, vol. 156, pp. 472–479. ISSN 0141-0296. Available at: <http://www.sciencedirect.com/science/article/pii/S0141029617309082>

Wu, F., Li, G., Li, H.N. and Jia, J.Q. (2013). Strength and stress-strain characteristics of traditional adobe block and masonry. *Materials and Structures/Materiaux et Constructions*, vol. 46, no. 9, pp. 1449–1457. ISSN 13595997.

Available at: <https://link.springer.com/article/10.1617/s11527-012-9987-y>

Zucchini, A. and Lourenço, P.B. (2007). Mechanics of masonry in compression: Results from a homogenisation approach. *Computers & Structures*, vol. 85, no. 3-4, pp. 193–204. ISSN 00457949.

Available at: <https://www.sciencedirect.com/science/article/pii/S0045794906003026>

Appendices

Appendix A

Masonry Unit

A.1 Loading Rate Summary

Table A.1: Summary of Loading Rates Used for Different Tests

Masonry Units & Mortar		
Compressive Strength Test		
Masonry Unit		0.75 mm/min
Mortar Cube		180 kN/min
Modulus of Elasticity Test		
Prismatic Specimens		
CMU & CSEB		135 N/s (0.04 MPa/s)
Adobe		13.5 N/s (0.004 MPa/s)
Cylindrical Specimens		
AACB & Mortar		90 kN/min
Masonry Wallets		
CMU		0.4 mm/min
CSEB		0.25 mm/min
Adobe		0.2 mm/min
AACB		0.3 mm/min

APPENDIX A. MASONRY UNIT

A.2 Compressive Strength Test Results**Table A.2:** Compressive Strength Test Results

Unit Type & Testing Time		Specimen								Average	Std	COV
		# 1	# 2	# 3	# 4	# 5	# 6	# 7	# 8			
CMU	28 Days	9.19	9.71	9.71	10.45	10.77	9.90	11.45	9.62	10.10	0.74	7.3 %
	Wall#1	14.75	13.52	13.74	15.65	15.31	15.65	14.71	-	14.76	0.86	5.8 %
	Wall#2	16.95	14.67	15.38	17.32	15.63	17.70	17.30	-	16.42	1.17	7.1 %
CSEB	28 Days	7.06	6.51	5.88	6.70	6.50	7.02	7.23	-	6.70	0.46	6.9 %
	Wall#1	9.15	8.77	8.25	8.28	7.85	7.66	8.09	8.17	8.28	0.48	5.8 %
	Wall#2	9.03	9.00	8.83	8.81	8.31	9.33	8.37	-	8.81	0.36	4.1 %
Adobe	28 Days	0.99	1.11	1.09	1.10	1.07	1.11	1.12	1.18	1.10	0.05	4.8 %
	Wall#1	1.17	1.20	1.03	1.05	1.10	1.19	1.09	-	1.12	0.07	6.1 %
	Wall#2	1.17	1.24	1.10	1.14	1.14	1.28	1.26	-	1.19	0.07	5.8 %
AACB	28 Days	17.84	17.35	20.52	19.91	20.19	18.09	17.38	20.84	19.01	1.49	7.8 %
	Wall#1	21.11	23.26	19.38	21.11	21.36	20.39	19.48	-	20.87	1.32	6.3 %
	Wall#2	22.45	21.46	22.33	24.49	22.83	21.73	21.81	-	22.44	1.02	4.5 %

Notes: Std = Standard Deviation

All unit compressive strength – f_u are expressed in [MPa]

APPENDIX A. MASONRY UNIT

A.3 Modulus of Elasticity Test Results

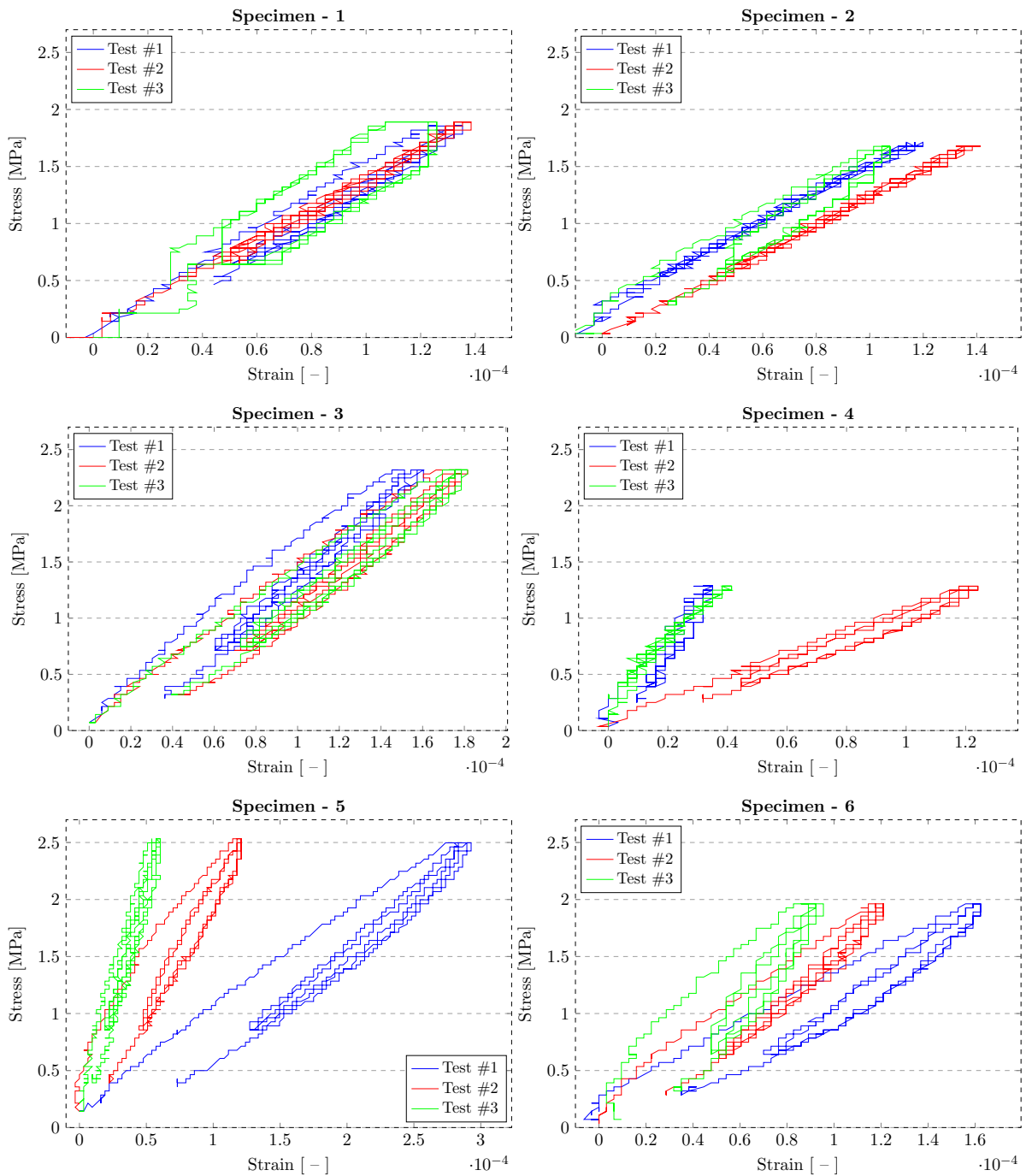


Figure A.1: CMU: Stress - Strain Responses at 28 days

APPENDIX A. MASONRY UNIT

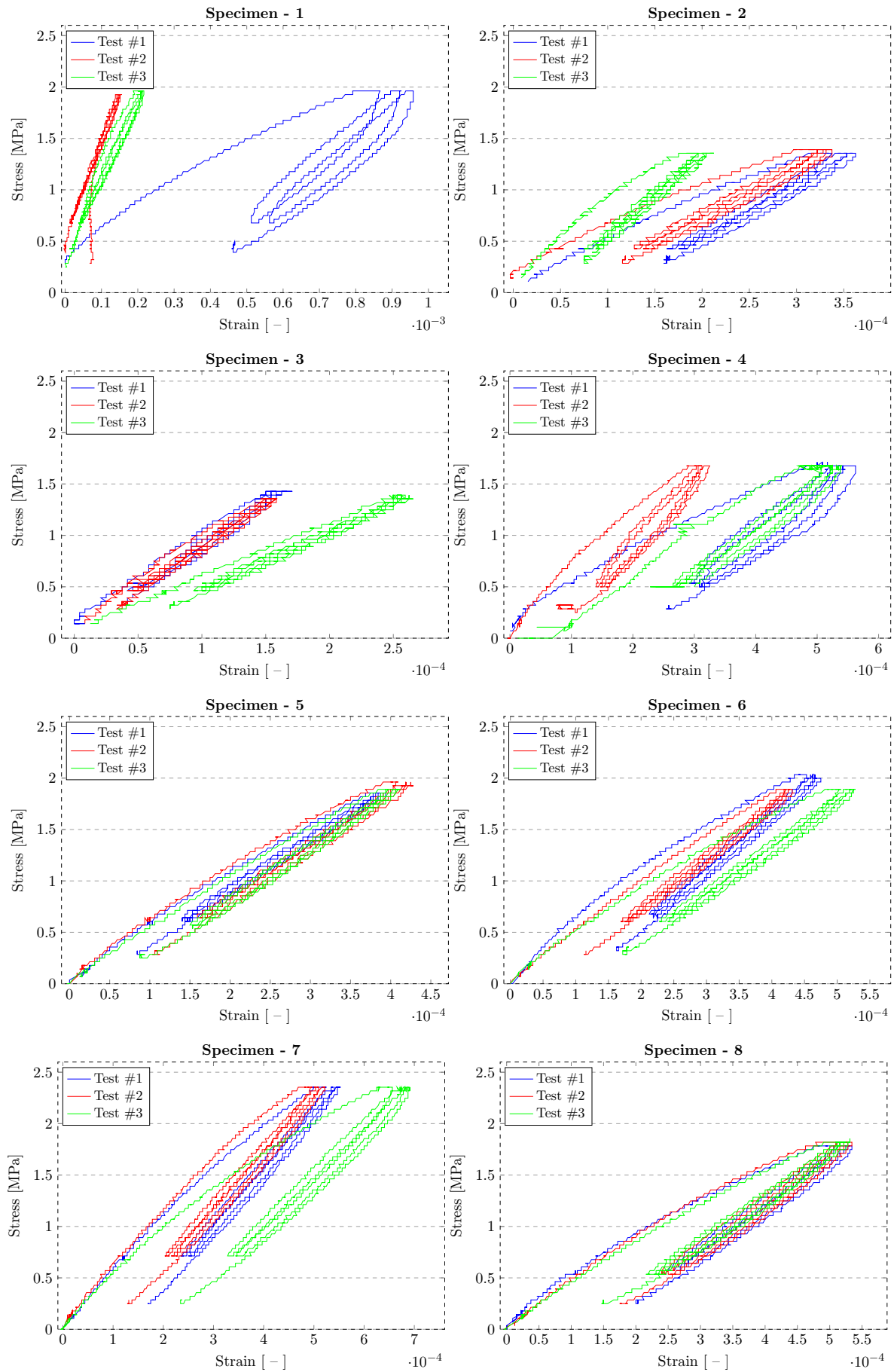


Figure A.2: CSEB: Stress - Strain Responses at 28 days

APPENDIX A. MASONRY UNIT

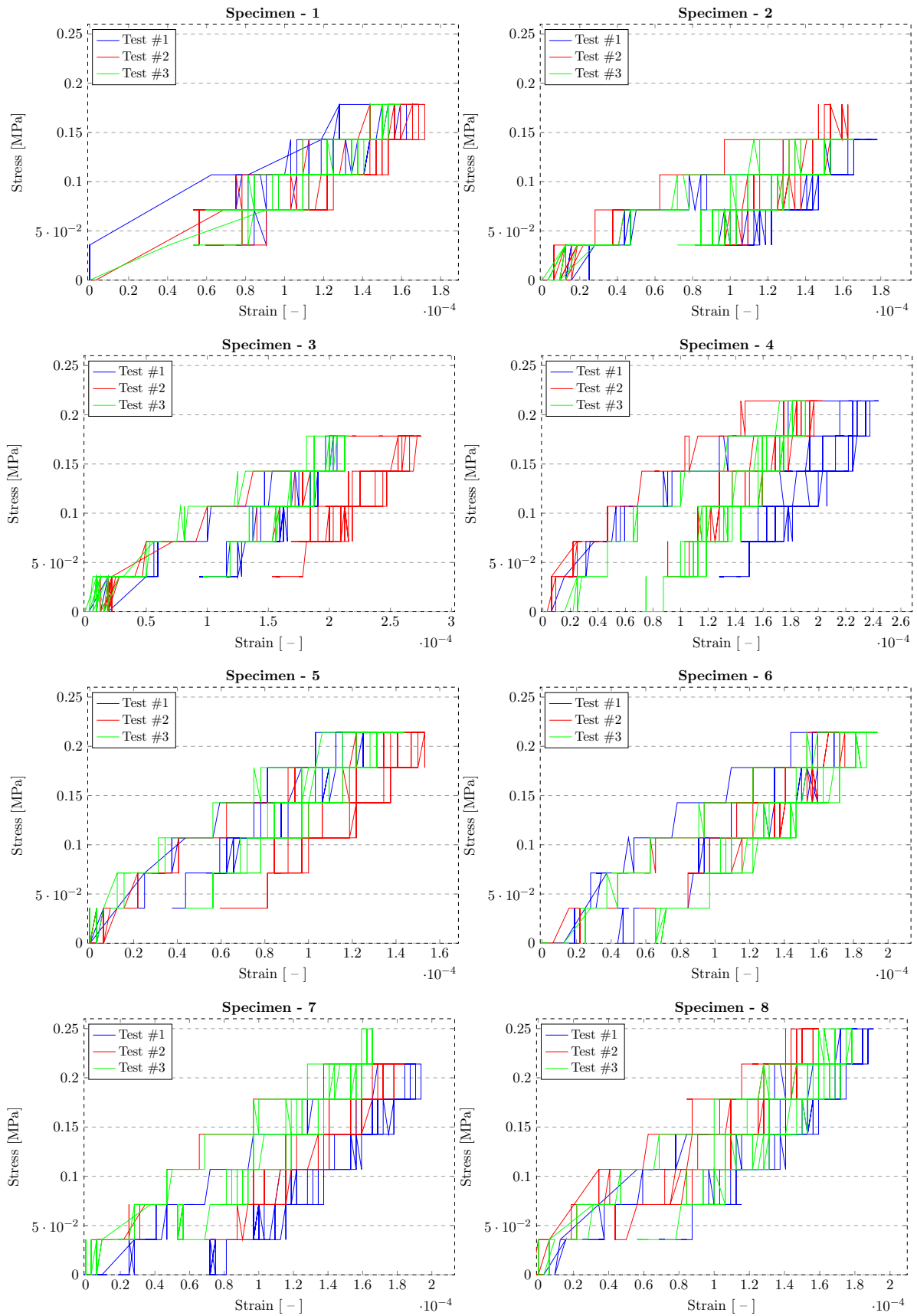


Figure A.3: Adobe: Stress - Strain Responses at 28 days

APPENDIX A. MASONRY UNIT

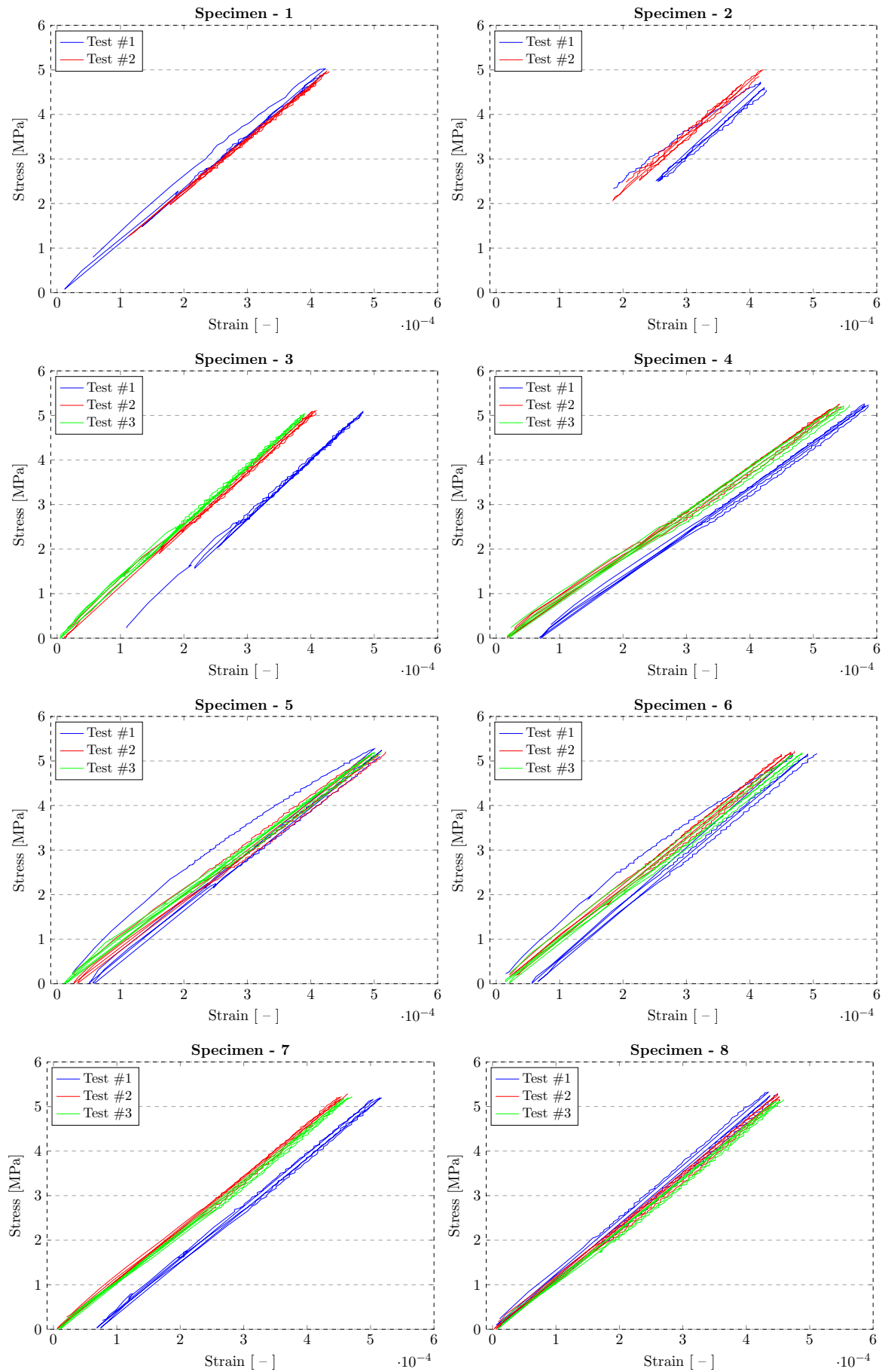


Figure A.4: AACB: Stress - Strain Responses at 28 days

Appendix B

Masonry Wallet

B.1 Modulus of Elasticity Test Results

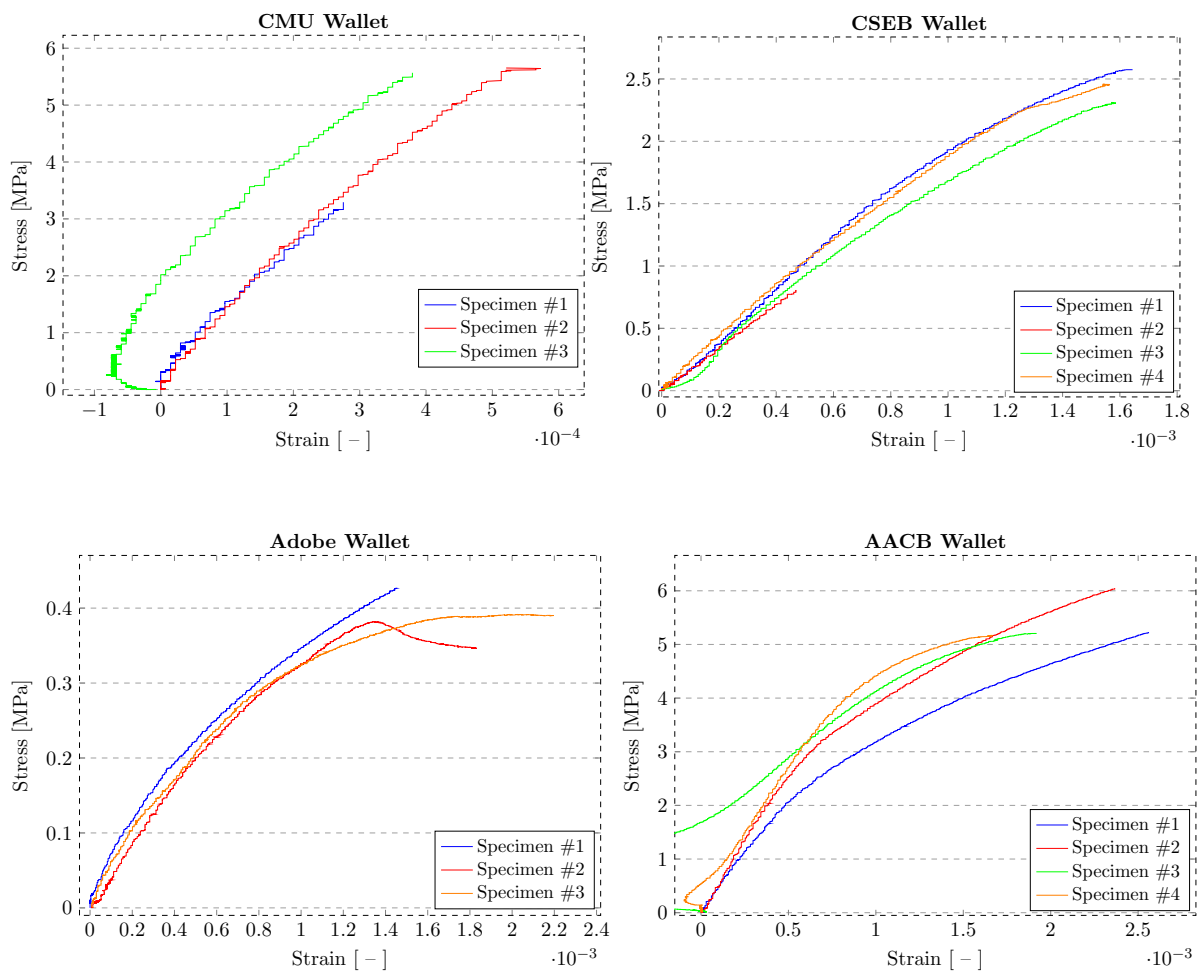


Figure B.1: Masonry Wallet: Stress - Strain Responses

Appendix C

Masonry Wall

C.1 LVDT and Applied Load Readings, & New Test Set-up

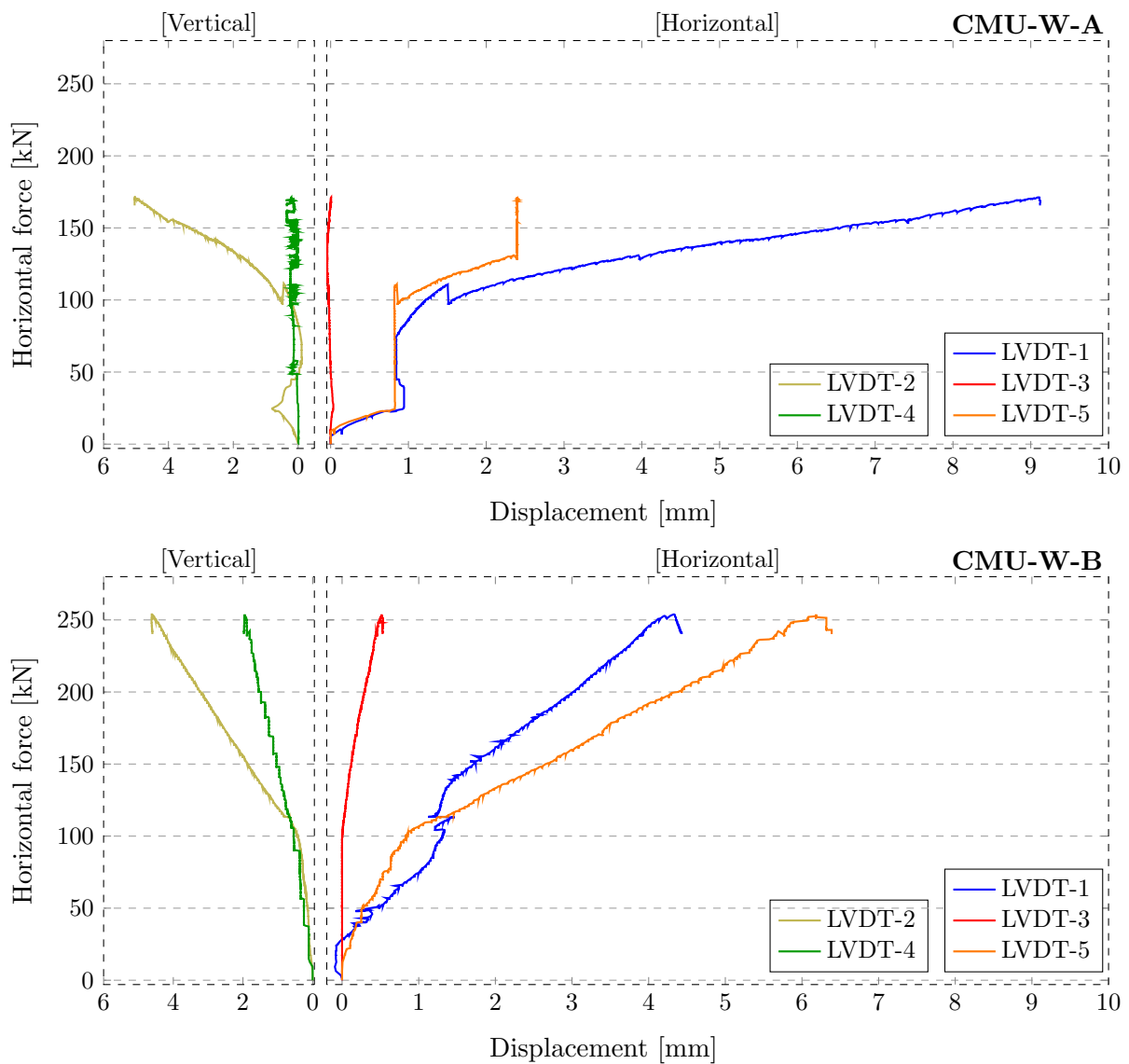
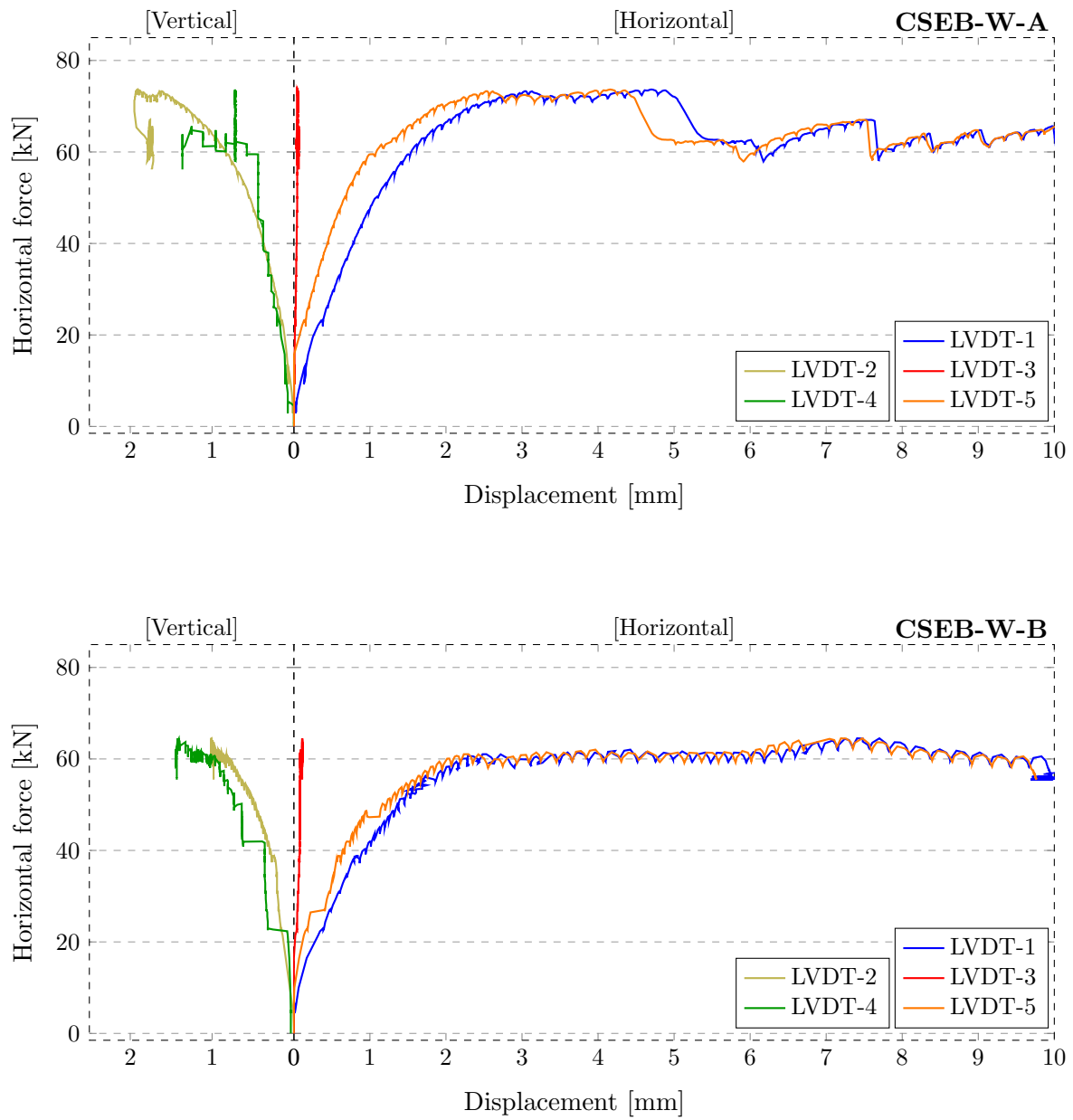
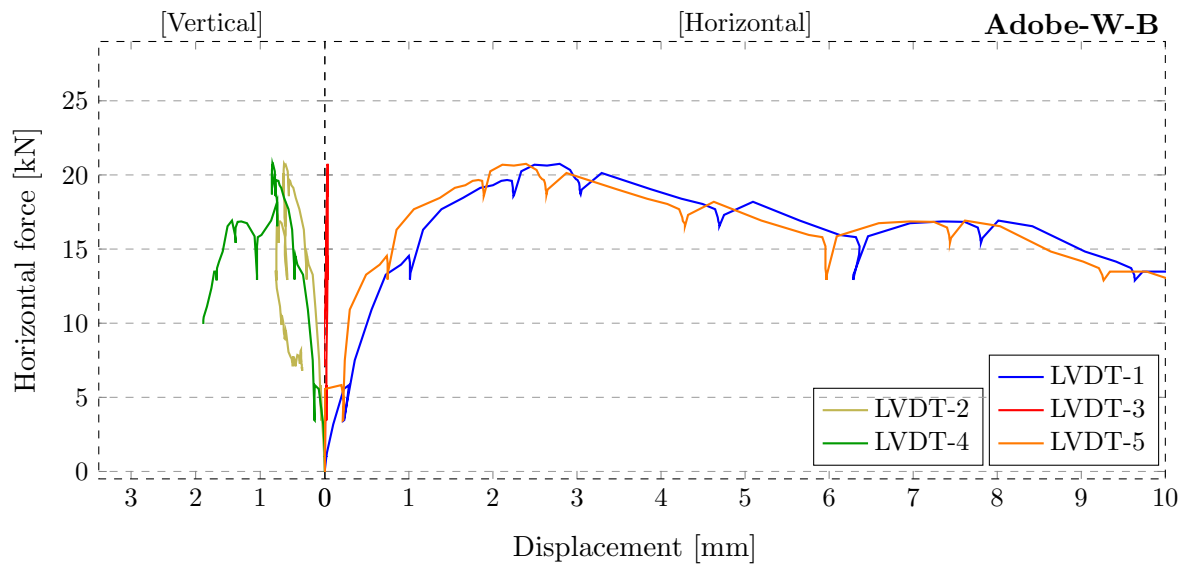
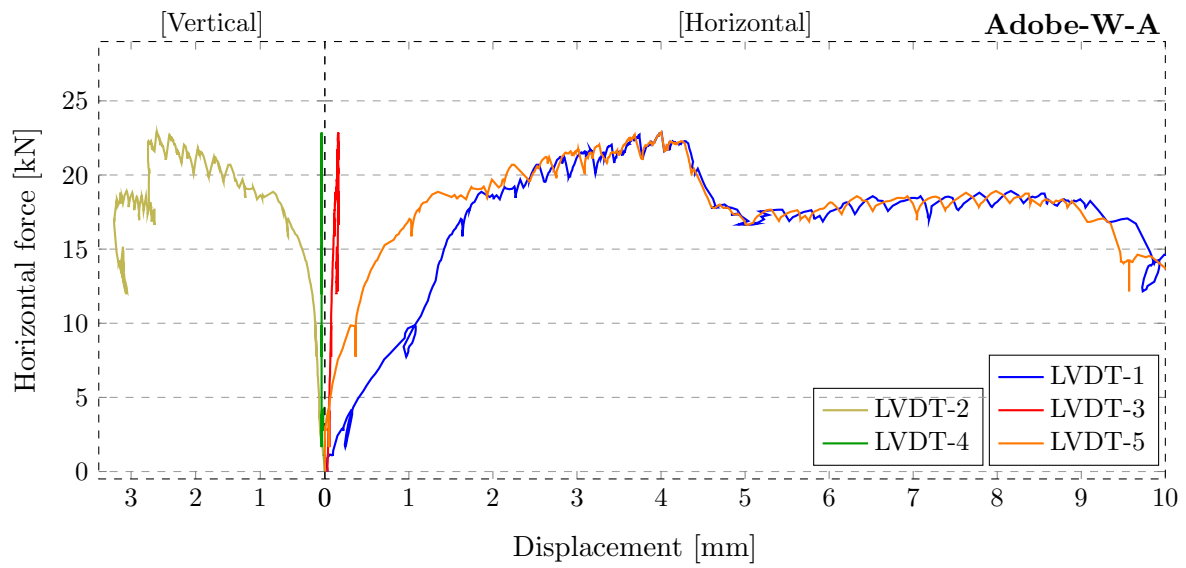


Figure C.1: CMU Walls: LVDT Readings

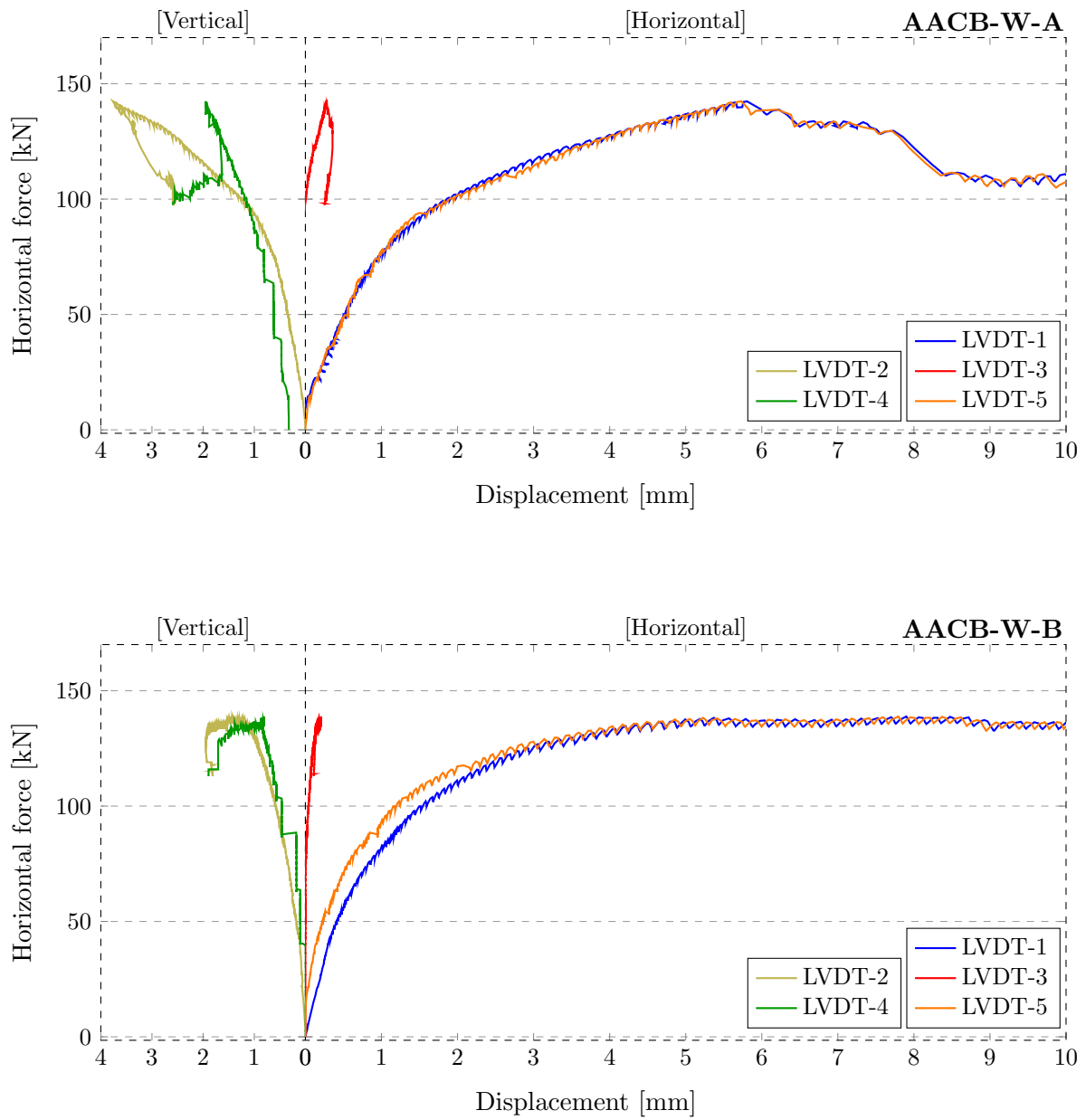
APPENDIX C. MASONRY WALL

**Figure C.2:** CSEB Walls: LVDT Readings

APPENDIX C. MASONRY WALL

**Figure C.3:** Adobe Walls: LVDT Readings

APPENDIX C. MASONRY WALL

**Figure C.4:** AACB Walls: LVDT Readings

APPENDIX C. MASONRY WALL

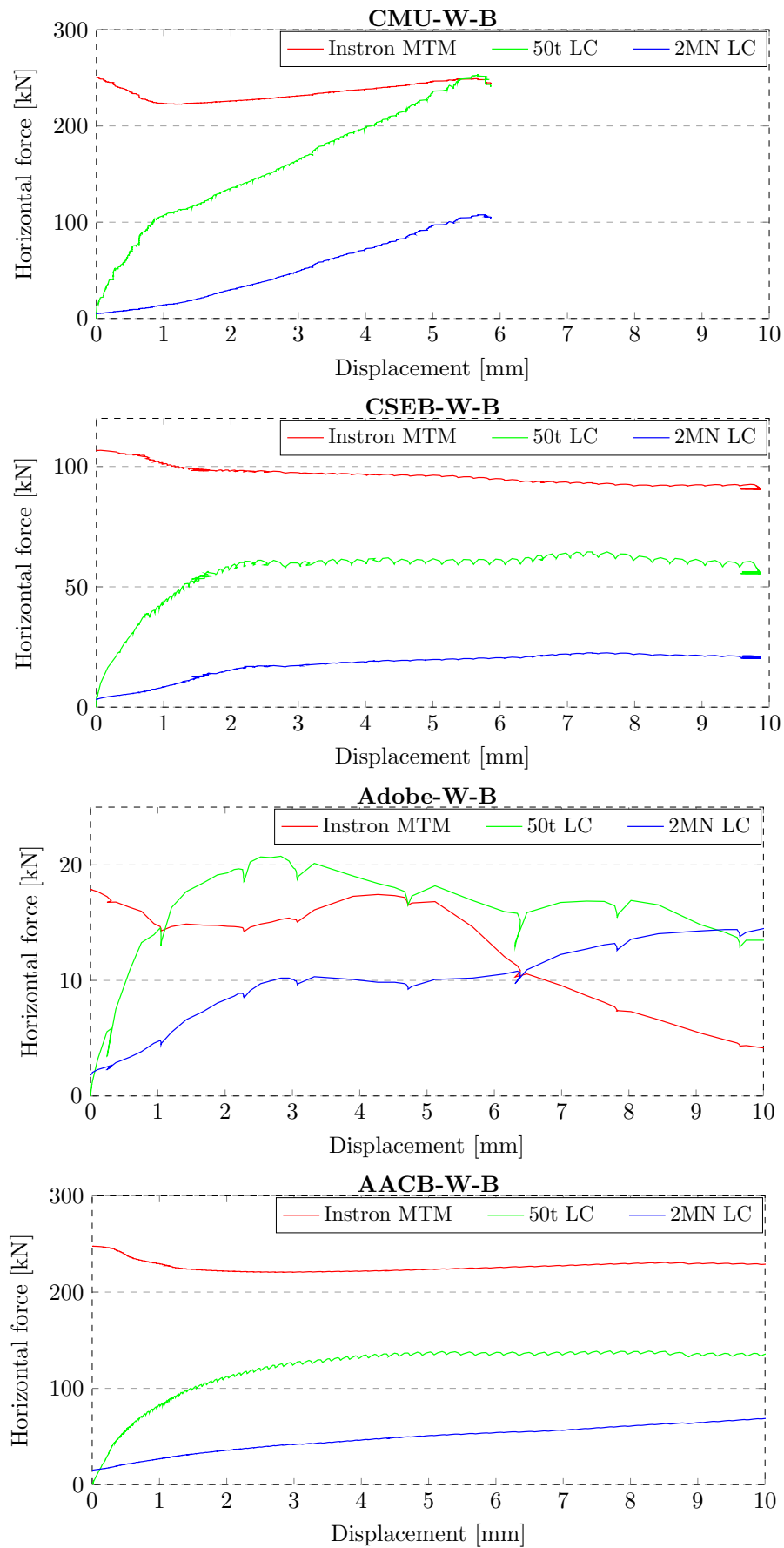


Figure C.5: Masonry Walls: Instron MTM, 50t & 2MN LC Readings

APPENDIX C. MASONRY WALL

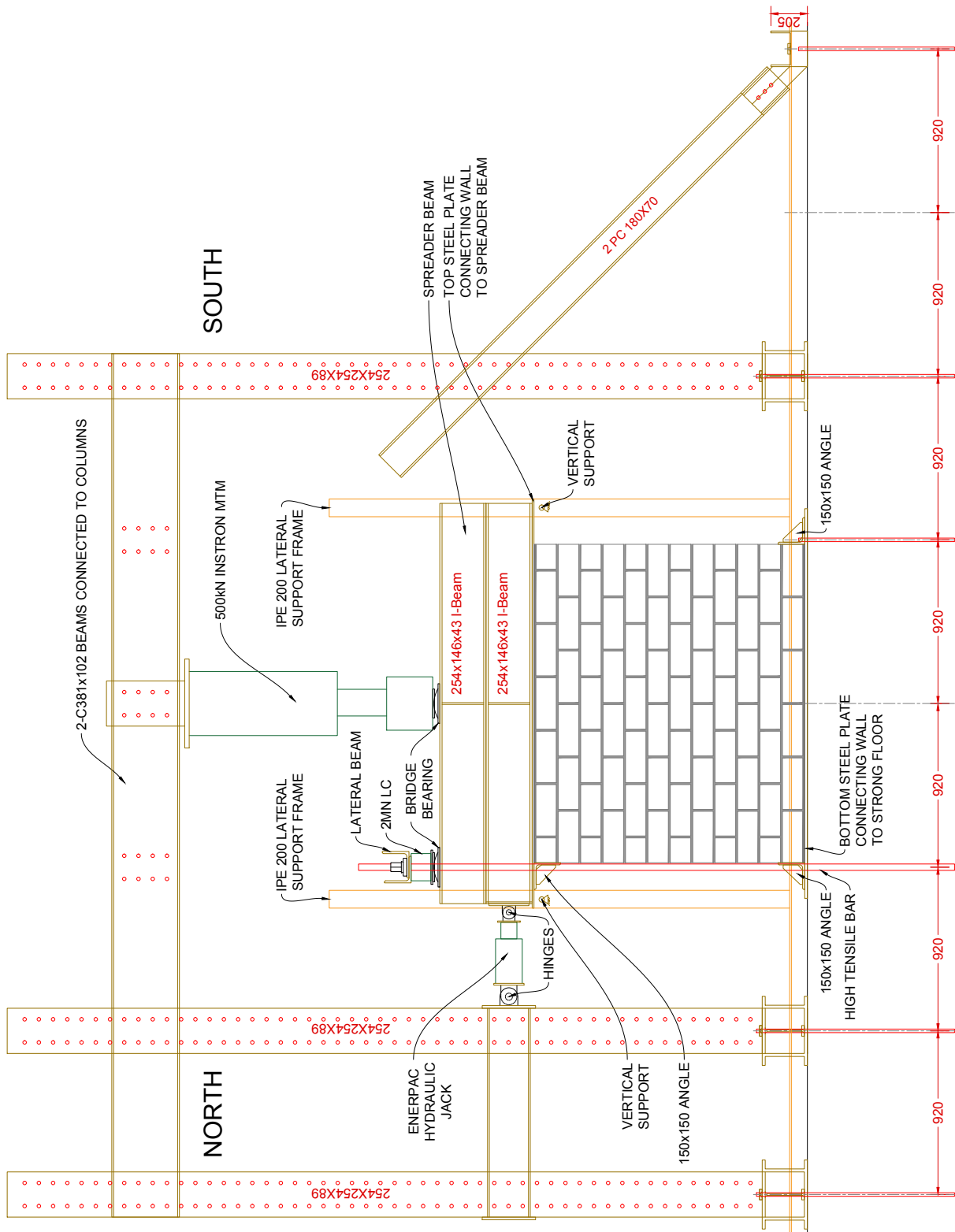


Figure C.6: New Test Set-up Proposal (all dimensions in mm)